Vacuum polarisation energies of two interacting scalar fields with a mass gap in $(1+1)$ dimensions

By

Martin Horst Capraro

Thesis presented in partial fulfilment of the requirements for the degree
of Master of Science in the Faculty of Science
at Stellenbosch University.

Supervisor: Prof. Herbert Weigel

December 2014

DECLARATION

By submitting this dissertation electronically, I declare that the entirety of the work contained therein is my own, original work, that I am the sole author thereof (save to the extent explicitly otherwise stated), that reproduction and publication thereof by Stellenbosch University will not infringe any third party rights and that I have not previously in its entirety or in part submitted it for obtaining any qualification.

December 2014

Abstract

The tools of perturbative Quantum Field Theory are by now a standard part of the theoretical physicist's arsenal. In this thesis we investigate the spectral method, an approach that uses tools from the quantum theory of scattering to calculate the $O(\hbar)$ corrections to fields. Specifically, we investigate whether the approach can be extended to deal with two interacting scalar fields with a mass gap in $(1+1)$ dimensions. To achieve this we need to verify the analyticity of the appropriate Jost function. All the machinery to do so is introduced during the course of the thesis. This includes the field theoretic formalism which describes such a system, and the derivation of a number of differential equations from which the density of states can be constructed. The numerical method is also outlined. Concrete results are presented to verify that the approach reproduces known results. Arguments related to Levinson's theorem are then presented that suggest that the Jost function is indeed analytic, with some caveats.

Opsomming

Die gereedskap van perturbatiewe Kwantumveld-teorie is teen diè tyd al ‘n standaard-deel van die teoretiese fisikus se werkskis. In hierdie tesis ondersoek ons die spektrale metode, ‘n benadering wat gereedskap van die kwantumteorie van verstrooing gebruik om die $O(\hbar)$ korreksie van velde te bereken. Ons ondersoek spesifiek of die metode uitgebrei kan word om toepaslik te wees in die geval van twee wisselwerkende skalaarvelde met ‘n massa-gaping in (1+1) dimensies. Vir hierdie doel moet ons bepaal of die toepaslike Jost-funksie analities is of nie. Al die masjinerie om dit te bepaal word deur die loop van hierdie tesis ingevoer. Dit sluit in die veld-teorietiese formalisme wat so ‘n stelsel beskryf, en die afleiding van ‘n aantal differensiaal vergelykings wat gebruik kan word om die digtheid van toestande te konstrueer. Die numeriese metode word ook beskryf. Konkrete resultate wat bevestig dat die metode die korrekte antwoorde in ‘n analities bekende geval weergee, word verskaf. Argumente wat verband hou met Levinson se stelling word gebruik om te bevestig dat die Jost-funksie inderdaad analities is, met sekere voorbehoude.

Acknowledgements

I would like to thank my supervisor, Professor Herbert Weigel, for his willingness to share his knowledge with me. Without his guidance and patience this thesis would not have come to fruition. I admire his dedication to his work, and attempted to emulate this as far as was possible.

My partner, Janel du Preez, deserves my thanks for putting up with my constant complaints. The support of her and my friends - Hannes, Chris, David, Willem and all the rest - has kept me more or less sane during the past two and a half years.

The various teachers who have, over the years, taught me mathematics and physics also deserve thanks. I am afraid that I have forgotten some of your names, but I thank all of you (except for those who didn't teach me anything).

I would also like to thank the National Institute for Theoretical Physics for providing the bulk of my funding in the form of a bursary. I would not have been able to pursue my studies without this.

CONTENTS

1 Introduction

Quantum Field Theory (QFT) is the most successful physical theory currently known. In the guise of the quantum theory of the electromagnetic force, Quantum Electrodynamics (QED), it correctly predicts the anomalous magnetic moment of the electron to better than one part in a billion [1]. Its genesis has been long and tortuous, consisting of the combination of Quantum Mechanics with the classical theory of fields and Einstein's theory of Special Relativity. As of the writing of this thesis, it underlies our understanding of three of the four known fundamental forces of Nature. The importance of the mathematical theory of groups in elucidating the relation between these forces generally, and the nature of symmetry breaking specifically, was an unexpected historical development. This has paved the way for fundamental insights into the importance of symmetry in Nature, culminating in the modern viewpoint that places gauge fields at the heart of our understanding of the microscopic laws that govern our Universe.

QFT has predicted more classically unexpected phenomena than it is reasonable to discuss in depth. The effect most relevant to this thesis is that attributed to Casimir and Polder [2]. The Casimir effect predicts that parallel conducting plates in a vacuum will experience an attractive force. In the context of QFT this can be traced to a shift in the zero-point energies that occurs because of the presence of the plates. This thesis deals with further manifestations of the Casimir effect. We are principally interested in extending an approach, called the spectral method, that uses results from the quantum theory of scattering, to study the $O(\hbar)$ corrections to fields. Specifically, we investigate whether we can apply this method to calculate the $O(\hbar)$ correction to the energy of two interacting scalar fields with a mass gap in $(1+1)$ dimensions.

The spectral method deals with the fundamental issue of what the appropriate way is to meaningfully sum the expression for the zero-point energies of the vacuum. The solution that is presented is to consider an expression like

$$\frac{1}{2}\sum_n(\omega_n - \omega_n^{(0)})|_{reg}, \tag{1.1}$$

where ω_n and $\omega_n^{(0)}$ are the energies of the interacting and free vacuum modes respectively, and the subscript implies that the expression has been suitably regularised and renormalised. We shall see during the course of this thesis how this can be related to the difference of the density of states between the interacting and free theories, and how this can be used to unambiguously compute the vacuum polarisation energy of a renormalisable field theory. The density of states, which is a measure of the inverse of the momentum spacing between adjacent states, will itself be constructed from the scattering phase shifts. The latter can be computed numerically on a computer. This procedure, including the necessary numerical algorithms, will also be outlined. The main strength of this approach is its computational efficiency.

A crucial ingredient of the spectral method is the identification of terms of the Born series with Feynman diagrams, which allows us to regularise the divergent pieces of the relevant integrals by shifting them into Feynman diagrams, which can then be renormalised by the standard method of adding counterterms to the Lagrangian density. This is one of two fundamental limitations of the method; the underlying field theory must be renormalisable. The other restriction is that the system must exhibit enough symmetry to permit a decomposition in terms of partial waves.

As this thesis progresses we shall have opportunities for digressions into a number of mathematical back alleys. The goal throughout is to maintain as much mathematical rigour as is necessary to clearly elucidate the principles that allow us to extract meaningful information from the physical system. References are given for many standard results, particularly from the quantum theory of scattering, that are taken for granted. On the other hand, while the extant literature on scattering theory is vast, the notation and terminology is often inconsistent and confusing, so that it is worthwhile to be somewhat pedantic with a number of the definitions and calculations.

1.1 Thesis organisation

Chapter 1 introduces some background material and notational conventions.

Chapter 2 is an introduction to the spectral method and the necessary tools from scattering theory. It includes a simple but concrete example of how the density of states can be constructed and used to calculate the vacuum polarisation energy of a scalar field interacting with a static background field.

Chapter 3 investigates an extension of certain scattering solutions in $(1+1)$ dimensions to two interacting scalar fields, with specific reference to a perturbative expansion about a classical soliton solution.

Chapter 4 introduces the model that underlies our approach. We quantise this model using the canonical approach of enforcing equal-time commutation relations between fields and their conjugate momenta, and then derive the necessary commutation relations between the annihilation and creation operators. We introduce a scattering ansatz, from which a set of differential equations are constructed. The scattering phase shifts can be extracted from the solution of these equations. An example is provided to establish that our model correctly calculates the vacuum polarisation energy for an analytically known case.

Chapter 5 contains numerical results and comments on the manner on which these numerical data were extracted. It also shows how the numerical data can be related to the topological structure of the Riemann surface of the appropriate Jost function, and how this can be used to investigate the analyticity of the Jost function.

The appendices contain a detailed proof of Levinson's theorem for s-wave and an overview of the various numerical methods used in this thesis.

1.2 Notation and conventions

The metric signature $g_{\mu\nu} = \mathrm{diag}(+,-,-,-)$ is used. Unless stated otherwise, the convention is to use natural units, with $\hbar = c = 1$. The usual Einstein summation convention for doubled indices is assumed. Operators, as opposed to their matrix representations, have hats, like $\hat{A}$. The conjugate transpose of a matrix is indicated by a dagger, like $A^\dagger$. The standard bra-ket notation for elements

of Hilbert spaces corresponding to quantum states is also used.

The only (slightly) non-standard notation is the use of the letter r to refer to the 'radial' coordinate in both (3+1) and (1+1) dimensions. In the latter case the metric signature is simply $g_{\mu\nu} = \mathrm{diag}(+,-)$. It should be clear from the context whether the coordinate is truly radial in the sense of three spatial dimensions. The symbol ∂_r is also used to refer to the ordinary, not partial, derivative with respect to r in $(1+1)$ dimensions. This is a purely typographical issue.

An unfortunate ambiguity in the terminology is the use of the word 'channel' to refer both to the partial wave decomposition, and to the various field components that are scattering. An effort has been made to ensure that it is obvious which meaning is intended.

2 The Spectral Method

The spectral method is an approach to Casimir-like effects in Quantum Field Theory (QFT) that uses a set of tools from potential scattering theory to calculate the quantities of interest. It has been developed over a number of years (see references [3], [4] and [5] for an introduction) and used to investigate a variety of problems within the context of QFT, including electroweak cosmic strings [6] and chiral soliton models stabilised by fermions [7].

This thesis is about the calculation of the vacuum polarisation energies (VPEs) of interacting scalar fields using the spectral method, and the analytic properties of related functions, so it is only reasonable that we discuss

i) the vacuum,
ii) vacuum polarisation energies,
iii) potential scattering theory in the spectral method,
iv) the spectral method itself.

We do so in this chapter, to the extent necessary to understand the context of the spectral method, and then introduce a concrete application of these ideas in the guise of the conceptually simple Klein-Gordon field coupled to a radial potential. This example serves to illustrate many of the rather abstract notions that we need to speak sensibly about our results. We also discuss the significance of zero-point energies in the context of the Casimir effect, and highlight the difficulty of uncritically accepting its existence as evidence for the 'reality' of zero-point energies. The section on the vacuum includes comments on technical difficulties in defining it in an unambiguous manner. We shall see during the course of this thesis that these difficulties do not in practice prevent us from performing physically sensible calculations with the spectral method.

2.1 The Vacuum

Classically, the vacuum is an area of space that contains 'nothing'. In QFT the vacuum state $|0\rangle$ is defined as the ground state of the system at hand, i.e. the state with the lowest energy for a given theory. This state is an element of some Hilbert space, with the additional requirement that the background spacetime be Minkowskian, with the physical symmetry being encoded in the Poincaré group. The vacuum ket state is then that state which is annihilated by all annihilation operators acting on it from the left:

$$\hat{a}_i(k)\,|0\rangle = 0 \qquad \forall k, i, \tag{2.1}$$

while the bra in the dual space is annihilated by all creation operators acting on it from the right:

$$\langle 0|\, \hat{a}_i^\dagger(k) = 0 \qquad \forall k, i. \tag{2.2}$$

It is understood that the creation and annihilation operators satisfy the standard commutation relations. The k in the equations above refer to the momentum of the particle state created/annihilated by the relevant operator, and i refers to any internal degrees of freedom (e.g. the spin quantum number).

Formally, a more general state of the form $|n\rangle$ is an eigenstate of the particle number operator $\hat{a}_i^\dagger(k)\hat{a}_i(k)$, which measures the number of quanta of a particular species with momentum k in a state. Such states are called Fock states (see [8]), a subset of states in Fock space. Fock spaces are created by summing the tensor products of Hilbert spaces spanned by single-particle states:

$$F(H) = \bigoplus_{n=0}^{\infty} S(H^{\otimes n}). \tag{2.3}$$

In this equation S is a symmetrising operator that symmetrises or antisymmetrises the Hilbert space H, depending on whether the states have integer or half-integer spin.

We should keep in mind that a theory may have sets of operators that create and annihilate different species of particles: the Dirac field for instance has two sets, one for positive frequency modes (particles with spin one half) and one for negative frequency modes (antiparticles with spin one half). This also highlights the fact that it is a misnomer to refer to 'the' vacuum, as different Lagrangians/models will have different vacua. There is the additional subtlety that if two observers are accelerating relative to each other, the state that the one observer measures as the vacuum state will be, from the other observer's perspective, filled with uniform thermal radiation (the Unruh Effect, see [9] and [10]). While the issue of accelerating frames of reference will not enter into our discussion of vacuum polarisation energies, it is helpful to keep in mind the range of applicability of our theory.

The possibility of a degenerate vacuum state leads to the mechanism of so-called spontaneous symmetry breaking, which is one part of the machinery that leads to the important Higgs mechanism, the origin of many particles' mass. However, no symmetry is truly broken: it is merely a case of a 'non-symmetric' choice of vacuum state, with the symmetry of the Lagrangian remaining unchanged. This is the case for potentials that allow an infinite number of degenerate vacua, forming a representation of some Lie group that depends on the specific form of the potential. Though the theory should respect this symmetry, the chosen vacuum configuration is not invariant under the corresponding transformation. We shall not consider continuous symmetries in this thesis. However, we shall see in section 3.1 how a theory with two degenerate vacua in one spatial dimension leads to soliton solutions that interpolate between them.

The magnitude of the vacuum energy of the Universe, E_Λ, has been speculated to be [11] the sum over the vacuum modes of a scalar field,

$$E_\Lambda = \frac{1}{2}\sum_n \hbar\omega_n. \tag{2.4}$$

We then recall[1] that the energy of a particle with momentum k and mass m is $\sqrt{k^2c^2 + m^2c^4}$, and perform the summation above by integrating over the momentum states, using the momentum phase space volume factor $4\pi k^2 dk$. We obtain an expression for the vacuum energy density,

$$\rho_\Lambda c^2 = 4\pi \int_0^\infty \frac{dk k^2}{(2\pi\hbar)^3} \sqrt{k^2c^2 + m^2c^4}, \tag{2.5}$$

which is divergent. However, we may guess that there is some energy scale at which new physics arises, of which our current models are effective field theories, so that the upper integration limit needs to be cut off there. This scale is typically taken to be of the order of the Planck scale, where we expect a complete theory of quantum gravity to be required. Substituting the Planck momentum,

$$K_{Pl} = \sqrt{\frac{\hbar c^2}{G_N}} \approx 10^{19}\text{GeV}/c \tag{2.6}$$

in the upper integration limit above, the integral yields a value

$$\rho_\Lambda \approx 2 \times 10^{91}\text{g/cm}^3. \tag{2.7}$$

Comparing this with the observed value of the cosmological constant (obtained from the measured acceleration of the observable Universe's expansion),

$$\rho \approx 2 \times 10^{-29}\text{g/cm}^3, \tag{2.8}$$

we see that there is a discrepancy of over 120 orders of magnitude. This enormous discrepancy between the theoretical prediction for the zero-point energy of the Universe and the experimental measurement of the cosmological constant provides us with a very glaring example of how attempting to combine concepts in an inappropriate manner can lead to serious difficulties (or interesting problems, depending on one's perspective [12]).

There are additional mathematical subtleties related to defining the vacuum state of an interacting field theory, and whether the Fock states above actually exist for such a theory, but for the purpose of this thesis the discussion in this section is sufficient. The interested reader is directed towards e.g. reference [13].

2.2 Vacuum Polarisation Energies and the Casimir Effect

The vacuum polarisation energy (VPE) of a given system is the $O(\hbar)$ correction to the classical energy of that system. In this context a classical field theory is one where the fields commute, so the VPE gives an indication of the leading quantum contribution to the energy. This contribution is equivalent to the energy change stemming from the polarisation of the vacuum modes, which in turn has its origin in the interaction of a quantum field with a background field or potential.

There are of course many examples of $O(\hbar)$ processes in QFT. For instance, the following Feynman diagram represents the one-loop correction to the photon propagator. The particle interpretation is that the virtual photon which mediates the electromagnetic force (represented by the wiggly line)

[1] In this section $\hbar$ and c are reinstated.

propagates, then splits into an electron-positron pair (the closed loop), which then annihilate to form a virtual propagating photon again (the X's at the endpoints mean that we can, by substitution, insert this graph in any QED diagram containing the photon propagator; this roughly corresponds to an extra integration over the momenta variables in the expression for the scattering amplitude of the associated process):

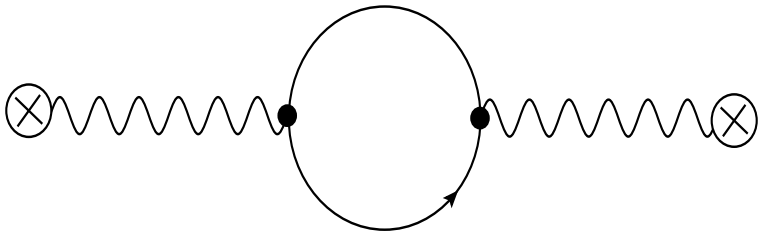

Figure 2.1: *Leading order correction to the photon propagator (see text for details)*

It is more-or-less trivial to write down the expression corresponding to this diagram, which contributes to the Lamb shift. However, the spectral method is not applicable to this diagram, because there is no classical analogue of 'a background electron field' (or indeed any other fermionic field). This need not discourage us, as there are still eminently physical processes that can be calculated in the context of the spectral method. We shall consider one such example in the next section.

In our case, the VPE is the quantity corresponding to the following diagrams:

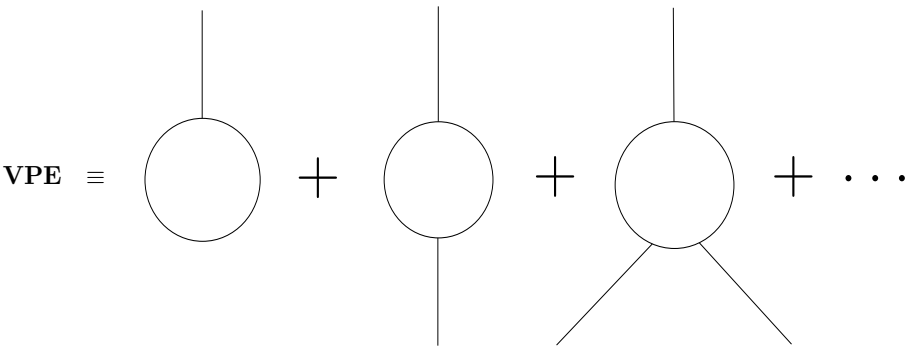

Figure 2.2: *All insertions of a background field to one-loop order*

Each external line here corresponds to one insertion of the static background field, and the loop represents the fluctuating quantum field.

2.2.1 The Casimir Effect

The Casimir effect, theoretically described in 1948 (see [2]) and experimentally confirmed in 1969 (see [14][2]), is a force between two parallel conducting plates in a vacuum, even though they are uncharged and there is no external field. The force per unit area of the plates, in (3+1) dimensions, is given by

[2]The purported results of earlier experiments were often of the same order of magnitude as the statistical uncertainty, e.g. [15].

$$\frac{F}{A} = -\frac{\hbar c \pi^2}{240 a^4}, \tag{2.9}$$

where a is the distance between the plates.

Although the absence of an external field means that this is classically impossible, we can interpret the force as arising from a shift in the zero-point energies of the quantum vacuum, which is essentially what the VPE measures. However, the effect can also be derived without reference to vacuum fluctuations [16]. In fact, in the context of relativistic quantum mechanics, the Casimir effect is the relativistic, retarded van der Waals force between two plates. This is obscured in the zero-point fluctuation calculation by the unphysical boundary condition that ALL the modes of the field between the plates are suppressed by them, even the ones with wavelengths much smaller than the typical interatomic spacing. This also highlights an interesting feature of the preceding equation: the QED coupling constant does not appear in it. This is clearly because the interaction at the plates' boundaries is taken to be infinitely strong. Presumably in a complete description the above would merely be the first term in a series, with a factor of $1/e^2$ occurring in the first correction.

Since the Casimir effect can be determined without any reference to the zero-point energy of the vacuum, which is what the spectral method does, the context is different. Whether one is then to consider the Casimir effect as a 'physical' manifestation of vacuum fluctuations is a matter of perspective, but the computational toolkit we shall consider is certainly still relevant. Despite all this, VPEs are often called 'Casimir energies' in the literature. We shall not follow this convention in this thesis.

2.3 Tools from Scattering Theory

In this section we shall review the scattering theory of particles insofar as it necessary to understand the spectral method. For an exhaustive treatment of the subject the reader is directed to references [17] and [18].

We restrict ourselves to spin 0 particles scattering off spherically symmetric potentials, $V = V(r)$, in three spatial dimensions (we shall later consider only $(1+1)$ dimensional scattering). Furthermore, we shall only consider potentials satisfying

$$\int_b^\infty dr |V(r)| r < \infty \tag{2.10}$$

for $b \geq 0$. We shall call such potentials 'regular'.

Applying separation of variables to Schrödinger's equation it follows that the solution can be factorised as

$$\psi(r, \theta, \phi) = R_l(r) Y_l^m(\theta, \psi), \tag{2.11}$$

where the $Y_l^m(\theta, \psi)$ are the spherical harmonics,[3],

$$Y_l^m(\theta, \phi) = \frac{(-1)^l}{2^l l!} \left(\frac{(2l+1)(l+m)!}{4\pi(l-m)!}\right)^{\frac{1}{2}} e^{im\phi} \frac{1}{\sin^m \theta} \frac{d^{l-m}}{d(\cos\theta)^{l-m}} [\sin(\theta)]^{2l}, \tag{2.12}$$

[3]The m occurring in the spherical harmonics is the magnetic quantum number, otherwise it refers to the mass of a particle.

and $w_l \equiv rR_l(r)$ satisfies the reduced radial Schrödinger equation[4]

$$-\frac{d^2w_l}{dr^2} + [V(r) + \frac{l(l+1)}{r^2}]w_l = Ew_l. \tag{2.13}$$

We note that this is identical to the time independent Schrödinger equation but with an extra term in the effective potential that tends to throw the particle outwards. The l's are the angular momentum quantum numbers.

The usual approach in potential scattering theory is to look for asymptotic solutions (i.e. solutions 'far away', where the effect of the potential can be ignored). One possible solution in the asymptotic regime is the combination of an incoming plane wave and an outgoing spherical wave at infinity, namely

$$\lim_{r\to\infty}[\psi(r,\theta,\phi) - (e^{i\vec{k}\cdot\vec{r}} + A(\theta,\phi)\frac{e^{ikr}}{r})] = 0. \tag{2.14}$$

The second, linearly independent, solution is obtained by complex conjugation and parameterisation of an incoming spherical wave.

The function $A(\theta,\phi)$[5], the amplitude of the outgoing wave, is called the scattering amplitude and leads to the probability of a particle being scattered in a certain direction, normalised with respect to the incoming flux:

$$\frac{d\sigma}{d\Omega} = |A(\theta,\phi)|^2. \tag{2.15}$$

This quantity is called the scattering cross-section, and plays a central role in the experimental scattering of particles.

2.3.1 Phase shifts and the S-matrix

Since the spherical harmonics form a complete orthonormal basis we can expand the scattering amplitude in terms of them. For any arbitrary function of the polar and azimuthal angles, $g(\theta,\phi)$, we have

$$g(\theta,\phi) = \sum_{l,m} c_{l,m}Y_l^m(\theta,\phi). \tag{2.16}$$

Examining the explicit formula for the spherical harmonics, and noting that the scattering amplitude for a spherically symmetric potential has no ϕ dependence, we see that all the m terms contribute equally to the sum in equation (2.16), yielding a degeneracy factor of $(2l+1)$, so that for a potential $V(r)$ the scattering amplitude is

$$A(\theta) = \sum_{l=0}^{\infty}(2l+1)a_l(k)P_l(\cos\theta), \tag{2.17}$$

where the $a_l's$ are as yet to be determined expansion coefficients and the $P_l(\cos\theta)$ are Legendre polynomials. The incoming plane wave can be expanded similarly,

[4]Reduced units, $\hbar = 1$ and $2m = 1$ (with m here the mass), are used throughout this section.
[5]The angles θ and ϕ are measured with respect to $\vec{k}$.

$$e^{i\vec{k}\cdot\vec{r}} = e^{ikr\cos\theta} = \sum_{l=0}^{\infty}(2l+1)i^l j_l(kr)P_l(\cos\theta) \tag{2.18}$$

with j_l a spherical Bessel function, which is a solution of (2.13) for the free case (i.e. $V(r) = 0$). Considering the asymptotic behaviour of j_l,

$$\lim_{r\to\infty}[i^l j_l(kr) - \frac{e^{ikr} - e^{-i(kr-l\pi)}}{2ikr}] = 0 \tag{2.19}$$

and inserting (2.18) and (2.17) in the ansatz (2.14) we get the asymptotic behaviour of the solution to the Schrödinger equation (2.11) for a radially symmetric potential as

$$\lim_{r\to\infty}(\psi(r,\phi) - \sum_{l=0}^{\infty}(2l+1)\frac{P_l(\cos\theta)}{2ik}[(1+2ika_l(k))\frac{e^{ikr}}{r} - \frac{e^{-i(kr-l\pi)}}{r}]) = 0. \tag{2.20}$$

This may be interpreted to mean that the scattering potential changes the coefficient of the outgoing wave by $1 + 2ika_l(k)$. We can use this to define the S-matrix element

$$S_l(k) \equiv e^{2i\delta_l(k)} \equiv 1 + 2ika_l(k). \tag{2.21}$$

The factor of two in the exponent is purely due to convention. The functions $\delta_l(k)$ are called the phase shifts. They play an important role in the spectral method, as we shall see.

We motivate here why we can define the S-matrix elements as pure phases. Intuitively the S-matrix is a representation of an operator that connects free states in the asymptotic past ('in' states) to states in the far future ('out' states). Since the Hamiltonian of a system with a spherically symmetric potential is itself rotationally invariant we know from Noether's theorem that angular momentum must be conserved. This is equivalent to requiring the S-matrix to be diagonal in the representation with angular momentum eigenkets as basis vectors. The hermiticity of the Hamiltonian, which is required for a sensible interpretation of quantum mechanics, forces the S-matrix to be unitary (via probability conservation). Then its eigenvalues (which are just the diagonal matrix entries) must have a magnitude of unity, so equation (2.21) is a valid parameterisation. We shall see later, in chapter 4, how to generalise these notions to two-channel scattering with a mass gap, in which case we shall deal with a conceptually simple 2×2 S-matrix.

2.3.2 The regular and Jost solutions

The free solution to the radial Schrödinger equation (2.13) is

$$u_l(kr) = kr\psi_l(kr) = (\frac{\pi kr}{2})^{\frac{1}{2}}J_{l+\frac{1}{2}}(kr), \tag{2.22}$$

where J is now the ordinary, not spherical, Bessel function. The general solution to the radial equation is a linear combination of spherical Bessel and von Neumann functions, but the spherical von Neumann function is singular at $r = 0$ and must be excluded if the origin is included to avoid unnormalisable wave functions. The asymptotic behaviour of (2.22) is

$$\lim_{r\to\infty}[u_l(kr) - \sin(kr - \frac{l\pi}{2})] = 0, \tag{2.23}$$

so that we regain the interpretation of the scatterer introducing phase shifts.

We define the *regular solution*, $\phi_l(k,r)$, by the boundary condition

$$\lim_{r\to 0}(2l+1)!!r^{-l-1}\phi_l(k,r)=1. \tag{2.24}$$

The existence of such a solution is guaranteed [17] if we consider regular potentials like (2.10). (Note that this boundary condition, unlike that of the 'physical' wave function $\psi_l(k,r)$, is k independent). Intuitively (2.24) means that the potential must be less singular than $\frac{1}{r}$ near the origin. It is known that the regular solution is the only one which vanishes at the origin [18] and since this is also required of the physical solution it must be a multiple of the regular solution.

We introduce the *Jost solution* to the radial Schrödinger equation as $f_l(k,r)$ with the boundary condition

$$\lim_{r\to\infty}(f_l(k,r)-e^{i\frac{l\pi}{2}}e^{ikr})=0 \tag{2.25}$$

and

$$\lim_{r\to\infty}(f_l'(k,r)-ike^{i\frac{l\pi}{2}}e^{ikr})=0, \tag{2.26}$$

where the prime denotes differentiation with respect to the spatial coordinate. The Wronskian of two functions is defined by

$$W(a,b)\equiv ab'-ba'. \tag{2.27}$$

If a and b are solutions to the reduced radial Schrödinger equation then

$$\frac{d}{dr}W(a,b)=0. \tag{2.28}$$

The above then allows us to see that

$$W[f_l(k,r),f_l(-k,r)]=2ik(-1)^{l+1}, \tag{2.29}$$

which indicates linear independence[6] for $k\neq 0$. Since there are only two linearly independent solutions of a second order differential equation the regular solution must be expressible as a linear combination of the Jost solutions (at least for $k\neq 0$). Defining the Jost *function*

$$F_l(k)=(-k)^l W[f_l(k,r),\phi_l(k,r)] \tag{2.30}$$

we can write the regular solution as

$$\phi_l(k,r)=\frac{1}{2}ik^{-l-1}[F_l(k)f_l(-k,r)-(-1)^l F_l(-k)f_l(k,r)]. \tag{2.31}$$

We state a number of properties and results (see ref. [17]) that will be relevant in the context of the spectral method:

1. The phase shift is equal to minus the phase of the Jost function

[6] This is a result of a theorem that says that two functions are linearly independent where their Wronskian does not disappear, as long as they have continuous first derivatives on that interval.

2. $F_l(-k) = [F_l(k)]^*$ and $F_l(-k) = |F_l|e^{i\delta_l(k)} \qquad \forall k \in \mathbb{R}$

3. $\lim_{|k|\to\infty} F_l(k) = 1$

4. $F_l(k)$ is analytic in the upper complex k-plane and has zeros on the positive imaginary axis corresponding to bound states, $k = i\kappa$, so that $E = -\kappa^2$ in the non-relativistic case (and these are all the bound states)

5. These zeros are finite in number and simple (except for $l \geq 1$ and $F_l(0) = 0$, in which case the zero at the origin would be double, i.e. then there is a pole of second order at $r = 0$ and a true bound state at $E = 0$)

6. For real k the phase shifts are given by $\delta_l(k) = \frac{1}{2i}\ln S_l(k) = \frac{1}{2i}[\ln F_l(-k) - \ln F_l(k)]$ (this statement is equivalent to item 2 above)

7. The phase shifts are odd for real k.

2.3.3 Levinson's Theorem

An important result which we shall need in the calculation presented in section 2.4 is Levinson's theorem, first published in 1949 [19]. A proof for the s-wave ($l = 0$) is presented in appendix A. The statement of the theorem is that for potentials of type (2.10), that permit n bound states, we have

$$\delta(0) - \delta(\infty) = \begin{cases} n\pi & \text{if} \quad F_l(0) \neq 0 \\ \pi(n + \frac{1}{2}) & \text{if} \quad F_l(0) = 0. \end{cases} \tag{2.32}$$

The convention is to take $\delta(\infty) = 0$. This reflects the fact that we do not expect a particle with infinite energy to be perturbed by a regular potential, and is equivalent to requiring the S-matrix to go to unity for large momenta.

This rather elegant result is of wide utility. If one is calculating the phase shift numerically, it is immediately obvious in which regime(s) a bound state appears. On the other hand, in certain analytic calculations involving integrals, it is convenient to perform integration by parts, which Levinson's theorem greatly facilitates. We shall later consider the scattering of two particles off a potential, in which case the quantity of interest will be the sum of the phase shifts of the diagonalised S-matrix. Even then, if the theory has a mass gap, we expect that a phase shift of some integer multiple of π inside this mass gap at threshold, where the energy equals the mass of the lighter field, will indicate the presence of a bound state below the mass gap when the off-diagonal coupling is omitted. We shall numerically investigate this issue later, in section 5.3, where we shall see that it provides evidence for the analyticity of the Jost function.

2.3.4 Density of states

The density of states plays an important role in the example provided in the next section. Intuitively it measures the number of states available in a given energy interval. We are only interested in the difference between the free and interacting density of states. We motivate the form of this quantity

by putting the system in a 'box' (in one spatial dimension) and considering the antisymmetric channel for simplicity.

In the free case the solution for the small oscillation modes is $\phi_k(r) = \sin kr$. In the presence of a potential we expect the solution to approach this one asymptotically, but with a possible phase shift,

$$\lim_{r\to\infty} \phi_k(r) \sin^{-1}(kr + \delta(k)) = 1. \tag{2.33}$$

Since the phase shift is only defined modulo π, we require it to be a continuous function of k that disappears as $k \to \infty$.

We then place the system in a 'box' by enforcing the boundary conditions $\phi_k(0) = \phi_k(L) = 0$, for some large L. This yields a discrete spectrum of allowed values of k, which we can enumerate as

$$\begin{aligned} &\vdots \\ k_{n+1}L + \delta(k_{n+1}) &= (n+1)\pi \\ k_n L + \delta(k_n) &= n\pi \\ &\vdots \end{aligned} \tag{2.34}$$

Next, we subtract the lower line from the upper, and divide by $\pi(k_{n+1} - k_n)$. If we assume that this last term is sufficiently small we can approximate the difference in phase shifts by a derivative,

$$\frac{1}{\pi}\left(L + \frac{d\delta(k)}{dk}\right) = \frac{1}{k_{n+1} - k_n}. \tag{2.35}$$

We see that the right hand side is the inverse of the momentum spacing between the states, i.e. the density of states.

We would like to take the continuum limit $L \to \infty$. However, the density of states in the equation above diverges in this limit as the momentum spacing becomes infinitely small. This can remedied by considering the difference between the density of states of the interacting and free systems,

$$\Delta\rho(k) \equiv \rho(k) - \rho^{(0)}(k) = \frac{1}{\pi}\frac{d\delta(k)}{dk}. \tag{2.36}$$

This quantity is finite. In higher spatial dimensions there may be additional degeneracy factors and a sum over partial waves (in one spatial dimension the analogue of angular momentum numbers are the odd and even channels, corresponding to antisymmetric and symmetric wavefunctions, respectively). A more rigorous definition makes use of the Green's function $G_l(r, r', k)$ so that

$$\Delta\rho(k) \equiv \frac{2k}{\pi}\mathrm{Im}\int_0^\infty dr[G_l(r, r, k + i\epsilon) - G_l^{(0)}(r, r, k + i\epsilon)]. \tag{2.37}$$

Here the superscript refers to the free Green's function. There are a number of alternative representations which are not immediately relevant to us. The actual form of the Green's function is also not of any immediate consequence for the illustration of the example of one scalar field which is to follow: it is sufficient that it exists as a solution to the inhomogeneous differential equation corresponding to the relevant particle equation(s) of motion. The interested reader is directed to reference [20]. We shall, in a later section, study the Green's function for two channel scattering in more detail.

2.4 Motivational Example

Let us consider what is perhaps the simplest example possible to illustrate the concepts outlined above: a scalar field in $(1+1)$ dimensions[7]. A number of the expressions we shall use are purely formal, in the sense that they may require regularisation. Nonetheless, we shall demonstrate how the spectral method allows physically meaningful information to be extracted from such expressions.

2.4.1 Lagrangian density and energy differences

The Lagrangian density of a Klein-Gordon field coupled to a static (i.e. time independent) and symmetric background potential is

$$\mathcal{L} = \frac{1}{2}[(\partial_\mu \phi)^2 - m^2\phi^2 - V(r)\phi^2]. \tag{2.38}$$

After the fields are quantised we are left with an infinite set of harmonic oscillators. Specifically, each normal mode ϕ_i is associated with a pair of creation/annihilation operators that respectively increment/decrement the occupation number n_i of that mode. The energy of each mode is

$$E_i = \omega_i(n_i + \frac{1}{2}), \tag{2.39}$$

where ω_i is the energy of mode i.

We immediately see that the naive vacuum, where $n_i = 0 \quad \forall i$, still has the divergent energy

$$E = \frac{1}{2}\sum_i \omega_i. \tag{2.40}$$

Another serious problem is that this expression is not really a sum, since we may need to include the energy of the continuum of scattering states in the form of an integral. The rest of this section deals with the appropriate way of extracting useful physical information from this divergent quantity. This will involve introducing the machinery from scattering theory necessary to rewrite (2.40) in a numerically tractable form.

We begin with the observation that in QFT, in contrast to General Relativity, we are only interested in energy *differences*, so that we define the quantity of interest to be

$$\Delta E \equiv \frac{1}{2}\sum_i \omega_i - \frac{1}{2}\sum_i \omega_i^{(0)} + E_{CT}, \tag{2.41}$$

where E_{CT} is the counterterm contribution. This expression is then the difference in vacuum energy between the full and free (i.e. where $V(r) = 0$) theories. While we may naively attempt to apply normal-ordering to get rid of this infinite constant, this would overlook the fact that the first two terms in expression (2.41) refer to different vacua. We may normal order the first term with respect to the true vacuum of the full theory, thus getting rid of this zero-point energy, but the second term will then not be normal ordered with respect to the non-interacting vacuum, which is the relevant state.

We now apply the tools discussed in the previous section to rewrite (2.41) as a sum over a finite

[7] The example in this section closely follows the discussion in chapters 1 and 3 of [3].

number of bound states and an integral weighted by the difference between the density of states in the free and interacting cases. The result is

$$\Delta E = \sum_j^{b.s.} \frac{1}{2}\omega_j + \frac{1}{2\pi}\int_0^\infty dk\omega \frac{d\delta(k)}{dk} + E_{CT}, \tag{2.42}$$

where the ω_j are the bound state energies, $\omega_j = \sqrt{m^2 - \kappa_i^2}$. We immediately note that, since the phase shift $\delta(k)$ goes like $\frac{1}{k}$ as k tends to infinity, the second term is still divergent, and so is the counterterm contribution. However, if the renormalisation scheme is to be consistent their combination must be finite. We need to choose a suitable regularisation for the combination of the two. The logarithmic divergence corresponds to the usual divergence of a scalar field theory in $(1+1)$ dimensions. We use Levinson's Theorem (see section 2.3.3) to write the above as

$$\Delta E = \sum_j^{b.s.} \frac{1}{2}(\omega_j - m) + \frac{1}{2\pi}\int_0^\infty dk(\omega - m) \frac{d\delta(k)}{dk} + E_{CT}. \tag{2.43}$$

The integral is still divergent. However, recalling that the Born approximations to the phase shifts are exact at large k, we subtract the first Born approximation to the phase shift to obtain the finite expression

$$\Delta E = \sum_j^{b.s.} \frac{1}{2}(\omega_j - m) + \frac{1}{2\pi}\int_0^\infty dk(\omega - m) \frac{d}{dk}[\delta(k) - \delta^{(1)}(k)] + E_{CT} + E_{FD}. \tag{2.44}$$

We have added the Born subtraction back in the form of a Feynman diagram, E_{FD}. This is legitimate because terms of the Born series can be identified with Feynman diagrams, as we shall see in the next section.

Applying integration by parts to the second term in the previous equation yields

$$\begin{aligned}\frac{1}{2\pi}\int_0^\infty dk(\omega - m)\frac{d}{dk}[\delta(k) - \delta^{(1)}(k)] &= \frac{1}{2\pi}(\omega - m)[\delta(k) - \delta^{(1)}(k)]\,|_0^\infty - \frac{1}{2\pi}\int_0^\infty dk\frac{k}{\omega}[\delta(k) - \delta^{(1)}(k)] \\ &= -\frac{1}{2\pi}\int_0^\infty dk\frac{k}{\omega}[\delta(k) - \delta^{(1)}(k)].\end{aligned} \tag{2.45}$$

The first two terms in the first line fall away because the Born approximation is exact as $k \to \infty$, so that $\delta(\infty) = \delta^{(1)}(\infty)$, and there are no bound states in the Born approximation, so that $\delta^{(n)}(0) = 0$ for all n, from Levinson's theorem. It is also the case that $\omega = m$ if $k = 0$.

After putting this all together, equation (2.44) becomes

$$\Delta E = \frac{1}{2}\sum_j^{b.s.}(\omega_j - m) - \frac{1}{2\pi}\int_0^\infty dk\frac{k}{\omega}[\delta(k) - \delta^{(1)}(k)] + E_{CT} + E_{FD}. \tag{2.46}$$

This expression is numerically very tractable. Furthermore, standard techniques from perturbative QFT can be applied to the sum $E_{CT} + E_{FD}$. For a scalar theory in $(1+1)$ dimensions, only the local tadpole diagram occurs, and $E_{CT} + E_{FD} = 0$. This is the general procedure in the spectral method: Subtract as many Born-approximations to the phase shift as are necessary to regularise the integrals, then add back the subtracted piece(s) via Feynman diagrams, which can be renormalised by the usual method of adding counterterms to the Lagrangian. For instance, if we repeat the preceding analysis

for a single fermion field in $(1+1)$ dimensions we find that two Born subtractions are necessary to render the relevant integral finite. It is clear that the application of this procedure is only valid when the underlying theory is renormalisable, so that the sum $E_{CT} + E_{FD}$ is finite. The following section contains a proof that the terms of the Born series can be identified with Feynman diagrams.

2.4.2 The relationship between Feynman diagrams and terms of the Born series

The vacuum to vacuum transition amplitude for a field ϕ in d spatial dimensions coupled to the background field $V(x)$ is given by

$$\left\langle \Omega^+ | \Omega^- \right\rangle_V \propto (\det[\partial_\mu \partial^\mu + m^2 + V - i\epsilon])^{-\frac{1}{2}}, \tag{2.47}$$

where $|\Omega^+\rangle$ and $|\Omega^-\rangle$ refer to the vacuum states at $t = +\infty$ and $t = -\infty$ respectively. This means that we are considering a scenario where the interaction $V(x)$ is adiabatically 'switched on' at an early time $-\frac{T}{2}$, and 'switched off' at time $+\frac{T}{2}$.

The energy density operator is the vacuum expectation value of the component $\hat{T}_{00}$ of the energy momentum tensor, $\epsilon(x) \equiv \langle 0 | \hat{T}_{00} | 0 \rangle$. For a single field ϕ coupled to the background $V(x)$ we have[8]

$$\epsilon(x) = \frac{1}{2} \frac{\int [d\phi] \phi(x) \hat{T}_x \phi(x) e^{i \int d^d y \frac{1}{2} [\dot{\phi}^2 - (\boldsymbol{\partial}\phi)^2 - (m^2+V)\phi^2]}}{\int [d\phi] e^{i \int d^d y \frac{1}{2} [\dot{\phi}^2] - (\partial\phi)^2 - (m^2 - V)\phi^2}}, \tag{2.48}$$

where $\hat{T}_x$ is the position space operator defined by

$$\hat{T}_x \equiv \overleftarrow{\partial_0}\overrightarrow{\partial_0} + \overleftarrow{\boldsymbol{\partial}} \cdot \overrightarrow{\boldsymbol{\partial}} + m^2 + V(x). \tag{2.49}$$

We would like to compute the vacuum expectation value of $\hat{T}_{00}$, as it occurs above. We note that the expression is quadratic in the field ϕ, so we add an interaction that couples it linearly to a source, compute the logarithmic derivative with respect to that source, and then set the source equal to zero[9]. We then have

$$\epsilon(x) = \frac{i}{2} \mathrm{Tr}[-\partial_\mu \partial^\mu - (m^2 + V)]^{-1} \delta^d(\hat{x} - x)[-\partial_0^2 - \boldsymbol{\partial}^2 + (m^2 + V)] \tag{2.50}$$

$$= -i \mathrm{Tr}[[-\partial_\mu \partial^\mu - (m^2 + V)]^{-1} \delta^d(\hat{x} - x) \partial_0^2] + ..., \tag{2.51}$$

where the ellipsis in the last line refers to contributions that do not involve V, and the notation Tr includes space-time integration. We note that the free propagator is $S_0 = [-\partial_\mu \partial^\mu - m^2]^{-1}$, so $[-\partial_\mu \partial^\mu - (m^2 + V)]^{-1} = [1 - S_0 V]^{-1} S_0$. Since V is static, we can introduce the frequency states $|\omega\rangle$ that satisfy $\langle \omega | V | \omega' \rangle = V \delta(\omega - \omega')$. Then the ν^{th} order term in the Feynman series of the energy density is

$$\epsilon_{FD}^{(\nu)}(x) = i \int \frac{d\omega}{2\pi} \mathrm{Tr}'[\omega^2 (S_0(\omega) V)^\nu S_0(\omega) \delta^{d-1}(\mathbf{x} - \hat{\mathbf{x}})], \tag{2.52}$$

where $S_0(\omega) = (\omega^2 + \boldsymbol{\partial}^2 - m)^{-1}$ and Tr' refers to the trace over the remaining degrees of freedom. Since this expression gives the $O(V^\nu)$ contribution to the energy density, we are justified in associating it with the Feynman diagram (with ν external legs) contribution to the energy density (up to total

[8] The following is from chapters 3.3 and 3.5 of [3], which can be consulted for further details.
[9] See chapters 5 and 6 of [21] for a general overview of this method.

derivatives that will not contribute to the integrated density).

2.4.3 Renormalisation of the tadpole graph

As stated earlier, subtracting the first Born approximation to the phase shift from the integrand occurring in the expression for the VPE is equivalent to subtracting the tadpole graph. The tadpole diagram is linear in the potential, so to renormalise it we must add a counterterm linear in the potential to the Lagrangian, $\mathcal{L}_{ct} = c_1 V(r)$. The integral corresponding to the tadpole diagram is proportional to

$$\int_{-\infty}^{\infty} dr V(r) \int_0^{\infty} \frac{dk}{k^2 - m^2}, \tag{2.53}$$

so we see that c_1 must be chosen so that its dependence on the regulator cancels the infinite constant coming from the tadpole diagram as we follow the renormalisation prescription. However, this diagram is not typical, since the spatial and momenta integration factorise in the equation above. This property allows us to choose the so-called 'no-tadpole renormalisation scheme', in which the sum $E_{CT} + E_{FD}$ vanishes.

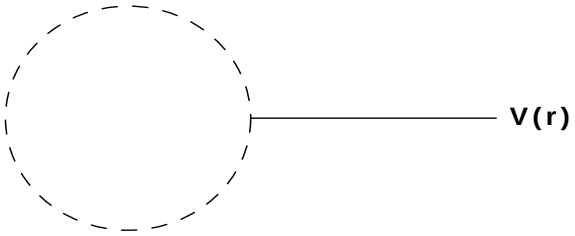

Figure 2.3: *The tadpole diagram, corresponding to one insertion of the background field*

2.4.4 Numerical Method

We have an expression, equation (2.46), that is amenable to numerical analysis. The question remains as to what the appropriate method is to calculate the phase shifts and their Born approximations. For this example we shall use a generalisation of the variable phase method (see [22]) of Calegero. For the antisymmetric channel (i.e. $\phi(0) = 0$) we make the ansatz for the scattering solution as

$$\phi_k(r) = \frac{1}{2i}(e^{ikr}e^{i\delta(k)}e^{i\beta_k(r)} - e^{-ikr}e^{-i\delta(k)}e^{-i\beta_k^*(r)}) \tag{2.54}$$

where the unknown function $\beta_k(r)$ satisfies the nonlinear differential equation

$$-i\beta_k''(r) + 2k\beta_k'(r) + [\beta_k'(r)]^2 + V(r) = 0. \tag{2.55}$$

The boundary conditions for this equation are $\lim_{r\to\infty} \beta_k'(r) = 0$ and $\lim_{r\to\infty} \beta_k(r) = 0$. Combined with the fact that the physical solution vanishes at the origin in the antisymmetric channel, we find that the phase shift can be extracted by

$$\delta(k) = -\mathrm{Re}[\beta_k(0)]. \tag{2.56}$$

Linearising and iterating equation (2.55) in powers of the potential yields differential equations (DEQs)

from which the Born approximations to the phase shifts can be computed. For instance, to first order in $V(r)$,

$$-i\beta_k^{\prime\prime(1)}(r) + 2k\beta_k^{\prime(1)}(r) + V(r) = 0, \tag{2.57}$$

from which we can, together with the appropriate boundary conditions, extract

$$\delta^{(1)}(k) = -\mathrm{Re}[\beta_k^{(1)}(0)]. \tag{2.58}$$

This expression allows us to numerically determine the VPE of this simple model to arbitrary precision, in the antisymmetric channel. To calculate the complete VPE it is necessary to sum over both channels, but for the purpose of illustration it is sufficient to consider only the antisymmetric channel.

We shall later see in section 4.4 how this approach can be modified to deal with the case of two fields that are scattering, where the quantity of interest is the sum of the phase shifts in the two channels.

3 Scattering solution for two interacting scalar fields

In this chapter we provide an example of how scattering methods can be applied to two coupled fields in the context of QFT. This serves both to introduce some useful conceptual tools from field theory, and to motivate the calculation of the VPE of two interacting scalar fields which occurs later.

Consider the Lagrangian density

$$\mathcal{L} = \mathcal{L}_1 + \mathcal{L}_2 + \mathcal{L}_{coupling}, \tag{3.1}$$

where

1. $\mathcal{L}_1 = \frac{1}{2}\partial_\mu\phi\partial^\mu\phi - \frac{\lambda}{4}(\phi^2 - \frac{m_1^2}{\lambda})^2$
2. $\mathcal{L}_2 = \frac{1}{2}\partial_\mu\psi\partial^\mu\psi - \frac{m_2^2}{2}\psi^2$
3. $\mathcal{L}_{coupling} = g\psi(\phi^2 - \frac{m_1^2}{\lambda})^2$,

which describes two fields with densities $\mathcal{L}_1$ and $\mathcal{L}_2$ interacting via $\mathcal{L}_{coupling}$. Here $m_2 > \sqrt{2}m_1$ and g is a coupling constant. The ϕ occurring in this equation should not be confused with the regular solution.

We shall consider a static (i.e. time independent) soliton solution of $\mathcal{L}_1$ that satisfies the classical equation of motion and expand around this, quantising the small oscillation field η which will be introduced shortly. This is equivalent to assuming that the fields commute, and calculating the $O(\hbar)$ corrections to the result obtained from this assumption. We shall then rewrite this as a matrix scattering equation.

3.1 Expansion around a static solution

We begin by considering fluctuations around a static solution of $\mathcal{L}_1$ which satisfies the Euler-Lagrange equation of motion in one spatial dimension,

$$\partial_r^2\phi = \lambda\phi(\phi^2 - \frac{m_1^2}{\lambda}). \tag{3.2}$$

We consider specifically the stationary *kink* solution

$$\phi_k = \frac{m_1}{\sqrt{\lambda}}\tanh(\frac{m_1}{\sqrt{2}}r), \tag{3.3}$$

which is a soliton [23] that reduces to the vacua $\pm\frac{m_1}{\sqrt{\lambda}}$ at positive/negative spatial infinity (we say that the solution interpolates between these two vacua). Defining the current

$$J^\mu = \frac{\sqrt{\lambda}}{m_1}\epsilon^{\mu\nu}\partial_\nu\phi_k \tag{3.4}$$

we see that we have a conserved (i.e. $\partial_\mu J^\mu = 0$) topological 'charge'

$$Q = \frac{1}{2}\int_{-\infty}^{\infty} dr J^0 = \frac{1}{2}\frac{m_1}{\sqrt{2}}\int_{-\infty}^{\infty} dr\,\mathrm{sech}^2(\frac{m_1}{\sqrt{2}}r) = 1 \tag{3.5}$$

for ϕ_k[10]. The conservation implies that this solution is topologically stable, in the sense that it cannot continuously decay to a solution with charge Q that differs from its initial value, as this would require infinite energy. We then look for solutions to small fluctuations around this field, i.e. solutions of $\mathcal{L}_1$ with

$$\phi = \phi_k + \eta. \tag{3.6}$$

After quantisation, these fluctuations η about the classical solution correspond to bosons with the mass of the lighter field ϕ.

To facilitate the use of results from scattering theory, we expand the complete Lagrangian to quadratic order in η,

$$\mathcal{L} = \frac{1}{2}\partial_\mu\eta\partial^\mu\eta + \frac{1}{2}\partial_\mu\psi\partial^\mu\psi - \frac{m_2^2}{2}\psi^2 - \frac{\lambda}{4}\eta^2(6\phi_k^2 - \frac{2m_1^2}{\lambda}) + 4g\phi_k(\phi_k^2 - \frac{m_1^2}{\lambda})\psi\eta \tag{3.7}$$

which yields the Euler-Lagrange equations for the fields ψ and η respectively as

$$\partial_\mu\partial^\mu\psi = -m_2^2\psi + 4g\phi_k(\phi_k^2 - \frac{m_1^2}{\lambda})\eta \tag{3.8}$$

and

$$\partial_\mu\partial^\mu\eta = 4g\phi_k(\phi_k^2 - \frac{m_1^2}{\lambda})\psi - \frac{\lambda}{2}(6\phi_k^2 - \frac{2m_1^2}{\lambda})\eta. \tag{3.9}$$

We can write this more succinctly as

$$\partial_\mu\partial^\mu\begin{pmatrix}\psi\\ \eta\end{pmatrix} = \begin{pmatrix}-m_2^2 & 4g\phi_k(\phi_k^2 - \frac{m_1^2}{\lambda})\\ 4g\phi_k(\phi_k^2 - \frac{m_1^2}{\lambda}) & -\frac{\lambda}{2}(6\phi_k^2 - \frac{2m_1^2}{\lambda})\end{pmatrix}\begin{pmatrix}\psi\\ \eta\end{pmatrix}. \tag{3.10}$$

We shall refer to this as the small oscillation equation.

The 2×2 matrix on the right hand side has the virtue of becoming a diagonal matrix as $r\to\infty$ because of the properties of the soliton solution ϕ_k. Specifically, it becomes the mass matrix

$$\begin{pmatrix}-m_2^2 & 0\\ 0 & -2m_1^2\end{pmatrix}. \tag{3.11}$$

We interpret this fact to mean that equation (3.10) describes asymptotically free scalar fields.

3.2 Regular solution in one channel

It is necessary at this point to return briefly to potential scattering theory in one spatial dimension. Specifically, for s-wave the boundary conditions for the regular solution become $\phi(k,0) = 0$ and $\phi'(k,0) = 1$. We can use this to convert the reduced radial Schrödinger equation into an integral

[10]Note that J^μ is conserved despite not being a Noether current.

equation (by the method of Green's functions) to obtain a Volterra integral of the second kind. We construct the Green's function explicitly as follows: The solution to the free equation (which is just the Helmholtz equation in one spatial dimension) satisfies[11]

$$(\partial_r^2 + k^2)\phi^{(0)}(k,r) = 0. \tag{3.12}$$

The solution is

$$\phi^{(0)}(k,r) = c_1 \cos(kr) + c_2 \sin(kr), \tag{3.13}$$

which the boundary conditions force to be

$$\phi^{(0)}(k,r) = \frac{\sin(kr)}{k}. \tag{3.14}$$

We note that if we ignore for the moment the fact that the delta function is actually a distribution, and hence only properly defined under an integral sign, the Green's function $G_k(r)$ satisfies, by definition,

$$(\partial_r^2 + k^2)G_k(r) = \delta(r), \tag{3.15}$$

and that this allows us to express $\phi(k,r)$ as

$$\phi(k,r) = \phi^{(0)}(k,r) + \int_0^r dr' G_k(r-r')V(r')\phi(r'), \tag{3.16}$$

since

$$\begin{aligned}(\partial_r^2 + k^2)\phi(k,r) &= \int_0^r dr' \delta(r-r')V(r')\phi(r') \\ &= V(r)\phi(k,r).\end{aligned} \tag{3.17}$$

Explicit computation verifies that the appropriate Green's function is

$$G_k(r-r') = \frac{\sin k(r-r')}{k}\theta(r'-r), \tag{3.18}$$

so that we are led to the regular solution,

$$\phi(k,r) = \frac{\sin(kr)}{k} + \int_0^r dr' \frac{\sin k(r-r')}{k} V(r')\phi(k,r'). \tag{3.19}$$

Substitution of this equation in (2.13) verifies that this is indeed the integral version of that equation (for $l = 0$).

If we define (for $n = 1, 2, \dots$)

$$\phi^{(n)}(k,r) \equiv \int_0^r dr' \frac{\sin k(r-r')}{k} V(r')\phi^{(n-1)}(k,r') \tag{3.20}$$

then the bounds [17]

[11] We use here reduced units, $\hbar = 1$ and $2m_1 = 1$.

$$\left|\frac{\sin kr'}{k}\right| \leq C\frac{r'}{1+|k|r'}e^{|\mathrm{Im}k|r'}, \tag{3.21}$$

for $r' > 0$ and complex k, and

$$\left|\frac{\sin k(r-r')}{k}\right| \leq C\frac{r}{1+|k|r}e^{|\mathrm{Im}k|(r-r')}, \tag{3.22}$$

for $r \geq r' \geq 0$, allow us to see that

$$\begin{aligned}|\phi^{(1)}(k,r)| &\leq \int_0^r dr' \left|\frac{\sin k(r-r')}{k}\right| |V(r')| \left|\frac{\sin kr'}{k}\right| \\ &\leq C\frac{r}{1+|k|r}\int_0^r dr'|V(r')|\frac{r'}{1+|k|r'}e^{|\mathrm{Im}k|(r-r')}e^{|\mathrm{Im}k|r'} \\ &= C\frac{r}{1+|k|r}e^{|\mathrm{Im}k|r}\int_0^r dr'|V(r')|\frac{r'}{1+|k|r'},\end{aligned} \tag{3.23}$$

where C is a numerical value independent of k or r. Iterating this calculation yields the general bound

$$|\phi^{(n)}(k,r)| \leq C\frac{r}{1+|k|r}e^{|\mathrm{Im}k|r}\frac{1}{n!}\left[C\int_0^r dr'\frac{r'}{1+|k|r'}|V(r')|\right]^n \tag{3.24}$$

for arbitrary complex k. This implies that the series

$$\phi(k,r) = \sum_{n=0}^{\infty}\phi^{(n)}(k,r) \tag{3.25}$$

is absolutely and uniformly convergent in any compact subset of the complex k-plane (and hence the unique solution to (3.19)) as long as the potential is regular. It is therefore important to keep in mind that the name regular *solution* is something of a misnomer for equation (3.19), as it is simply the radial Schrödinger equation, subject to specific boundary conditions, that we have rewritten as an integral equation. Its actual solution would depend on as many terms of equation (3.25) as are needed to achieve the desired level of precision.

A very similar argument, using the same inequalities as above and an additional step which can be found in reference [17], shows that the series expansion of the Jost solution is also absolutely and uniformly convergent, but only for $\mathrm{Im}k \geq 0$. The Jost solution also solves equation (3.12), but with the boundary conditions (2.25) and (2.26). This is accomplished by the integral equation

$$f(k,r) = e^{ikr} + \int_r^{\infty} dr'\frac{\sin k(r-r')}{k}V(r')f(k,r'). \tag{3.26}$$

The relevant series expansion is defined by

$$f^{(0)}(k,r) = e^{ikr} \tag{3.27}$$

and

$$f^{(n)}(k,r) = e^{ikr} + \int_r^{\infty} dr'\frac{\sin k(r-r')}{k}V(r')f^{(n-1)}(k,r'). \tag{3.28}$$

3.3 From the small oscillation equation to the regular solution in two channels

We shall now show how the small oscillation equation leads to a matrix equation that is analogous to the regular solution. For two fields it seems reasonable to expect equation (2.13) to become, in one spatial dimension and for the s-wave,

$$[\partial_r^2 + \begin{pmatrix} k_\phi^2 & 0 \\ 0 & k_\eta^2 \end{pmatrix}] \begin{pmatrix} \psi \\ \eta \end{pmatrix} = V(r) \begin{pmatrix} \psi \\ \eta \end{pmatrix}, \tag{3.29}$$

where $V(r)$ is a 2×2 matrix. This equation has a solution equivalent to the regular solution, but now in two channels (as can again be verified by substitution)

$$\begin{pmatrix} \psi \\ \eta \end{pmatrix} = \begin{pmatrix} \frac{\sin k_\phi r}{k_\phi} \\ \frac{\sin k_\eta r}{k_\eta} \end{pmatrix} + \int_0^r dr' \begin{pmatrix} \frac{\sin k_\phi (r-r')}{k_\phi} & 0 \\ 0 & \frac{\sin k_\eta (r-r')}{k_\eta} \end{pmatrix} V(r') \begin{pmatrix} \psi(r') \\ \eta(r') \end{pmatrix}. \tag{3.30}$$

Equation (3.29) can in fact be obtained from the small oscillation equation if we make the stationary ansatz,

$$\psi(r,t) = \psi(r) e^{-iEt} \tag{3.31}$$

and

$$\eta(r,t) = \eta(r) e^{-iEt}, \tag{3.32}$$

which is equivalent to energy conservation.

Substitution of this ansatz in the small oscillation equation (3.10) yields

$$[\partial_r^2 + \begin{pmatrix} -m_2^2 & 4g\phi_k(\phi_k^2 - \frac{m_1^2}{\lambda}) \\ 4g\phi_k(\phi_k^2 - \frac{m_1^2}{\lambda}) & -\frac{\lambda}{2}(6\phi_k^2 - \frac{2m_1^2}{\lambda}) \end{pmatrix}] \begin{pmatrix} \psi \\ \eta \end{pmatrix} = -E^2 \begin{pmatrix} \psi \\ \eta \end{pmatrix} \tag{3.33}$$

If we recall that energy is the same in both channels, but with different momenta, we have the dispersion relations

$$E^2 = k_\phi^2 + m_2^2 \tag{3.34}$$

and

$$E^2 = k_\eta^2 + 2m_1^2. \tag{3.35}$$

Substitution then yields

$$[\partial_r^2 + \begin{pmatrix} k_\phi^2 & 0 \\ 0 & k_\eta^2 \end{pmatrix}] \begin{pmatrix} \psi \\ \eta \end{pmatrix} = [\begin{pmatrix} -m_2^2 & 0 \\ 0 & -2m_1^2 \end{pmatrix} - \begin{pmatrix} -m_2^2 & 4g\phi_k(\phi_k^2 - \frac{m_1^2}{\lambda}) \\ 4g\phi_k(\phi_k^2 - \frac{m_1^2}{\lambda}) & -\frac{\lambda}{2}(6\phi_k^2 - \frac{2m_1^2}{\lambda}) \end{pmatrix}] \begin{pmatrix} \psi \\ \eta \end{pmatrix} \tag{3.36}$$

which is of the same form as (3.29), so that (3.30) is a solution, with the first factor on the right-hand side in the equation above playing the role of $V(r)$. The properties of the soliton solution ensure that this reduces to the equation describing non-interacting fields at spatial infinity.

To summarise, we have constructed a solution for small fluctuations around a static soliton configuration and established that it is analogous to a two channel version of the regular solution from scattering theory. The analytic properties of the regular solution do unfortunately not carry over simply to the two channel case. It is easy to see why: it follows from the dispersion relations that while, for instance, the ϕ channel may be analytic in the upper complex momentum plane, making the other field's momentum complex will produce a divergence because of the exponential increase in $\sin k(r - r')$. It is clear that if k_1 is taken real then k_2 will be purely imaginary inside the momentum gap, $0 < k_1 < \sqrt{m_2^2 - m_1^2}$, so this may appear to be a serious problem. Fortunately, there are ways around this (see chapter 17.1 of [17]).

Another important issue that is relevant with regard to the numerical results is the form of the equation which relates k_1 and k_2 via the energy momentum relation. Specifically, naively choosing $k_2 = \sqrt{k_1^2 - \Delta m^2}$, where $\Delta m \equiv \sqrt{m_2^2 - m_1^2}$, leads to an incorrect sign for the imaginary/real part of k_2 as k_1 takes values in the complex momentum plane. To get around this issue we choose to define $k_2 = k_1\sqrt{1 - \frac{\Delta m^2}{k_1^2}}$. We must use this form of the expression in the numerical program that solves the differential equations from which the phase shifts are extracted to avoid sign errors. More specifically, this ensures that

$$\mathrm{sgn}(k_1) = \mathrm{sgn}(k_2), \tag{3.37}$$

which is necessary if we want $\delta(k) = -\delta(-k)$, as demanded by the properties of the phase shifts outlined in chapter 2.

4 The model

In this chapter we define our model within the context of QFT, and confirm that it is self-consistent by performing the standard calculations associated with the canonical quantisation of a field theory. An expression for the vacuum polarisation energy is derived based on a Fock decomposition of two interacting scalar fields. We then make a connection with the spectral method by introducing a scattering ansatz that allows us to extract the scattering phase shifts (and the Born approximations thereof) from certain differential equations (DEQs) that can be solved by a computer. We also describe how the discrete binding energies enter into the calculation of the VPE, and how they can be obtained numerically.

A concrete example of this procedure is then provided and compared to the known analytic results for a specific uncoupled problem, with positive results.

4.1 Quantum Field Theory Formalism

4.1.1 Lagrangian density

Our model consists of two coupled (real) scalar fields, in $(1+1)$ dimensions, with a mass gap $(m_1 < m_2)$ interacting via a static, spherically symmetric background potential $V = V(r)$. We shall use $|\Omega\rangle$ to denote the vacuum of this full, interacting theory. The Lagrangian density corresponding to two scalar fields coupled by a potential with these properties is

$$\mathcal{L} = \frac{1}{2}(\partial_\mu \Phi^\dagger \partial^\mu \Phi - \Phi^\dagger M^2 \Phi - \Phi^\dagger V(r) \Phi), \tag{4.1}$$

where we have introduced the two-component field

$$\Phi(r,t) = \begin{pmatrix} \phi_1(r,t) \\ \phi_2(r,t) \end{pmatrix} \tag{4.2}$$

and the mass matrix

$$M = \begin{pmatrix} m_1 & 0 \\ 0 & m_2 \end{pmatrix} \tag{4.3}$$

for notational convenience. The radial potential that couples the two fields is likewise represented by a 2×2 matrix $V(r)$ that we leave unspecified for the moment, beyond requiring it to be Hermitian, $V^\dagger(r) = V(r)$.

An alternative viewpoint of our model is possible. If we consider the density of our system to be rather

$$\mathcal{L} = \frac{1}{2}\partial_\mu \Phi^\dagger \partial^\mu \Phi - \frac{1}{2}\Phi^\dagger M^2 \Phi - \sigma(\Phi), \tag{4.4}$$

and if $\phi_0(r)$ is a stationary point of the classical action, then equation (4.1) corresponds to the harmonic approximation

$$\mathcal{L} = \frac{1}{2}\partial_\mu \Phi^\dagger \partial^\mu \Phi - \frac{1}{2}\Phi^\dagger M^2 \Phi - \frac{1}{2}\Phi^\dagger \sigma''(\phi_0(r))\Phi + \cdots \tag{4.5}$$

if $V(r) \equiv \sigma''(\phi_0(r))$. This makes the origin of the one-loop, or $O(\hbar)$, truncation of the spectral method clear: The Φ fields describe small fluctuations about the solution ϕ_0.

This viewpoint is of course equivalent to the preceding one. Besides its numerical efficiency, the strength of the spectral method lies in the fact that there are no approximations made beyond the harmonic one, so that we have a 'non-perturbative' method up to $O(\hbar)$, in the sense that it includes all contributions from the potential, as in diagram 2.2. It is still perturbative in the sense that we ignore effects of $O(\hbar^2)$ and higher, so that truly non-perturbative effects cannot occur.

4.1.2 Quantisation

To quantise the system described by the Lagrangian density (4.1) above, we elevate the field $\Phi(r,t)$ to an operator

$$\hat{\Phi}(r,t) = \begin{pmatrix} \hat{\phi}_1(r,t) \\ \hat{\phi}_2(r,t) \end{pmatrix} \tag{4.6}$$

that acts on the Hilbert (or Fock) space of the quantum states of the system, and enforce the equal-time commutation relations between the field components and the components of the conjugate momenta in the Heisenberg picture:

$$[\hat{\phi}_a(r,t), \hat{\Pi}_b(r',t)] = i\delta(r-r')\delta_{ab} \tag{4.7}$$

and between the field components at equal time:

$$[\hat{\phi}_a(r,t), \hat{\phi}_b(r',t)] = 0. \tag{4.8}$$

It is understood that a and b label the field components, so that these equations correspond to the four entries in a 2×2 matrix as the Latin indices vary over their domain.

In the present case it follows from the definition of the conjugate momenta,

$$\hat{\Pi} \equiv \frac{\partial \mathcal{L}}{\partial(\partial_0 \Phi)}, \tag{4.9}$$

that

$$\hat{\Pi} = \partial_0 \hat{\Phi}^\dagger(r,t), \tag{4.10}$$

i.e. in our notation it is a two-component row vector. We shall see in the next section how these commutation relations for the fields and their conjugate momenta lead to the canonical commutation relations (CCR) for the annihilation and creation operators.

4.1.3 Equations of motion and canonical commutation relations

We start by assuming the stationary ansatz, so that

$$\hat{\Phi}(r,t) = \begin{pmatrix} \hat{\phi}_1(r,t) \\ \hat{\phi}_2(r,t) \end{pmatrix} = \hat{\Phi}(r)e^{-iEt}, \tag{4.11}$$

where

$$E = \sqrt{k_1^2 + m_1^2}\,. \tag{4.12}$$

As a result of this, the particles associated with these fields obey the following stationary wave equation, which should be familiar from the previous chapter:

$$(\partial_r^2 + K^2)\phi(E,r) = V(r)\phi(E,r). \tag{4.13}$$

It is understood that $\phi(E,r)$ is the two-component solution of this matrix differential equation, and K^2 is the 2×2 matrix in equation (3.29) with the squared momenta on the diagonal. In the general case the $\phi(E,r)$ occurring here can be treated as a 2×2 matrix. The two columns are solutions of the equation that only differ in their boundary conditions. We shall restrict ourselves for the moment to a specific boundary condition that will appear shortly. The alert reader will also notice that this equation is very similar in form to the reduced radial Schrödinger equation (2.13) for the s-wave, which, in view of the discussion in the preceding chapter, makes the applicability of scattering theory in this context obvious. The Lagrangian density is, however, more general than that occurring there. This stationary wave equation can be derived by applying the Euler-Lagrange equation,

$$\frac{\partial \mathcal{L}}{\partial \hat{\Phi}} - \partial^\mu \frac{\partial \mathcal{L}}{\partial(\partial^\mu \hat{\Phi})} = 0, \tag{4.14}$$

to the Lagrangian density (4.1) and using the stationary ansatz, as before. Following on from this, we can define annihilation and creation operators by

$$\hat{a}_\alpha(E) = i\sum_{a=1,2}\int dr \phi_{a,E}^{(\alpha)}(r)[\partial_0\hat{\phi}_a(r) - iE\hat{\phi}_a(r)]e^{iEt} \tag{4.15}$$

and

$$\hat{a}_\alpha^\dagger(E) = -i\sum_{a=1,2}\int dr \phi_{a,E}^{(\alpha)*}(r)[\partial_0\hat{\phi}_a(r) + iE\hat{\phi}_a(r)]e^{-iEt} \tag{4.16}$$

respectively. The subscript E in $\phi_{a,E}^{(\alpha)}(r)$ serves to remind us that this $\phi^{(\alpha)}(r)$ is the Jost solution of the stationary wave equation above at the energy E, with the subscript a labelling the component. The $\hat{\phi}_a(r)$ are the time independent field components.

We would like to determine all the possible commutation relations between these operators. To do so we must first fix our normalisation. We choose the so-called covariant normalisation for the fields, with the associated Fock decomposition as

$$\hat{\Phi}(r,t) = \sum_{\alpha=1,2}\int_0^\infty \frac{dk_1}{(2\pi)2E}[\begin{pmatrix} \phi_{1,E}^{(\alpha)}(r) \\ \phi_{2,E}^{(\alpha)}(r) \end{pmatrix} e^{-iEt}\hat{a}_\alpha(E) + \begin{pmatrix} \phi_{1,E}^{(\alpha)*}(r) \\ \phi_{2,E}^{(\alpha)*}(r) \end{pmatrix} e^{iEt}\hat{a}_\alpha^\dagger(E)]. \tag{4.17}$$

The Greek letter labels the two independent solutions[12].

Because of the profusion of super- and sub- scripts, it will be convenient in the calculations which will appear shortly to refer to the two column vectors occurring in the integrand above as $\phi_{\alpha,E}(r)$ and $\phi^*_{\alpha,E}(r)$. This means that $\phi^\dagger_{\alpha,E}(r)\phi_{\alpha,E}(r)$ is an inner product. It is hoped that this will not cause confusion.

We expect the fields to decouple and their solutions to reduce to plane waves at spatial infinity (that this is the case can be seen from the consideration of their Wronskian, as we shall see in the next section), so that the vectors have the asymptotic behaviour

$$\lim_{r\to\infty}\phi_{1,E}(r)e^{-ik_1 r} = \begin{pmatrix}1\\0\end{pmatrix} \quad \text{and} \quad \lim_{r\to\infty}\phi_{2,E}(r)e^{-ik_2 r} = \begin{pmatrix}0\\1\end{pmatrix}. \tag{4.18}$$

The reader will notice that this is the extension of the boundary condition for the Jost solution introduced in section 2.3.2 to two fields (and for the s-wave). We also see from the definition of the annihilation and creation operators above that they 'mix' the field components.

To calculate the CCR for the model, we straightforwardly substitute equation (4.17) in the expressions for the relevant operators, and use the equal-time commutation relations from the previous section. For example,

$$\begin{aligned}[\hat{a}_1(E),\hat{a}_1^\dagger(E')] &= e^{i(E-E')t}\sum_{a=1,2}\int dr\int dr'\left[\phi^{(1)}_{a,E}(\hat{\Pi}_a(r,t)-iE\hat{\phi}_a(r,t))\,,\,\phi^{(1)*}_{a,E'}(\hat{\Pi}_a(r',t)+iE'\hat{\phi}_a(r',t))\right]\\ &= e^{i(E-E')t}\sum_{a=1,2}\int dr\int dr'\phi^{(1)}_{a,E}(r)\phi^{(1)*}_{a,E'}(r')(E'+E)\delta(r-r')\\ &= e^{i(E-E')t}\sum_{a=1,2}\int dr\phi^{(1)}_{a,E}(r)\phi^{(1)*}_{a,E'}(r)(E'+E).\end{aligned} \tag{4.19}$$

It is clear that if the Jost solutions $\phi_{\alpha,E}(r)$ and $\phi^*_{\alpha,E}(r)$ are orthonormal,

$$\sum_{a=1,2}\int dr\phi^{(\alpha)}_{a,E}(r)\phi^{(\beta)*}_{a,E'}(r) = 2\pi\delta(k_1-k_1')\delta_{\alpha,\beta}, \tag{4.20}$$

then the commutator above is

$$[\hat{a}_1(E),\hat{a}_1^\dagger(E')] = (2\pi)2E\delta(k_1-k_1'). \tag{4.21}$$

The other cases proceed similarly, so we see that the choice of covariant normalisation, together with the orthonormality condition for the wave solutions, lead to the canonical commutation relations

$$[\hat{a}_\alpha(E),\hat{a}_\beta^\dagger(E')] = (2\pi)2E\delta(k_1-k_1')\delta_{\alpha,\beta}. \tag{4.22}$$

These serve to define the annihilation/creation algebra for our model. The interacting vacuum ket in the space of the combined system is then annihilated by all the annihilation operators acting on it

[12]The reader may be concerned about the absence of the bound states wavefunctions. However, as we shall see in the next section, the relevant Green's function can be constructed to have simple poles at the bound state energies. After rotation to the imaginary axis the contribution from the bound state wavefunctions disappears.

from the left,

$$\hat{a}_\alpha(E)\,|\Omega\rangle = 0 \quad \forall\alpha, \tag{4.23}$$

while the interacting vacuum bra in the dual space is annihilated by all creation operators acting on it from the right,

$$\langle\Omega|\,\hat{a}^\dagger_\alpha(E) = 0 \quad \forall\alpha. \tag{4.24}$$

These two equations serve to define the Fock space of the system.

4.1.4 Energy density operator

The calculation of the vacuum polarisation energy requires an expression for the energy density operator, which is the component $\hat{T}_{00}$ of the energy momentum tensor

$$\hat{T}_{\mu\nu} = \frac{\partial\mathcal{L}}{\partial(\partial^\mu\hat{\Phi})}\partial_\nu\hat{\Phi} - g_{\mu\nu}\mathcal{L}. \tag{4.25}$$

We see from this that the energy density operator is given by

$$\hat{T}_{00} = \frac{1}{2}[\partial_0\hat{\Phi}^\dagger\partial_0\hat{\Phi} + \partial_1\hat{\Phi}^\dagger\partial_1\hat{\Phi} + \hat{\Phi}^\dagger(M^2+V)\hat{\Phi}]. \tag{4.26}$$

We can construct an expression for the vacuum polarisation energy from the spatial integral over the energy density. The energy density is by definition the VEV of the energy density operator,

$$\epsilon(r) \equiv \langle\Omega|\,\hat{T}_{00}\,|\Omega\rangle\,. \tag{4.27}$$

To evaluate this expression we must first calculate $\hat{T}_{00}$ by inserting the Fock decomposition in (4.26). Starting with the time derivative,

$$\partial_0\hat{\Phi}(r,t) = \sum_{\alpha=1,2}\int_0^\infty \frac{dk_1}{(2\pi)2E}[-iE\begin{pmatrix}\phi^{(\alpha)}_{1,E}(r)\\ \phi^{(\alpha)}_{2,E}(r)\end{pmatrix}e^{-iEt}\hat{a}_\alpha(E) + iE\begin{pmatrix}\phi^{(\alpha)*}_{1,E}(r)\\ \phi^{(\alpha)*}_{2,E}(r)\end{pmatrix}e^{iEt}\hat{a}^\dagger_\alpha(E)], \tag{4.28}$$

so

$$\begin{aligned}\langle\Omega|\,\partial_0\hat{\Phi}^\dagger\partial_0\hat{\Phi}\,|\Omega\rangle &= \frac{1}{4\pi^2}\sum_{\alpha,\beta}\int_0^\infty dk_1\int_0^\infty dk_1'[\frac{EE'}{4EE'}(\phi^{(\alpha)}_{1,E}\phi^{(\beta)*}_{1,E'} + \phi^{(\alpha)}_{2,E}\phi^{(\beta)*}_{2,E'})]\\ &\qquad\times e^{-it(E-E')}\,\langle\Omega|\,\hat{a}_\alpha(E)\hat{a}^\dagger_\beta(E')\,|\Omega\rangle\\ &= \frac{1}{4\pi}\sum_{\alpha,\beta}\int_0^\infty dk_1\int_0^\infty dk_1'[E(\phi^{(\alpha)}_{1,E}\phi^{(\beta)*}_{1,E'} + \phi^{(\alpha)}_{2,E}\phi^{(\beta)*}_{2,E'})]\\ &\qquad\times e^{-it(E-E')}\delta(k_1-k_1')\delta_{\alpha,\beta}\\ &= \frac{1}{4\pi}\sum_{\alpha=1,2}\int_0^\infty dk_1 E\phi^\dagger_{\alpha,E}(r)\phi_{\alpha,E}(r).\end{aligned} \tag{4.29}$$

Note that we have used the following 'trick' that follows from the commutation relations,

$$\begin{aligned}\langle\Omega|\,\hat{a}_\alpha(E)\hat{a}^\dagger_\beta(E')\,|\Omega\rangle &= \langle\Omega|\,[\hat{a}_\alpha(E),\hat{a}^\dagger_\beta(E')]\,|\Omega\rangle - \langle\Omega|\,\hat{a}^\dagger_\beta(E)\hat{a}_\alpha(E')\,|\Omega\rangle \\ &= [\hat{a}_\alpha(E),\hat{a}^\dagger_\beta(E')]\,\langle\Omega|\Omega\rangle \\ &= (2\pi)2E\delta(k_1-k_1')\delta_{\alpha,\beta} \end{aligned} \tag{4.30}$$

since we are free to choose an orthonormal basis so that $\langle\Omega|\Omega\rangle = \mathbb{I}$.

Similarly[13],

$$\partial_1\hat{\Phi}(r,t) = \sum_{\alpha=1,2}\int_0^\infty \frac{dk_1}{(2\pi)2E}[\begin{pmatrix}\phi'^{(\alpha)}_{1,E}(r)\\ \phi'^{(\alpha)}_{2,E}(r)\end{pmatrix}e^{-iEt}\hat{a}_\alpha(E) + \begin{pmatrix}\phi'^{(\alpha)*}_{1,E}(r)\\ \phi'^{(\alpha)*}_{2,E}(r)\end{pmatrix}e^{iEt}\hat{a}^\dagger_\alpha(E)], \tag{4.31}$$

so

$$\begin{aligned}\langle\Omega|\,\partial_1\hat{\Phi}^\dagger\partial_1\hat{\Phi}\,|\Omega\rangle &= \frac{1}{4\pi^2}\sum_{\alpha,\beta}\int_0^\infty dk_1\int_0^\infty [\frac{dk_1'}{4EE'}(\phi'^{(\alpha)}_{1,E}\phi'^{(\beta)*}_{1,E'} + \phi'^{(\alpha)}_{2,E}\phi'^{(\beta)*}_{2,E'})e^{-it(E-E')}]\,\langle\Omega|\,\hat{a}_\alpha(E)\hat{a}^\dagger_\beta(E')\,|\Omega\rangle \\ &= \frac{1}{4\pi}\sum_{\alpha=1,2}\int_0^\infty \frac{dk_1}{E}\phi'^\dagger_{\alpha,E}(r)\phi'_{\alpha,E}(r). \end{aligned} \tag{4.32}$$

Before evaluating the last term of $\langle\Omega|\,\hat{T}_{00}\,|\Omega\rangle$ we note that

$$\begin{aligned}\phi'^\dagger_{\alpha,E}(r)\phi'_{\alpha,E}(r) &= \frac{1}{2}\partial_r(\phi^\dagger_{\alpha,E}(r)\phi_{\alpha,E}(r)') - \frac{1}{2}\phi^\dagger_{\alpha,E}(r)\phi''_{\alpha,E}(r) + \frac{1}{2}\partial_r(\phi'^\dagger_{\alpha,E}(r)\phi_{\alpha,E}(r)) - \frac{1}{2}\phi''^\dagger_{\alpha,E}(r)\phi_{\alpha,E}(r) \\ &= \frac{1}{2}\partial_r(\partial_r(\phi^\dagger_{\alpha,E}(r)\phi_{\alpha,E})(r)) - \phi^\dagger_{\alpha,E}(r)(V(r)-K^2)\phi_{\alpha,E}(r), \end{aligned} \tag{4.33}$$

where we have substituted the stationary wave equation (4.13). The hermiticity of $V(r)$ and the symmetry of K^2 ensure that the equation above holds if we take the conjugate transpose of $\phi_{\alpha,k_1}(r)$. By a similar method

$$\begin{aligned}\langle\Omega|\,\hat{\Phi}^\dagger(M^2+V)\hat{\Phi}\,|\Omega\rangle &= \frac{1}{4\pi^2}\sum_{\alpha,\beta}\int_0^\infty dk_1\int_0^\infty dk_1'\frac{1}{4EE'}\phi^\dagger_{\alpha,E}(r)(M^2+V)\phi_{\beta,E'}(r)e^{-it(E-E')} \\ &\qquad\qquad \times\langle\Omega|\,\hat{a}_\alpha(E)\hat{a}^\dagger_\beta(E')\,|\Omega\rangle \\ &= \frac{1}{4\pi}\sum_{\alpha=1,2}\int_0^\infty\frac{dk_1}{E}\phi^\dagger_{\alpha,E}(r)(M^2+V)\phi_{\alpha,E}(r). \end{aligned} \tag{4.34}$$

Combining this with equations (4.32), (4.33) and (4.34) we have the expression for the energy density as

$$\epsilon(r) = \frac{1}{4\pi}\sum_{\alpha=1,2}\int_0^\infty dk_1 E(1+\frac{\partial_r^2}{4E^2})\phi^\dagger_{\alpha,E}(r)\phi_{\alpha,E}(r) + \text{bound state piece}. \tag{4.35}$$

[13]Primed dependent variables in the following equations denote ordinary differentiation with respect to the spatial coordinate.

4.2 Extension of scattering theory to two coupled fields

We now introduce the Green's function by

$$G(r,r',k_1) = -\frac{2}{\pi}\sum_{\alpha=1,2}\int_0^\infty dq \frac{\phi_{\alpha,q}(r)\otimes\phi^\dagger_{\alpha,q}(r')}{(k_1+i\epsilon)^2-q^2} + \text{bound state piece.} \tag{4.36}$$

The $i\epsilon$ prescription leads to this Green's function being meromorphic in the upper complex k_1-plane, with poles at the bound state energies on the imaginary axis. Recalling the notation introduced previously, the factor like $\phi\otimes\phi^\dagger$ is a tensor product, so the Green's function is matrix-valued (it is in fact a 2×2 matrix).

This matrix Green's function must satisfy, by definition, the following equation of the interacting fields,

$$[\partial_r^2 + K^2 - V(r)]G(r,r',k_1) = \mathbb{I}_2\delta(r-r'). \tag{4.37}$$

We need to generalise the notions of the Jost and regular solutions discussed in section 2.3 to matrices. To do so, we recognise that the appropriate extension of the definition of the Wronskian to matrices is

$$\begin{aligned} W(A,B) &\equiv A^TB' - A'^TB \\ &= \begin{vmatrix} A^T & A'^T \\ B & B' \end{vmatrix}. \end{aligned} \tag{4.38}$$

The introduction of the transpose is necessary to ensure that the Wronskian of two *different* matrix solutions of the particle equation of motion be constant [17]. This in turn ensures that these two solutions are linearly independent. If we take A to be one of these matrix solutions, we have $W(A,A) = A^TA' - A'^TA$, which we may suspect is some non-zero quantity. However,

$$\begin{aligned} W'(A,A) &= A^TA'' - A''^TA \\ &= A^TCA - A^TCA \\ &= 0, \end{aligned} \tag{4.39}$$

where $C = -V(r) + K^2$. So even if $W(A,A)\neq 0$, it will still be independent of r. If this solution A is the Jost solution, then we know that it becomes diagonal in the limit as $r\to\infty$, and this implies that the constant must be 0, so that $W(A,A) = 0$, as is required for a sensible notion of a Wronskian.

We can then define the 2×2 Jost function by

$$F(E) \equiv W(f(E),\phi(E)), \tag{4.40}$$

where the Jost solution $f(E)$ and the regular solution $\phi(E)$[14] satisfy respectively the boundary conditions

$$\lim_{r\to\infty} e^{-iKr}f(E,r) = \mathbb{I}_2 \tag{4.41}$$

[14]This $\phi(E)$ does not correspond to the $\phi_{\alpha,E}(r)$'s in the Fock decomposition, but the notation in this section has been chosen to maintain consistency with reference [17], the notation of which it is notoriously tedious to keep track of.

and

$$\lim_{r\to 0}\phi(E,r)=0. \tag{4.42}$$

This regular solution can then also be written as

$$\phi(E,r)=\frac{1}{2i}[f(E)K^{-1}F(-E)-f(-E)K^{-1}F(E)], \tag{4.43}$$

where K is the matrix with the momenta on the diagonal. The S-matrix can then be constructed as

$$S(E)=F(-E)F^{-1}(E). \tag{4.44}$$

4.3 Energy density

If we define the local spectral density for real k_1 as

$$\rho(k_1,r)\equiv\frac{k_1}{i}\mathrm{tr}G(r,r,k_1) \tag{4.45}$$

we see that this is related to the Green's function by

$$\mathrm{Re}[\rho(k_1,r)]=\sum_{\alpha=1,2}\phi^{\dagger}_{\alpha,E}(r)\phi_{\alpha,E}(r)=\mathrm{Im}[k_1\mathrm{tr}G(r,r,k_1)]. \tag{4.46}$$

We now make use of the following to rewrite the expression for the energy density: the imaginary part of the Green's function at $r=r'$ is an odd function of k_1, while the real part is even. Then $\mathrm{Re}[k_1G(r,r,k_1)]$ is odd, so that $\mathrm{Re}[f(k_1^2)k_1G(r,r,k_1)]$ is odd, while $\mathrm{Im}[f(k_1^2)k_1G(r,r,k_r)]$ is even (the function $f(k_1^2)$ here should not be confused with the Jost function). Then we can write, from equation (4.35),

$$\begin{aligned}\epsilon(r)&=\frac{1}{4\pi}\int_0^{\infty}dk_1E(1+\frac{\partial_r^2}{4E^2})\mathrm{Im}[k_1\mathrm{tr}G(r,r,k_1)]+\text{bound state piece}\\&=\frac{1}{2\pi}\int_{-\infty}^{\infty}\frac{dk_1}{i}E(1+\frac{\partial_r^2}{4E^2})(\mathrm{Re}[k_1\mathrm{tr}G(r,r,k_1)]+i\mathrm{Im}[k_1\mathrm{tr}G(r,r,k_1)])+\text{bound state piece}\\&=\frac{1}{2\pi i}\int_{-\infty}^{\infty}dk_1E(1+\frac{\partial_r^2}{4E^2})k_1\mathrm{tr}G(r,r,k_1)+\text{bound state piece.}\end{aligned} \tag{4.47}$$

It is convenient to calculate this as a contour integral in the upper complex k_1-plane. However, we first need to subtract a few Born terms from the integrand to ensure that the contribution from the semi-circle at infinity disappears. These must then be added back later as Feynman diagrams. We define the N times Born-subtracted spectral density as

$$\begin{aligned}[\rho(k_1,r)]_N&\equiv[\rho(k_1,r)-\rho^{(0)}(k_1,r)-\rho^{(1)}(k_1,r)-...-\rho^{(N)}(k_1,r)]\\&=\frac{k_1}{i}\mathrm{tr}[G(r,r,k_1)-G^{(0)}(r,r,k_1)-G^{(1)}(r,r,k_1)...-G^{(N)}(r,r,k_1)].\end{aligned} \tag{4.48}$$

The superscript labels the order of the term in the Born expansion. For our purposes (i.e. for two interacting scalar fields in (1+1) dimensions) we can restrict our attention to $[\rho(k_1,r)]_1$, (as this is the only subtraction that is required to render the integral finite), while deriving the general case here. The subtraction of the free spectral density $\rho^{(0)}(k_1,r)$ corresponds to the subtraction of the energy

of the trivial non-interacting vacuum, which has not appeared in our expressions up to this point. It should be clear that this is justified by the form of the Born-subtracted spectral density, and means that we are in fact calculating the *difference* in energy between the free and interacting vacua.

Choosing the contour of integration as in figure 4.1 and substituting the expression above, we have

$$\epsilon(r) = \frac{1}{2\pi}\oint_C dk_1 \sqrt{k_1^2 + m_1^2}\,(1 + \frac{\partial_r^2}{4(k_1^2 + m_1^2)})[\rho(k_1, r)]_N + \sum_{i=1}^{N} \epsilon_{FD}^{(i)}(r) + \epsilon_{CT}(r) + \text{bound state piece}, \tag{4.49}$$

where $\sum_{i=1}^{N} \epsilon_{FD}^{(i)}(r)$ and $\epsilon_{CT}(r)$ refer to the Feynman diagram and counterterm contributions respectively.

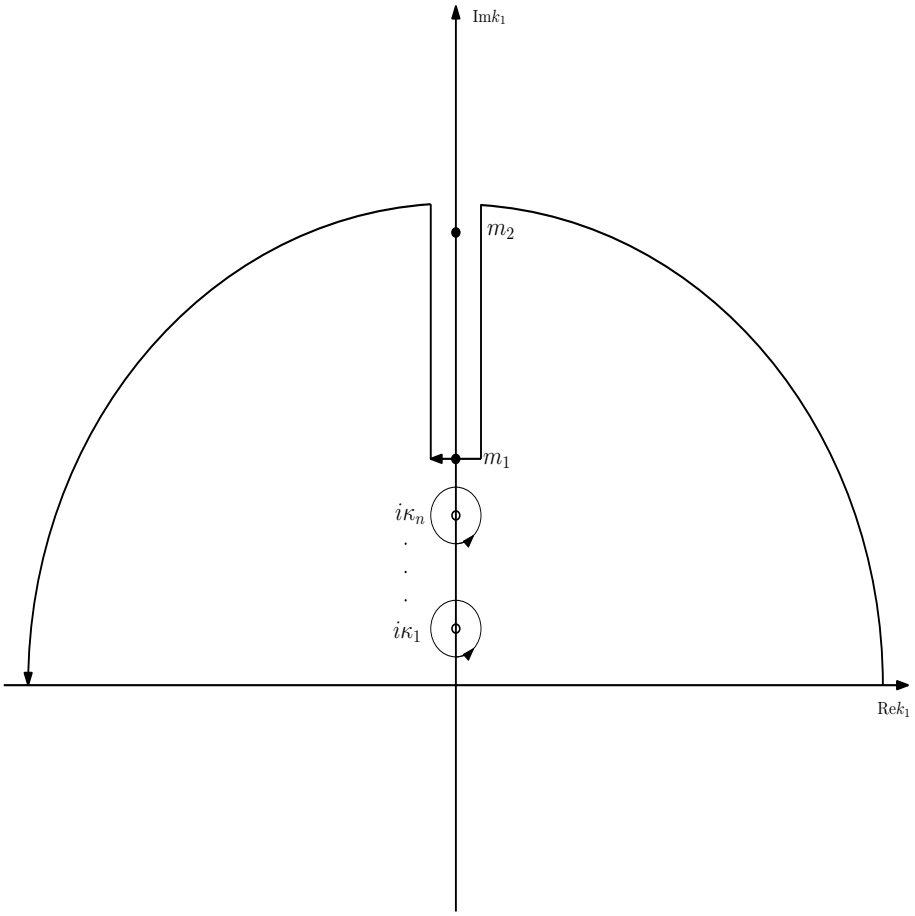

Figure 4.1: *The assumed contour of integration appearing in equation (4.49)*

By construction, the Green's function will lead to the contour integral above picking up contributions at the poles corresponding to these bound states (assuming the function has the indicated analytic structure). These exactly cancel the sum over the bound states, and since the Born subtractions eliminate the contribution from the semi-circle at infinity without introducing any poles themselves (because there are no bound states in the Born approximation), we are left with the discontinuity along the cut from $k_1 = im_1$ to $k_1 = i\infty$. The expression for the energy density in the

variable $k_1 = it$ is then

$$\begin{aligned}\epsilon(r) &= \frac{1}{2\pi}\int_{m_1}^{\infty} idt\sqrt{-(t^2-m_1^2)}\left(1+\frac{\partial_r^2}{4(-t^2+m_1^2)}\right)[\rho(t,r)]_N + \sum_{i=1}^{N}\epsilon_{FD}^{(i)}(r)+\epsilon_{CT}(r)\\ &= -\int_{m_1}^{\infty}\frac{dt}{2\pi}\sqrt{t^2-m_1^2}\left(1-\frac{\partial_r^2}{4(t^2-m_1^2)}\right)[\rho(t,r)]_N + \sum_{i=1}^{N}\epsilon_{FD}^{(i)}(r)+\epsilon_{CT}(r). \qquad (4.50)\end{aligned}$$

The minus sign in the final expression reflects the fact that we must choose the positive branch of the square root (i.e. $\sqrt{k_1^2+m_1^2}$ has become $+i\sqrt{t^2-m_1^2}$) as we can see from the above figure.

A crucial point has however been swept under the carpet, so to speak. We do not know a priori whether or not figure 4.1 correctly reflects the analytic structure of $\rho(t,r)$. The main issue that this thesis is supposed to address is whether the threshold at m_2 leads to the appearance of any additional singularities in $\rho(t,r)$. If it does, then expression (4.50) is invalid. Fortunately, as we shall see later by using Levinson's theorem to count the bound states, this does not appear to be the case (with some caveats).

To calculate the total energy we integrate over the energy density,

$$E[V(r)] = \int_0^{\infty} dr\epsilon(r). \qquad (4.51)$$

We see that the total energy is formulated as an integral over the radial coordinate. In one spatial dimension this implies invariance of the interaction with respect to reflection at the origin.

The integral over t is absolutely convergent, so the order of the t and r integration can be exchanged, and the total derivative term integrated to zero, to obtain

$$E[V(r)] = -\int_{m_1}^{\infty}\frac{dt}{2\pi}\sqrt{t^2-m_1^2}\int_0^{\infty} dr[\rho(t,r)]_N + \sum_{i=1}^{N}E_{FD}^{(i)}+E_{CT}. \qquad (4.52)$$

What remains is to find an efficient numerical method of calculating the quantity $[\rho(k_1,r)]_N$. But by strict analogy with the motivational example in section 2.4 we identify this as a Jost-like function (up to prefactors and, depending on the parameterisation, simple factors involving powers of the energy and momentum in the integrand). In the next section we turn to the question of how to construct this function; or at least how to extract phase shifts from the S-matrix, which is closely related to the Jost function, as we have seen. In practice the phase shifts and bound states are all that are required, because the density of states can be constructed from them. The identification of any specific function related to the scattering of the fields as central to the determination of the $O(\hbar)$ correction to the energy of two interacting scalar fields with a mass gap is then unnecessary, even though the formulation in terms of standard methods from scattering theory can give us confidence that the problem is physically well-defined and consistent. If we can construct DEQs related to our scattering ansatz, solve them on a computer and extract the phase shifts from their solution, then all that remains is to construct and solve the relevant integral related to the total energy. The caveat is that the Jost-like solution, whatever its form, must be analytic if we are to trust our results. If it is not, then the rotation of the integral onto the imaginary axis as in equation (4.49) is not defined, as the required analytic continuation does not exist. The determination of analyticity is therefore an important part of this thesis, as is the derivation of the necessary differential equations in the next

section.

4.4 Derivation of the differential equations required for the numerical calculation of the phase shifts in one spatial dimension

4.4.1 Two interacting scalar fields with equal masses

In analogy with the example in section 2.4.4, we now derive the differential equation required to extract phase shifts from the two-channel scattering problem for scalar fields with equal masses.

We start with the second-order relativistic wave equation

$$(\partial_r^2 + K^2)\phi(E,r) = V(r)\phi(E,r), \tag{4.53}$$

which we introduced in the previous section as the stationary wave equation for two scalar fields coupled by a radially symmetric potential $V(r)$. In the present case $m_1 = m_2$, so that K^2 is just the identity matrix multiplied by k^2. We could equally well write the k's in terms of the energy and the masses, since they are related by the relativistic energy-momentum relation

$$E^2 = m_1^2 + k_1^2 = m_2^2 + k_2^2, \tag{4.54}$$

but there is nothing to be gained by doing so in the present case. However, when $m_1 \neq m_2$ we shall do so, since momentum is no longer equal in the two channels, while energy is. We may therefore restrict ourselves to $E > 0$.

Equation (4.53) has the well-known solution (see [7]), which we call the scattering solution, that can be written as

$$\psi_{scatt}(E,r) = -\psi_a^*(E,r) + \psi_a(E,r)S(E), \tag{4.55}$$

where $S(E)$ is the appropriate 2×2 S-matrix and the subscript a stands for 'ansatz'. Since the scattering solution disappears at the origin in the antisymmetric channel, $\psi_{scatt}(E,0) = 0$, we can construct the S-matrix in that case by

$$S(E) = \lim_{r\to 0} \psi_a^{-1}(E,r)\psi_a^*(E,r). \tag{4.56}$$

Next, we make the ansatz that

$$\psi_a(E,r) = F(E,r)A(E,r), \tag{4.57}$$

where $A(E,r)$ contains the free plane wave solutions [15],

$$A(E,r) = \begin{pmatrix} e^{-ik_1 r} & 0 \\ 0 & e^{-ik_2 r} \end{pmatrix}. \tag{4.58}$$

[15] While the equality of the masses implies that $k_1 = k_2$, so that $A(E,r)$ is just a factor of $e^{ik_1 r}$, this form is relevant for the general case where $m_1 \neq m_2$. It is therefore convenient to already use this notation at this stage.

The S-matrix at fixed energy can then be obtained (in the antisymmetric channel) by

$$\begin{aligned} S(E) &= \lim_{r\to 0} \psi_a^{-1}(E,r)\psi_a^*(E,r) \\ &= \lim_{r\to 0} A^{-1}(E,r)F^{-1}(E,r)F^*(E,r)A^*(E,r) \\ &= \lim_{r\to 0} F^{-1}(E,r)F^*(E,r), \end{aligned} \tag{4.59}$$

since $\lim_{r\to 0} A(E,r) = \mathbb{I}_2$. The requirement that the S-matrix be unitary provides us with a convenient consistency check for the numerical output of our program, although the off-diagonal elements must first be multiplied by factors like $\sqrt{\frac{k_i}{k_j}}$ to normalise the S-matrix relative to the incoming flux.

Inserting the ansatz (4.57) in equation (4.53) yields

$$F'' - 2ikF' - VF = 0, \tag{4.60}$$

which is well-suited to numerical analysis, being both linear and ordinary (this is the case for all the DEQs we shall consider). It remains to choose appropriate boundary conditions. The choice is motivated by the physical requirement that the solutions reduce to plane waves at spatial infinity. This is equivalent to the conditions

$$\lim_{r\to\infty} F(r) = \mathbb{I}_2 \tag{4.61}$$

and

$$\lim_{r\to\infty} F'(r) = 0, \tag{4.62}$$

which should be compared with the Jost solution boundary conditions.

The solution of equation (4.60) subject to these boundary conditions allows us to construct the S-matrix in the antisymmetric channel via (4.59), from which we can then extract the sum of the eigenphase shifts as $\frac{1}{2i}\ln\det S$. The construction of the S-matrix is similar in the symmetric channel (except that $\psi'(E,0) = 0$) but this case has not been included, as we are actually interested in the case where the masses are not equal.

The case where $m_1 \neq m_2$ is similar, but the differential equation for F requires more attention. We also have two different matrix DEQs, one when the energy is in the mass gap and one when it is outside. We now turn to this case.

4.4.2 Two interacting scalar fields with unequal masses

The discussion is broadly similar to the previous section. All the equations (4.53) - (4.60) still hold, except for (4.58), which is no longer an acceptable ansatz for energy values inside the gap. We see from (4.54) that since $m_1 \neq m_2$, $A(E,r)$ is no longer proportional to the unit matrix, so that we need to pay specific attention to the commutativity of the terms. We also have two different cases, one where the energy is in the gap (i.e. $m_1 < E < m_2$) and another where it is outside (i.e. $m_1 < m_2 < E$). They require different differential equations if the associated wave-function is to be normalisable. In the latter case substitution of the derivatives of $A(E,r)$ followed by right multiplication by $A^{-1}(E,r)$

yields straightforwardly

$$F'' - 2iF' \begin{pmatrix} \sqrt{E^2 - m_1^2} & 0 \\ 0 & \sqrt{E^2 - m_2^2} \end{pmatrix} + [K^2, F] - VF = 0, \tag{4.63}$$

where the term $[K^2, F]$ is the commutator of the matrix

$$K^2 = \begin{pmatrix} E^2 - m_1^2 & 0 \\ 0 & E^2 - m_2^2 \end{pmatrix} \tag{4.64}$$

and F, which vanishes trivially if $m_1 = m_2$.

In the gap the lower matrix entry $\sqrt{E^2 - m_2^2}$ must become $\sqrt{m_2^2 - E^2}$. We can see this by noting that at spatial infinity, where we assume $V(r) \to 0$, the stationary wave equation is of the form

$$\phi''(E, r) = - \begin{pmatrix} E^2 - m_1^2 & 0 \\ 0 & E^2 - m_2^2 \end{pmatrix} \phi(E, r). \tag{4.65}$$

The upper channel is a simple harmonic oscillator, while the lower channel has solutions $e^{-\sqrt{m_2^2 - E^2}r}$ and $e^{\sqrt{m_2^2 - E^2}r}$. This suggests that the appropriate ansatz for $A(E, r)$ that leads to a normalisable wavefunction is

$$A(E, r) = \begin{pmatrix} e^{-i\sqrt{E^2 - m_1^2}r} & 0 \\ 0 & e^{-\sqrt{m_2^2 - E^2}r} \end{pmatrix} \tag{4.66}$$

which yields the DEQ for $m_1 < E < m_2$ as

$$F'' - 2F' \begin{pmatrix} i\sqrt{E^2 - m_1^2} & 0 \\ 0 & \sqrt{m_2^2 - E^2} \end{pmatrix} + [K^2, F] - VF = 0. \tag{4.67}$$

The boundary conditions for F are the same as for the case of equal masses, so that the rest of the analysis proceeds along lines analogous to the previous section. The phase shifts must however still be extracted from the DEQs. We turn to this in the next section.

4.4.3 Extracting phase shifts in the antisymmetric channel

We assume here that we have constructed the relevant S-matrix as per the discussion in the preceding section. After diagonalisation by some appropriate unitary matrix U we expect to find, above the gap, the phase shifts on its diagonal,

$$US(E)U^\dagger = \begin{pmatrix} e^{2i\delta_1(E)} & 0 \\ 0 & e^{2i\delta_2(E)} \end{pmatrix}. \tag{4.68}$$

It is then clear that we can extract the sum of the phase shifts at a certain energy in the antisymmetric

channel from the S-matrix as follows[16]:

$$\begin{aligned}\sum_j \delta_j(E) &= \frac{1}{2i}\ln\det(U(E)S_A(E)U(E)^\dagger)\\ &= \frac{1}{2i}\ln\det S_A(E)\\ &= \frac{1}{2i}\mathrm{tr}\left[\ln S_A(E)\right]\\ &= \frac{1}{2i}\mathrm{tr}\left[\ln\lim_{r\to 0}F^{-1}(E,r)F^*(E,r)\right].\end{aligned} \tag{4.69}$$

The subscript A refers to the antisymmetric channel, while the last step follows from equation (4.59). The factors like $\sqrt{\frac{k_i}{k_j}}$ by which A must be multiplied to normalise the S-matrix relative to the incoming flux cancel in $\det S$.

This can be easily incorporated in a numerical routine. However, the expression only gives the phase shift modulo π. To avoid this problem we construct a function that depends on r in such a manner that it reduces to the phase shift at $r = 0$, and then include the derivative of this function in the numerical routine that solves the differential equations for F. A convenient (and obvious) choice, which does not have the discontinuities of π, is

$$\sum_j \delta_j(E,r) = \frac{1}{2i}\mathrm{tr}\left[\ln F^{-1}(E,r)F^*(E,r)\right], \tag{4.70}$$

which we can see is real by considering $\delta^*(E,r)$. We then include

$$\frac{d}{dr}\sum_j \delta_j(E,r) = \frac{1}{2i}\mathrm{tr}\left[\frac{dF^*}{dr}(F^*)^{-1} - \frac{dF}{dr}F^{-1}\right] \tag{4.71}$$

in the numerical routine that solves the differential equations for F, with the boundary condition $\lim_{r\to\infty}\sum_{j=1,2}\delta_j(E,r) = 0$ (see reference [7]). This allows us to unambiguously extract the sum of the phase shifts from the numerical solution $\sum_j \delta_j(E,r)$. We recall that inside the mass gap we are only interested in the element S_{11} of the S-matrix, since the other channel is not scattering.

4.4.4 Extracting phase shifts in the symmetric channel

The argument for the symmetric channel is very similar to that for the antisymmetric channel, except that it is the derivative of the scattering solution which disappears at the origin, $\psi'_{scatt}(r) = 0$. The construction of the S-matrix is then slightly more involved. Specifically, following strictly the same procedure as before, we have

$$\begin{aligned}S_S(E) &= \lim_{r\to 0}\psi_a'^{-1}(E,r)\psi_a'^*(E,r)\\ &= \lim_{r\to 0}[F'(E,r)A(E,r) + F(E,r)A'(E,r)]^{-1}[F'(E,r)A(E,r) + F(E,r)A'(E,r)]^*\\ &= \lim_{r\to 0}[F'(E,r) + F(E,r)A'(E,r)]^{-1}[F'(E,r) + F(E,r)A'(E,r)]^*.\end{aligned} \tag{4.72}$$

[16]The value of the subscript j varies over the set $\{1\}$ or $\{1,2\}$, depending on whether we are respectively inside or outside the mass gap. In the former case only the lighter field is scattering.

In contrast to the antisymmetric channel, where the S-matrix is given by the same expression inside and outside the mass gap, we see that in the symmetric channel the presence of $A'(E,r)$ means that there will be two different expressions, as well as two different DEQs from which the phase shifts are to be extracted. The expression is

$$S_S(E) = \lim_{r\to 0} B(E,r)^{-1} B^*(E,r), \tag{4.73}$$

where in the gap

$$B(E,r) = F'(E,r) + F(E,r) \begin{pmatrix} -i\sqrt{E^2-m_1^2} & 0 \\ 0 & \sqrt{m_2^2-E^2} \end{pmatrix}, \tag{4.74}$$

while outside it

$$B(E,r) = F'(E,r) - iF(E,r) \begin{pmatrix} \sqrt{E^2-m_1^2} & 0 \\ 0 & \sqrt{E^2-m_2^2} \end{pmatrix}. \tag{4.75}$$

The phase shifts are then obtained as before, from

$$\sum_j \delta_j(E,r) = \frac{1}{2i}\mathrm{tr}\left[\ln \lim_{r\to 0} B(E,r)^{-1} B^*(E,r)\right], \tag{4.76}$$

with the appropriate $B(E,r)$.

The possibility of discontinuities of π exists, as in the odd channel. The independent differential equation which rectifies this is

$$\frac{d}{dr}\sum_j \delta_j(E,r) = \frac{1}{2i}\mathrm{tr}\left[\frac{dB^*}{dr}(B^*)^{-1} - \frac{dB}{dr}B^{-1}\right], \tag{4.77}$$

with the same boundary conditions as before for F and F'.

4.4.5 The Born approximation to the phase shifts

We have seen in the preceding sections how to extract phase shifts from differential equations related to the relativistic wave equations. However, in general analogy with the example of one scalar field outlined in section 2.4, the integrals associated with the VPE are still divergent, and can be regularised by subtracting Born approximations to the phase shifts from the integrand. This is because terms of the Born series coincide term-by-term with Feynman diagrams, as shown in section 2.4.2.

We introduce the Born series expansion of the matrix F as

$$F = \mathbb{I}_2 + F_1 + F_2 + \ldots, \tag{4.78}$$

where the subscript labels the order in the potential. The Born series' terms have the boundary condition

$$\lim_{r\to\infty} F_j = \lim_{r\to\infty} F_j' = 0 \quad \forall j. \tag{4.79}$$

The general method of calculating the Born approximation of order j to the phase shifts is to use the term of order $(j-1)$ as a source term in the relevant differential equation. For instance, to calculate F_1 for the case of two interacting scalar fields for $m_1 < E < m_2$, we use equation (4.67) to get

$$F_1'' - 2F_1' \begin{pmatrix} i\sqrt{E^2 - m_1^2} & 0 \\ 0 & \sqrt{m_2^2 - E^2} \end{pmatrix} + [K^2, F_1] - V = 0. \tag{4.80}$$

This is an expansion of the differential equation in powers of the potential, so the generalisation to higher orders should be clear.

It turns out that in the case of two scalar fields in $(1+1)$ dimensions we only need one Born subtraction to regularise the integrals. The Born approximation to the phase shift (in the antisymmetric channel) can be calculated as follows. We start by noting that $\ln(1+x) \approx x$ if x is small. Then

$$\begin{aligned} \ln S_A(E) &= \lim_{r\to 0} \ln[F^{-1}(r)F^*(r)] \\ &= \lim_{r\to 0} \ln[(\mathbb{I}_2 + F_1 + F_2 + \ldots)^{-1}(\mathbb{I}_2 + F_1 + F_2 + \ldots)^*] \\ &= \lim_{r\to 0} [-\ln(\mathbb{I}_2 + F_1 + F_2 + \ldots) + \ln(\mathbb{I}_2 + F_1 + F_2 + \ldots)^*] \\ &\approx \lim_{r\to 0} [-(F_1 + F_2 + \ldots) + (F_1^* + F_2^* + \ldots)]. \end{aligned} \tag{4.81}$$

So, for instance, the first Born approximation to $\ln S(E)$ in the antisymmetric channel is

$$\ln S_A^{(1)}(E) = \lim_{r\to 0} [F_1^*(E,r) - F_1(E,r)], \tag{4.82}$$

where F_1 can be obtained from the solution of equation (4.80) above, together with the appropriate boundary condition. In this case, the first Born approximation to the sum of the phase shifts is [17]

$$\begin{aligned} \sum_j \delta_j^{(1)}(E) &= \frac{1}{2i}\mathrm{tr}\left[\ln S_A^{(1)}(E)\right] \\ &= \frac{1}{2i}\mathrm{tr}\left[\lim_{r\to 0}[F_1^*(E,r) - F_1(E,r)]\right] \\ &= -\mathrm{tr}\left[\lim_{r\to 0} \mathrm{Im}[F_1(E,r)]\right]. \end{aligned} \tag{4.83}$$

This last expression is well-suited to numerical computation, as all it requires is the solution of equation (4.80). We recall that in the case of the odd channel the phase shifts inside and outside the gap are obtained from the same expression.

A similar calculation in the symmetric channel yields

$$\ln S_S^{(1)}(E) = -2i(\lim_{r\to 0} \mathrm{Im}[F_1'(E,r) \begin{pmatrix} -i\sqrt{E^2 - m_1^2} & 0 \\ 0 & \sqrt{m_2^2 - E^2} \end{pmatrix}^{-1} + F_1(E,r)]) \tag{4.84}$$

[17] See footnote 13 in section 4.4.3.

in the gap, and

$$\ln S_S^{(1)}(E) = -2i(\lim_{r\to 0} \mathrm{Im}[F_1'(E,r) \begin{pmatrix} -i\sqrt{E^2-m_1^2} & 0 \\ 0 & -i\sqrt{E^2-m_2^2} \end{pmatrix}^{-1} + F_1(E,r)]) \tag{4.85}$$

outside it. The generalisation to equation (4.83) should be clear, and has been omitted due to the cumbersome nature of the expression.

4.5 Numerical calculation of binding energies

The binding energies at which bound states occur are a crucial part of the calculation of the VPEs along the real momentum axis, so a rigorous way of determining them is vital. While shooting methods are popular, we shall take a different approach. We start by looking to solutions of the small oscillation equation in the free case,

$$(\partial_r^2 + K^2)\phi(r) = 0. \tag{4.86}$$

The reader will realise that in the odd/antisymmetric channel (where $\phi(0) = 0$) this is the pair

$$\phi_{n,1}^{(0)}(r) = \begin{pmatrix} \sqrt{\frac{2}{L}} \sin k_n r \\ 0 \end{pmatrix} \quad \text{and} \quad \phi_{n,2}^{(0)}(r) \begin{pmatrix} 0 \\ \sqrt{\frac{2}{L}} \sin \tilde{k}_n r \end{pmatrix}, \tag{4.87}$$

while in the even/symmetric channel (where $\phi'(0) = 0$) the sines are replaced by cosines, for a total of four linearly independent solutions. The prefactor $\sqrt{\frac{2}{L}}$ serves to normalise the solutions when the system is discretised by putting it in a 'box' of length L, so that the set of solutions is orthonormal. This discretisation also implies that the momentum/energy values are discretised, as in the familiar case of the infinite square well. This follows from the boundary condition that the wavefunction must disappear at the boundary, so that $\sin(kL) = 0$, implying that $k_n = \frac{n\pi}{L}$ (for $n = 1, \ldots, N$), or equivalently for the relativistic energy, $E_n^2 = \frac{n^2\pi^2}{L^2} + m_1^2$.

To find the binding energies, we then construct the interacting Hamiltonian via

$$H_{n,m}^{(I)} = \frac{2}{L}\int_0^L dr \left(\begin{array}{c|c} \phi_{n,1}^{\dagger(0)}(r)V(r)\phi_{m,1}^{(0)}(r) & \phi_{n,1}^{\dagger(0)}(r)V(r)\phi_{m,2}^{(0)}(r) \\ \hline \phi_{n,2}^{\dagger(0)}(r)V(r)\phi_{m,1}^{(0)}(r) & \phi_{n,2}^{\dagger(0)}(r)V(r)\phi_{m,2}^{(0)}(r) \end{array} \right), \tag{4.88}$$

where each block is an $N \times N$ submatrix. In the odd channel this is simply

$$H_{n,m}^{(I)} = \frac{2}{L}\int_0^L dr \left(\begin{array}{c|c} V_{11}(r)\sin(k_n r)\sin(k_m r) & V_{12}(r)\sin(k_n r)\sin(\tilde{k}_m r) \\ \hline V_{21}(r)\sin(\tilde{k}_n r)\sin(k_m r) & V_{22}(r)\sin(\tilde{k}_n r)\sin(\tilde{k}_m r) \end{array} \right), \tag{4.89}$$

while cosines are substituted for the sines in the even case. The discretisation procedure also differs in the even channel, in that the momentum values are restricted to half integer values of $\frac{\pi}{L}$.

In practice this can be computed numerically (see appendix B (section 6) for a concise overview of the integration method). The binding energies are found after calculating (again, numerically) the full Hamiltonian

$$H_{n,m} = (E_n)^2\delta_{n,m} + H_{n,m}^{(I)}. \tag{4.90}$$

Upon diagonalisation (see appendix B again for a concise overview of the diagonalisation method) the eigenvalues corresponding to the energies squared appear on the diagonal. These energies will in practice depend very specifically on both the numerical parameter L (the length of the 'box') and the integer $nmax$, that places an upper limit on the energy of the system or, equivalently, the subscripts n and m in the Hamiltonian. However, once these two parameters are chosen 'large enough', in a manner which depends on the specific details of the potential, the number of eigenvalues which are smaller than the square of the smaller mass m_1, and their values, should be stable. These are the squares of the binding energies. The other eigenvalues cannot be trusted, since they are scattering states that depend on the discretisation parameters, but this need not concern us, as they do not enter into the calculation of the VPEs in this manner.

The astute reader may guess that the integral in equation (4.89) has an analytic solution, and this is indeed the case for many typical potentials, as may be verified with a Computer Algebra System. However, given the relatively light computational overhead required to solve the integrals numerically, it is preferable to do so rather than e.g. writing a wrapper to a CAS. The analytic solutions themselves may involve special functions, which require time to be properly incorporated in a program. For example, choosing a Gaussian potential $\propto e^{-\mu x^2}$ yields an analytic solution containing the complex error function, which is not an intrinsic Fortran 90 function. Solving the integrals numerically therefore allows for more robustness in an approach that already requires a considerable investment time-wise if it is to be executed competently.

4.6 Example: Two uncoupled Pöschl-Teller potentials

To test the consistency and applicability of our method we checked our numerical results against the analytically known case of the $n = 2$ member of the Pöschl-Teller [24] family of potentials (this n is not related to the one in the previous section). Specifically, we checked whether the results for two uncoupled Pöschl-Teller potentials with different masses corresponded to the vacuum polarisation energy calculated by our numerical program. Fortunately, as we shall see, they did. While this does not tell us anything about the general coupled case, it does strongly suggest that the method developed in this chapter for setting up a scattering problem, extracting phase shifts and bound state energies, and numerically integrating the scattering data is valid. This is an important consistency check for the numerical program. The program has been coded so that the following analysis only required a different definition for the potential matrix $V(r)$, from a general 2×2 Hermitian matrix to a diagonal matrix (i.e. a change in two lines of code). The logical flow of the program is unaltered, as are all the other parameters; so agreement with the analytic result indicates a certain level of consistency in the implementation of the Runge-Kutta algorithm and the setup of the scattering problem. Analytic results are not known for the general coupled case; if they were this thesis would not be well-motivated.

The overview of the comparison is as follows: we start with the Lagrangian density for two uncoupled ϕ^4 kinks,

$$\mathcal{L} = \mathcal{L}_1 + \mathcal{L}_2 \tag{4.91}$$

where

$$\mathcal{L}_1 = \frac{1}{2}\partial_\mu\phi_1\partial^\mu\phi_1 - \frac{\lambda_1}{4}\left(\phi_1^2 - \frac{m_1^2}{2\lambda_1}\right)^2 \tag{4.92}$$

and

$$\mathcal{L}_2 = \frac{1}{2}\partial_\mu\phi_2\partial^\mu\phi_2 - \frac{\lambda_2}{4}\left(\phi_2^2 - \frac{m_2^2}{2\lambda_2}\right)^2. \tag{4.93}$$

These each have the non-perturbative and stationary kink solution (which should be familiar from chapter 3)

$$\phi_i(r) = \frac{m_i}{\sqrt{2\lambda_i}}\tanh\left(\frac{m_i r}{2}\right). \tag{4.94}$$

As before, we consider small fluctuations around these solutions and expand the resultant Lagrangian density to quadratic order in the small oscillation fields η_1 and η_2.

The result can be written as the following small oscillation equation for two uncoupled fields:

$$[\partial_r^2 - \partial_0^2 - \begin{pmatrix} m_1^2 & \\ & m_2^2 \end{pmatrix}]\begin{pmatrix} \eta_1 \\ \eta_2 \end{pmatrix} = \begin{pmatrix} -\frac{3m_1^2}{2}\mathrm{sech}^2(\frac{m_1 r}{2}) & 0 \\ 0 & -\frac{3m_2^2}{2}\mathrm{sech}^2(\frac{m_2 r}{2}) \end{pmatrix}\begin{pmatrix} \eta_1 \\ \eta_2 \end{pmatrix}. \tag{4.95}$$

To continue we note that the $n = 2$ Pöschl-Teller potential is given (in one spatial dimension) by

$$V_2(r) = -\frac{3m^2}{2}\mathrm{sech}^2(\frac{mr}{2}). \tag{4.96}$$

This is analytically solvable [24]. We therefore see that the small oscillation equation corresponding to small fluctuations around the two kink solutions corresponds to one of the few potentials with a known closed form solution. This will allow us to check the accuracy and applicability of the numerical method for extracting phase shifts developed in this chapter.

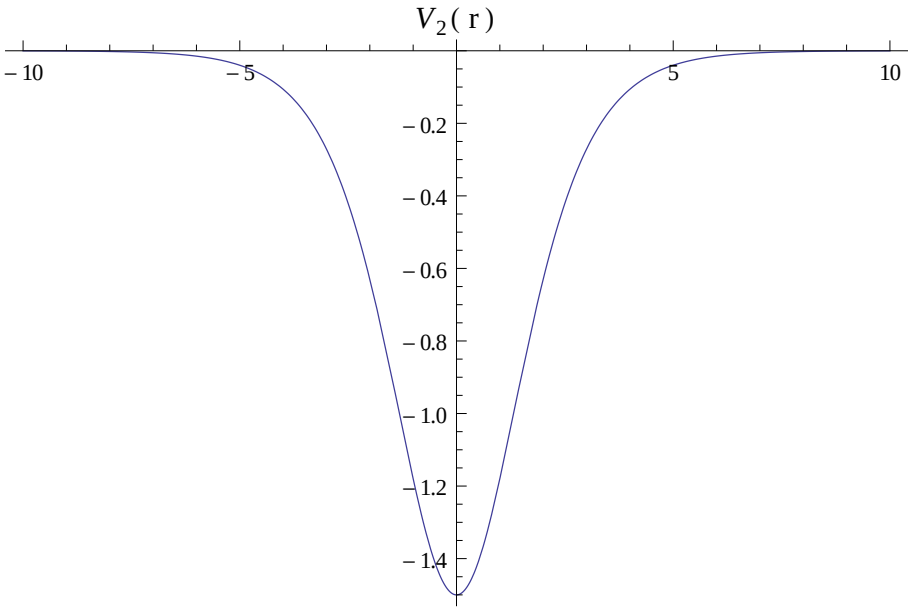

Figure 4.2: *Pöschl-Teller potential $V_2(r)$ with $m = 1$*

The phase shifts in the odd and even channels will be the same, because the potential is reflectionless. The analytic expression for the phase shifts of a field with mass m is [3]

$$\delta_S^{\text{kink}}(k) = \delta_A^{\text{kink}}(k) = \arctan\left(\frac{m}{k}\right) + \arctan\left(\frac{m}{2k}\right). \tag{4.97}$$

Considering the previous discussion, we attempt to determine the vacuum polarisation energy numerically, using the expression

$$\Delta E = \frac{1}{2}\sum_j(\omega_j - m) - \int_0^\infty \frac{dk}{2\pi}\frac{k}{\omega(k)}\left(\delta_A(k) + \delta_S(k) + \frac{< V >}{k}\right), \tag{4.98}$$

for each field of mass m, where the ω_j are the bound state energies, and the phase shifts and bound state energies are themselves to be determined numerically using the methods described in this thesis. The addition of $\frac{<V>}{k}$ corresponds to the first Born subtraction.

The numerical evaluation of this expression for each field should be compared with the analytic result for the total vacuum polarisation energy in the no-tadpole renormalisation scheme [25],

$$\Delta E = (m_1 + m_2)\left(\frac{1}{4\sqrt{3}} - \frac{3}{2\pi}\right). \tag{4.99}$$

We shall check the integral and bound state contributions separately, as they are computed using different methods.

The bound state momenta for this potential are given by $k_j = -\frac{j^2 m_i^2}{4}$, with $j = 1, 2$. This corresponds to relativistic bound state energies

$$E = \{\sqrt{\frac{3}{4}}\, m_i, 0\}. \tag{4.100}$$

The zero energy mode arises from translational invariance, which must be included in the sum in equation (4.98). The analytic expressions for the first Born approximation to the phase shifts are also known, and are given by

$$\begin{aligned}\delta_S^{(1)}(k) &= \frac{3m_i^2}{2k}\int_0^\infty dr \operatorname{sech}^2\left(\frac{m_i r}{2}\right)\cos^2(kr)\\ \delta_A^{(1)}(k) &= \frac{3m_i^2}{2k}\int_0^\infty dr \operatorname{sech}^2\left(\frac{m_i r}{2}\right)\sin^2(kr).\end{aligned} \tag{4.101}$$

The results (up to four decimal places) for a number of different masses follow in the form of tables of numerical data. All results are in natural units (i.e. the mass parameters are in the same units as the energies). For clarity, the relevance of the technical parameters are as follows:

1. m_1 and m_2 are the mass parameters of the theory.
2. ϵ is the numerical error tolerance parameter in the adaptive RK45 algorithm (see appendix B for details).
3. ntt is the numerical parameter that sets the number of momentum intervals inside the mass gap.
4. There is another variable (which is not indicated in the tables), $ntt2$, which determines the number of momentum intervals outside the mass gap. It is chosen so that the size of the momentum intervals outside and inside the gap are (more or less) equal.
5. $\tilde{k}_1$ is the upper limit of the momentum interval over which the integral term of the VPE occurring in equation (4.98) is numerically computed[18].

[18] See section (5.1.2) for an overview of how this can be used to estimate the value of the same integral over an

	$m_1 = 0.4,\ m_2 = 0.6$			$m_1 = 0.5,\ m_2 = 1$		
	$ntt = 101$	$ntt = 201$	$ntt = 1001$	$ntt = 101$	$ntt = 201$	$ntt = 1001$
		$\int dk = 0.2338$			$\int dk = 0.3502$	
$\epsilon = 10^{-6}$						
$\int dk$(num.)	0.2328	0.2334	0.2338	0.3480	0.3498	0.3507
$\epsilon = 10^{-8}$						
$\int dk$(num.)	0.2328	0.2334	0.2338	0.3480	0.3498	0.3507

Table 4.1: Integral contribution in equation (4.98): Comparison of numerical and analytic results for the VPE of two uncoupled $n = 2$ Pöschl-Teller potentials with differing masses ($\tilde{k}_1 = 10, rmax = 100$)

6. Similarly, nk specifies the number of momentum intervals in the module that computes the bound states energies.

7. $nttH$ specifies the number of spatial intervals used for the numerical integration over the 'box' which is used to discretise the system in momentum space, allowing numerical computation of the bound state energies.

8. BSE refer to the bound state energies in equation (4.98).

9. L is the size of the 'box' in which the system is placed to compute the bound state energies.

10. $\int dk$ is the value of the integral term in equation (4.98).

11. $rmax$ is the upper limit of the independent spatial variable r in the Runge-Kutta solver.

12. Finally, the parenthesis '(num.)' refers to the numerical results.

The analytic result is provided near the top of the table.

It is evident from the data in the first table that the numerical program produces very accurate results, even for fairly large error tolerances. Similarly, it is seen that the bound state energies are reproduced accurately, as long as $nttH$ is chosen large enough.

The agreement between the numerical and analytic results is encouraging, and indicates that the numerical program functions in a satisfactory manner in the uncoupled case[19]. We shall turn in the next chapter to the general coupled case.

4.7 Calculating the vacuum polarisation energies of two interacting scalar fields with a mass gap in $(1+1)$ dimensions

In this section we bring together the machinery described in the preceding sections to derive the expression which will allow us to calculate the vacuum polarisation energies of two scalar fields

unbounded interval.

[19]The slightly anomalous result for $m_1 = 0.5$, $m_2 = 1$, $nk = 401$ and $nttH = 101$ in the second table, and the result for the entry two rows further down in the same column, is an artifact that indicates that the spatial interval of numerical integration has not been chosen small enough. It vanishes if an appropriately small value of the spatial interval is used in the numerical integrator (i.e. for an appropriately small value of $\frac{L}{nttH}$).

	$m_1 = 0.4$, $m_2 = 0.6$		
	$nttH = 101$	$nttH = 201$	$nttH = 1001$
	$BSE = -0.5669$		
$nk = 201$			
BSE(num.)	-0.5524	-0.5626	-0.5669
$nk = 401$			
BSE(num.)	-0.5495	-0.5595	-0.5669
$nk = 801$			
BSE(num.)	-0.5484	-0.5579	-0.5668

Table 4.2: Bound state contribution in equation (4.98): Comparison of numerical and analytic results for the VPE of two uncoupled $n = 2$ Pöschl-Teller potentials($m_1 = 0.4$, $m_2 = 0.6$ and $L = 60$)

	$m_1 = 0.5$, $m_2 = 1$		
	$nttH = 101$	$nttH = 201$	$nttH = 1001$
	$BSE = -0.8504$		
$nk = 201$			
BSE(num.)	-0.8296	-0.8439	-0.8504
$nk = 401$			
BSE(num.)	-0.6995	-0.8394	-0.8504
$nk = 801$			
BSE(num.)	-0.6890	-0.8373	-0.8502

Table 4.3: Bound state contribution in equation (4.98): Comparison of numerical and analytic results for the VPE of two uncoupled $n = 2$ Pöschl-Teller potentials($m_1 = 0.5$, $m_2 = 1$ and $L = 60$)

of given masses interacting via a radially symmetric potential that is assumed to be regular as in equation (2.10)[20]. In strict analogy with the example in section 2.4 we write the energy difference between the free and interacting cases as a sum over a finite number of bound states and an integral weighted by a factor that is essentially the difference between the density of states in the free and interacting cases. The lower integration bound is now $E = m_1$, which corresponds to $k_1 = 0$ in the first channel. The relevant equation is then

$$\Delta E = \frac{1}{2}\sum_{j}^{b.s.}(\omega_j - m_1) + \frac{1}{2\pi i}\int_{m_1}^{\infty} dE(E - m_1)\frac{d}{dE}[\ln\det S(E)]_N + \sum_{i=1}^{N} E_{FD}^{(i)} + E_{CT}. \tag{4.102}$$

It is understood that the subscript N means that that factor is already Born subtracted (to order N), and the ω_j are the binding energies of section 4.5. The factor of $(E - m_1)$ in the integrand ensures that the integral exists: the Born approximation goes like $\frac{1}{k}$, so without this factor the integrand would diverge at small k_1 (or for E near m_1).

[20] We shall find an additional bound for the exponential potential, as we shall see in a later section.

Integration by parts on the second term yields

$$\begin{aligned}\frac{1}{2\pi i}\int_{m_1}^{\infty} dE(E-m_1)\frac{d}{dE}[\ln\det S(E)]_N &= \frac{1}{2i}(E-m_1)[\ln\det S(E)]_N|_{m_1}^{\infty} - \frac{1}{2i}\int_{m_1}^{\infty} dE[\ln\det S(E)]_N \\ &= \frac{1}{2\pi i}[(\infty-m_1)[\ln\det S(\infty)]_N] - \frac{1}{2\pi i}\int_{m_1}^{\infty} dE[\ln\det S(E)]_N \\ &= -\sum_{p=+1,-1}\int_{m_1}^{\infty}\frac{dE}{\pi}[\delta_p(E)-\delta_p^{(1)}(E)]. \qquad (4.103)\end{aligned}$$

Here the fact that the S-matrix goes to unity at large momenta was used in the last line. Note also that from equation (4.69) it follows that $\sum_j \delta_j(E) = 2i\ln\det S(E)$. The sum over p refers to the parity, i.e. $\delta(E)$ is already the sum of the phase shifts and the summation sign refers to the summation over the symmetric and antisymmetric channels.

Combining this with the previous equation, the quantity of interest is

$$\Delta E = \frac{1}{2}\sum_{j}^{b.s.}(\omega_j - m_1) - \sum_{p=+1,-1}\int_{m_1}^{\infty}\frac{dE}{\pi}[\delta_p(E)-\delta_p^{(1)}(E)] + \sum_{i=1}^{N} E_{FD}^{(i)} + E_{CT}. \qquad (4.104)$$

It should be clear at this point how the actual calculation of the VPE in $(1+1)$ dimensions is to proceed: For two masses, $m_1 \neq m_2$, and a potential that is Hermitian, radial and regular, we calculate the sum of the phase shifts and the Born approximations thereof numerically by solving equations (4.69), (4.83), and the relevant equations for the symmetric channel, on a computer. This then allows the integral in the expression above to be calculated numerically, and this quantity is then added to the sum over the bound states, which are also computed numerically as described in section 4.5.

5 Numerical Analysis

All the machinery required to calculate the VPE has been been assembled. In this chapter we bring all of this together to give the numerical results for a number of potentials with varying parameters, as well as general comments on the analyticity of the Jost function and some further comments on how the numerical data were computed. See the appendices for details of the relevant numerical methods.

5.1 Comments on the numerical aspect of the problem

Analyticity (in the sense of the satisfaction of the Cauchy-Riemann equations and the absence of singularities) of the generalised Jost function is essential for the success of the spectral method. This can be checked numerically by comparing the integrals associated with the VPE along the real and positive imaginary momentum axes. If the Jost function is analytic, then the integral must have the same value along both axes. If the function is *not* analytic, we must reconsider our assumptions and find the reason for the non-analyticity by reexamining the analytic structure with respect to poles and branch cuts. However, before we can make statements about the analyticity it is important that we deal appropriately with the various numerical issues that already occur along the real axis.

The starting point is the integral appearing in equation (4.104). Due to the (integrable) singularities appearing near threshold (i.e. at $E = m_1$), it is convenient to reparameterise it as a function of the momentum k_1. We do so, perform some integration 'tricks', and identify the sum of the phase shifts as the trace of the logarithm of the generalised Jost function. Doing so, we have

$$\begin{aligned} I &= -\sum_{p=+1,-1}\int_0^\infty \frac{dk_1}{\pi}\frac{k_1}{\sqrt{{k_1}^2+m_1^2}}[\delta_p(k_1)-\delta_p^{(1)}(k_1)] \\ &= -\frac{1}{2\pi i}\int_0^\infty dk_1\frac{k_1}{\sqrt{{k_1}^2+m_1^2}}\mathrm{tr}[\ln F(-k_1)-\ln F(k_1)]_1 \\ &= -\frac{1}{2\pi i}\int_{-\infty}^\infty dk_1\frac{k_1}{\sqrt{{k_1}^2+m_1^2}}\mathrm{tr}[\ln F(k_1)]_1 \\ &= -\frac{1}{2\pi i}\int_{-\infty}^\infty dk_1\sqrt{{k_1}^2+m_1^2}\,\frac{d}{dk_1}\mathrm{tr}[\ln F(k_1)]_1. \end{aligned} \tag{5.1}$$

It is understood that the subscript in $\mathrm{tr}[\ln F]_1$ implies that the first Born term has been subtracted from the expression.

We now have an integral along the whole real k_1 axis. We can relate this to the contour integral of the analytic continuation of the relevant function along the path illustrated in diagram 4.1 by the judicious use of Cauchy's theorem[21]. The poles corresponding to bound states on the imaginary axis

[21] See appendix A for a derivation of Levinson's theorem for s-wave which follows the same general procedure as this calculation.

cancel the contribution from the sum in (4.104). We are left with the following integral along the imaginary axis from the cut at $k_1 = im_1$ in the parameter $t = -ik_1$:

$$\begin{aligned}\Delta E &= -\int_{m_1}^{\infty} \frac{dt}{2\pi} \sqrt{t^2 - m_1^2}\, \frac{d}{dt} \mathrm{tr} \ln F(it) + \sum_{i=1}^{N} E_{FD}^{(i)} + E_{CT} \\ &= -\int_{m_1}^{\infty} \frac{dt}{2\pi} \frac{t}{\sqrt{t^2 - m_1^2}} \mathrm{tr} \ln F(it) + \sum_{i=1}^{N} E_{FD}^{(i)} + E_{CT}. \end{aligned} \tag{5.2}$$

This should be compared to equation (4.52), which was derived in the context of QFT without explicit reference to phase shifts or a Jost-like function. This leads to the identification

$$\frac{d}{dt} \mathrm{tr}[\ln F(it)]_N = \int_0^{\infty} dr [\rho(t, r)]_N, \tag{5.3}$$

which allows us to make contact between the numerical (LHS) and formal QFT (RHS) formalisms. Without this identification our approach would be ambiguous. It is clear that for our approach to be applicable the expression above for ΔE must be equal to (4.104) (or the equivalent expression in the k_1 parameterisation).

5.1.1 Singularities at small momenta

It is in practice convenient to calculate the relevant integrals in the k_1 parameterisation. This is because of the behaviour of the integrand near the threshold. This is clear if we consider the analytic expressions for the first Born approximation (which are known, in contrast to the exact phase shift). In $n = 1$ spatial dimension and one channel, for an arbitrary radial potential, they are given in the symmetric and antisymmetric channels respectively by [3]

$$\begin{aligned}\delta_S^{(1)}(k) &= -\frac{1}{k} \int_0^{\infty} dr V(r) \cos^2(kr) \\ \delta_A^{(1)}(k) &= -\frac{1}{k} \int_0^{\infty} dr V(r) \sin^2(kr). \end{aligned} \tag{5.4}$$

This gives us some insight into what to expect in the two channel case. Specifically, if we compute the integrand in the E parameterisation we expect to find two (integrable) singularities in the even channel, one at $E = m_1$, because of the $\frac{1}{k_1}$ behaviour there, and the other at $E = m_2$. However, in the k_1 parameterisation the factor of k_1 cancels the first singularity, and the other one is shifted to $k_1 = \Delta m = \sqrt{m_2^2 - m_1^2}$. The latter is an integrable square root singularity in the E parameterisation, but still requires special treatment numerically. We do so as follows: If we denote the integrand by $g(k_1)$, then the preceding comments on the behaviour for small momenta is equivalent to expecting

$$g(k_1)|_{k_1 \sim \Delta m} = \frac{C k_1}{\sqrt{k_1^2 - \Delta m^2}}, \tag{5.5}$$

where C is some appropriate numerical constant. Then we may perform the integration over k_1 near the mass gap by

$$\begin{aligned}\int_{\Delta m}^{\Delta m+\delta k_1} dk_1 g(k_1) &= \int_{\Delta m}^{\Delta m+\delta k_1} dk_1 \frac{Ck_1}{\sqrt{k_1^2-\Delta m^2}} \\ &\approx C\Delta m \int_0^{\delta k_1} dq \frac{1}{\sqrt{2q\Delta m}} \\ &= C\sqrt{2\Delta m \delta k_1}, \end{aligned} \tag{5.6}$$

where δk_1 is the size of the momentum interval in the numerical program. If this ansatz for the behaviour of $g(k_1)|_{k1\sim\Delta m}$ is correct, then we may extract C from the numerical data by

$$C = \lim_{k_1\to\Delta m} \frac{g(k_1)\sqrt{k_1^2-\Delta m^2}}{k_1}. \tag{5.7}$$

In practice, the numerical parameters need to be tweaked to make sure that the integral does not have a dependence on the upper momentum limit. If this is not an issue we can perform the numerical integration from $k_1 = \Delta m$ to $k_1 = \Delta m + \delta k_1$ using this method. This is implicitly the case for the rest of the discussion in this chapter. Note also that this issue does not occur at all in the odd channel.

5.1.2 Numerical integration over unbounded intervals

The integral which gives the expression for the VPE must be computed numerically over an unbounded interval. It is clearly not possible to calculate an infinite number of points on a computer. However, the following trick allows us to get around this limitation. Let us consider some integral

$$I = \int_a^\infty dk_1 g(k_1). \tag{5.8}$$

If it so happens that there exists a number $\tilde{k}_1$ such that $\forall k_1 \geq \tilde{k}_1$ the function $g(k_1) \approx \frac{D}{k_1^n}$, where D is an appropriate constant and n an integer, then

$$\begin{aligned} I &= \int_a^{\tilde{k}_1} dk_1 g(k_1) + \int_{\tilde{k}_1}^\infty dk_1 \frac{D}{k_1^n} \\ &= \int_a^{\tilde{k}_1} dk_1 g(k_1) + \frac{D}{(n-1)\tilde{k}_1^{n-1}} \\ &= \int_a^{\tilde{k}_1} dk_1 g(k_1) + \frac{\tilde{k}_1}{n-1} g(\tilde{k}_1). \end{aligned} \tag{5.9}$$

It is fortunately known [18] that our integrand is of $O(1/k_1^3)$ on the real axis, and of $O(1/k_1^2)$ on the imaginary axis, so we can make use of this method to integrate over the unbounded interval. We must however be sure to choose a large enough numerical upper bound on the integral. We can check this by varying the upper parameter $\tilde{k}_1$. It is implicitly the case for all the results that follow that this parameter was chosen suitably large.

5.1.3 Summary of the approach to performing the numerical integration

It is convenient to summarise the previous discussion regarding the numerical integration. The figure below breaks the integral on the real axis into a number of intervals. The dependent variable is the integrand $g(k_1) \equiv \frac{k_1}{E}\sum_{p=+1,-1}[\delta_p(k_1) - \delta_p^{(1)}(k_1)]$. Considering them one by one, with reference to figure 5.1:

(1) $\int_{\epsilon}^{\Delta m-\epsilon} dk_1 g(k_1)$; in this case we can compute and tabulate $g(k_1)$ numerically, and then integrate using the numerical method discussed in appendix B.

(2) $\int_{\Delta m-\epsilon}^{\Delta m} dk_1 g(k_1)$; if ϵ is taken small enough we can simply ignore this piece.

(3) $\int_{\Delta m}^{\Delta m+\delta k_1} dk_1 g(k_1)$; we make the ansatz as in section 5.1.1 and get the contribution $C\sqrt{2\Delta m \delta k_1}$.

(4) [22] $\int_{\Delta m+\delta k_1}^{k_1 max} dk_1 g(k_1)$; in this case we can compute and tabulate $g(k_1)$ numerically, and then integrate using the numerical method discussed in appendix B.

(5) $\int_{k_1 max}^{\infty} dk_1 g(k_1)$; the integration over the unbounded interval is performed as in equation (5.9).

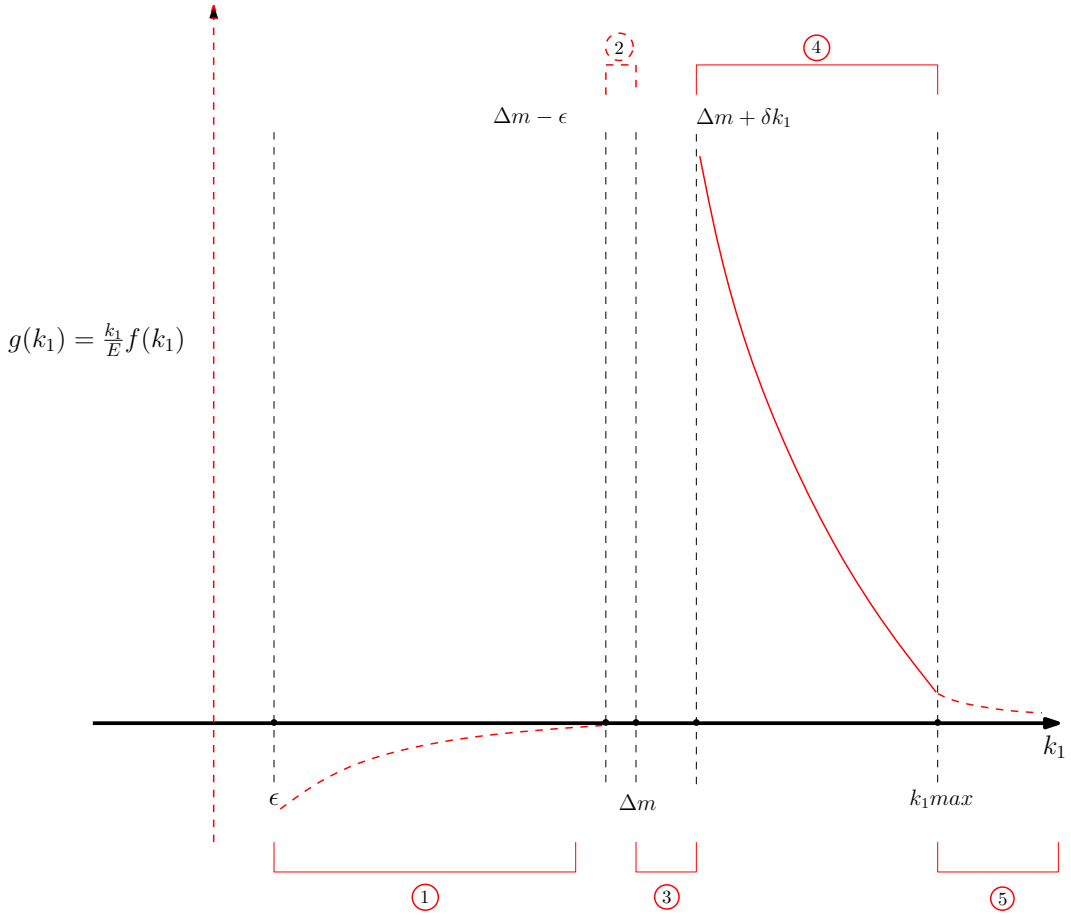

Figure 5.1: *The various integration intervals involved in the computation of ΔE on the real axis. The plot itself is just for illustration of the general behaviour of the integrand in the even channel.*

[22] Number four only occurs in the even channel, as has been discussed previously.

5.1.4 A note on the numerical instability of the exponential potential in (1+1) dimensions, and the continuity of the S-matrix

There are certain technical difficulties associated with investigating the exponential potential $\propto e^{-\mu r}$. Specifically, an imprudent choice of the parameter μ leads to a strong dependence of the solution of the DEQs on the maximum value of the independent variable r in the numerical integrator. This is evident from the equations in section 4.4 if we introduce the notation $V = (V_{ij})e^{-\mu r}$ for the potential matrix, where the subscripts label the entries of that matrix. The second derivative of the second field is then

$$\phi_2''(r) = (\Delta m^2 - k_1^2)\phi_2 + e^{-\mu r}(V_{21}\phi_1 + V_{22}\phi_2), \tag{5.10}$$

where $\Delta m = \sqrt{m_2^2 - m_1^2}$. We want the potential to disappear at spatial infinity, so that the two fields decouple and $\phi_2 \sim (\Delta m^2 - k_1^2)\phi_2$. In the gap the lighter and heavier fields go respectively like $\phi_1 \sim e^{ik_1 r}$ and $\phi_2 \sim e^{-\kappa r}$ (where $\kappa = \sqrt{\Delta m^2 - k_1^2}$) as $r \to \infty$, i.e. the heavier field is exponentially damped. Substituting this in the expression above we then have

$$\kappa^2 = (\Delta m^2 - k_1^2) + V_{21}e^{(\kappa-\mu)r}e^{ik_1 r}, \tag{5.11}$$

which describes the large r behaviour. Note that the term like $V_{22}\phi_2$ has been omitted because it includes a factor $e^{-\mu r}$ which suppresses it as $r \to \infty$.

Clearly, if $\kappa > \mu$, then the dominant term on the right hand side of this equation is the second one, rather than the first one, which is required if the equation is to satisfy the boundary condition $\lim_{r\to\infty} F = \mathbb{I}_2$. The simplest resolution of this problem is simply to restrict our investigation to values of the parameter $\mu > \Delta m$.

In fact, the issue is with the assumption of regular potentials. If we make the more restrictive choice, that our potential must satisfy

$$\int_0^\infty dr V(r) e^{\sqrt{m_2^2 - m_1^2}\, r} < \infty, \tag{5.12}$$

then the numerical instability does not occur. The reader can verify that if one chooses an exponential potential this integral diverges for $\Delta m > \mu$, and converges otherwise. So for the case of two scalar fields with a mass gap coupled by a exponential potential we find that it is the size of the mass gap Δm relative to the magnitude of the coupling μ that determines whether the solution has the appropriate asymptotic behaviour.

Stated differently, if the the parameter μ is not suitably restricted then we would have to change the ansatz (4.66) to something like

$$A = \begin{pmatrix} e^{-ik_1 r} & 0 \\ 0 & e^{-\mu r} \end{pmatrix}, \tag{5.13}$$

and the fields would not decouple to two plane waves: There would be a field decaying exponentially (i.e. something like a bound state), with this decay dependent not on the momentum but on the parameter μ. The other channel would, however, still be scattering.

Because the simplest way to increase the number of bound states is to decrease the size of the

parameter μ, this result has serious consequences for any attempt verify Levinson's theorem for two coupled fields. We shall see that while Levinson's theorem holds for potentials that allow one bound state, we cannot speak with certainty for potentials that allow more, precisely because of this restriction. This is not, however, a fundamental limitation, as we can adapt the differential equations as in the preceding discussion to take the necessary boundary conditions into consideration.

The discussion in this section is summarised by the following figures, which show the dependence of the phase shifts on the upper limit of the independent variable $rmax$ if the parameter μ is chosen improperly/properly for an exponential potential. Plots for a Gaussian potential are also included. The exponential potential corresponds to potential P_4 in appendix C, while the Gaussian potential corresponds to P_5. Explicitly, figures 5.2 and 5.4 have unacceptable values of μ, while the rest are acceptable, in the sense that they do not depend on $rmax$. Some comments on the continuity of the S-matrix follow the figures.

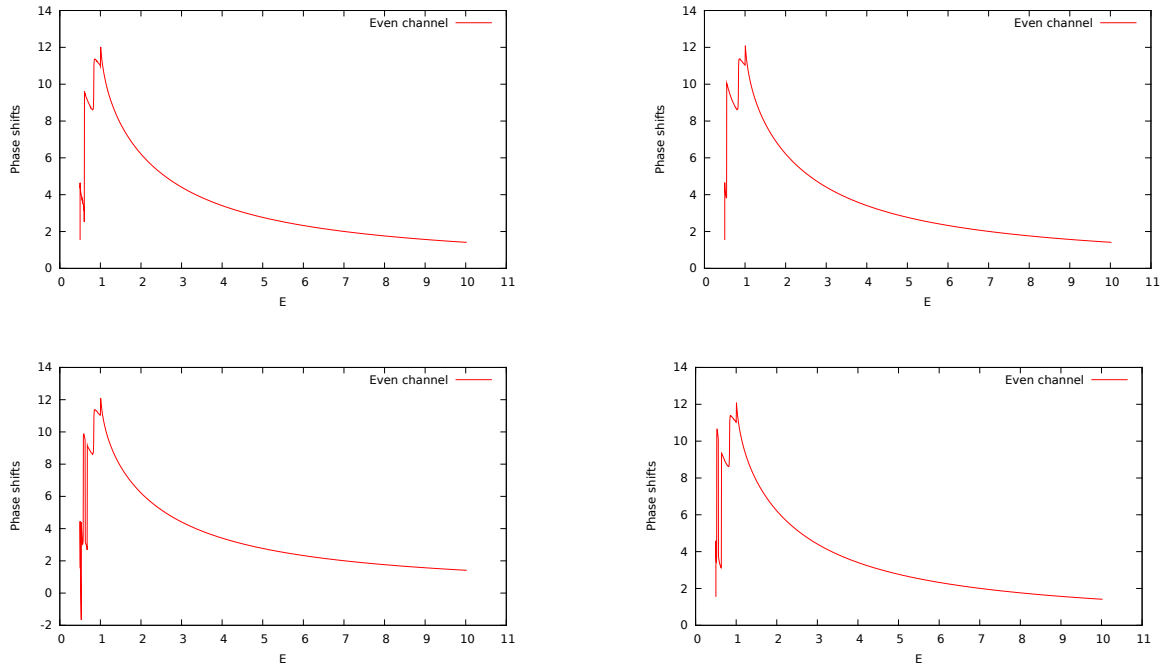

Figure 5.2: Behaviour of phase shifts for the exponential potential P_4 if $\mu < \Delta m$. Clockwise from top left: rmax = 10, 20, 30, 40 (even channel, $m_1 = 0.5$, $m_2 = 1$, $\mu = 0.4$).

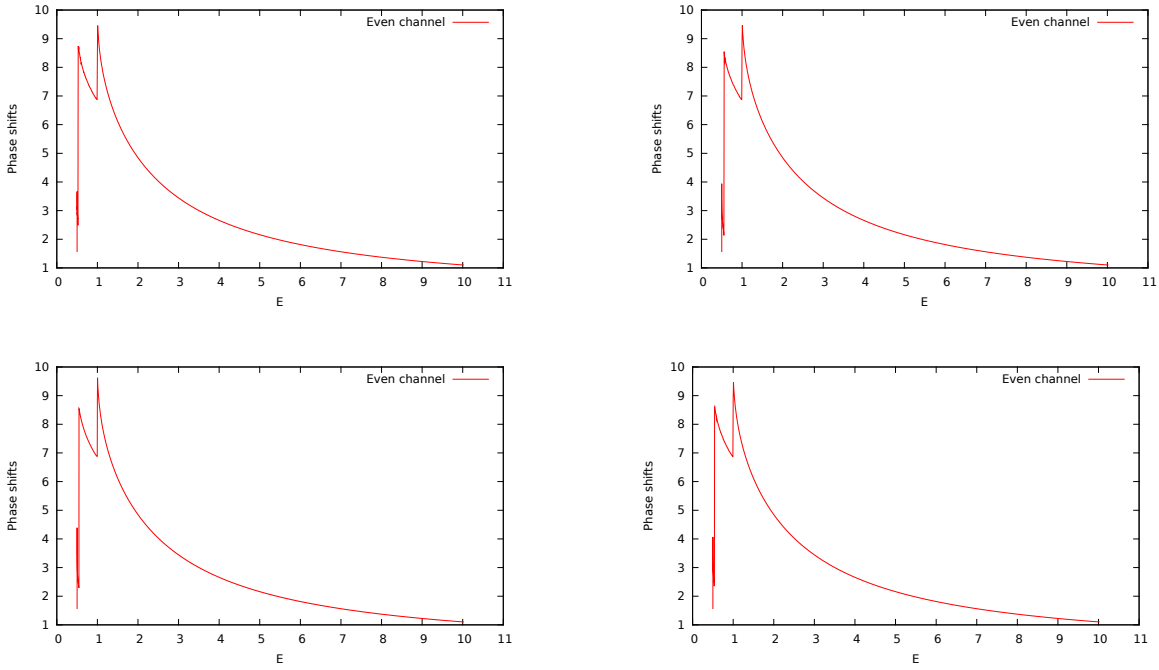

Figure 5.3: Behaviour of phase shifts for the exponential potential P_4 if $\mu > \Delta m$. Clockwise from top left: rmax = 10, 20, 30, 40 (even channel, $m_1 = 0.5$, $m_2 = 1$, $\mu = 0.9$).

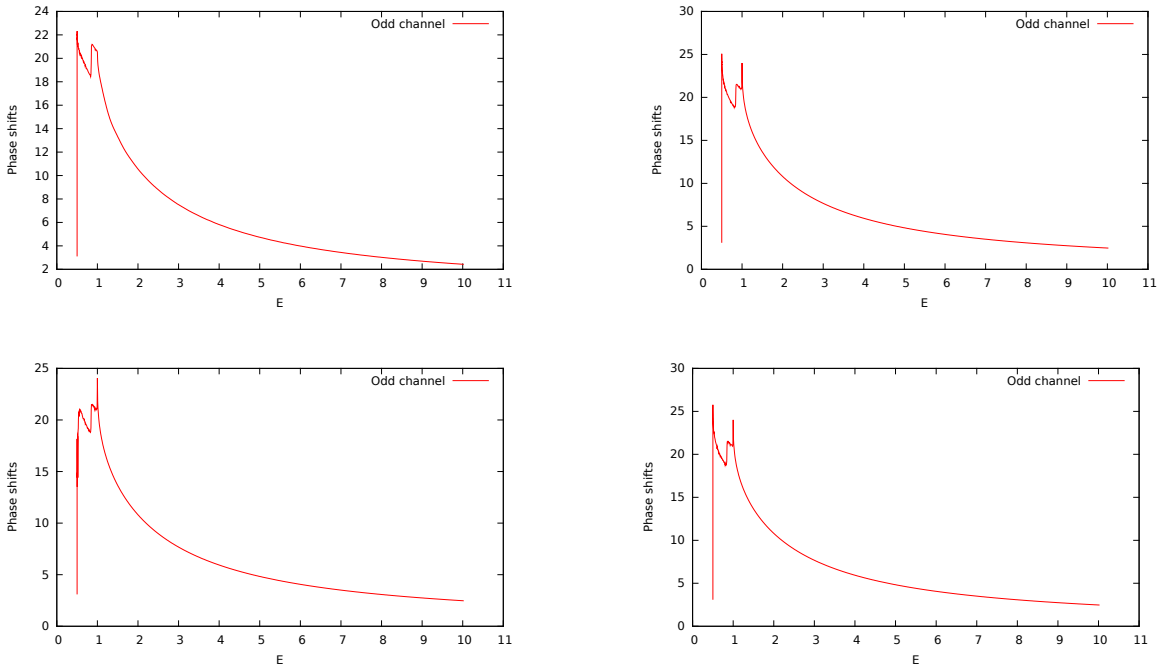

Figure 5.4: Behaviour of phase shifts for the exponential potential P_4 if $\mu < \Delta m$. Clockwise from top left: rmax = 10, 20, 30, 40 (odd channel, $m_1 = 0.5$, $m_2 = 1$, $\mu = 0.4$).

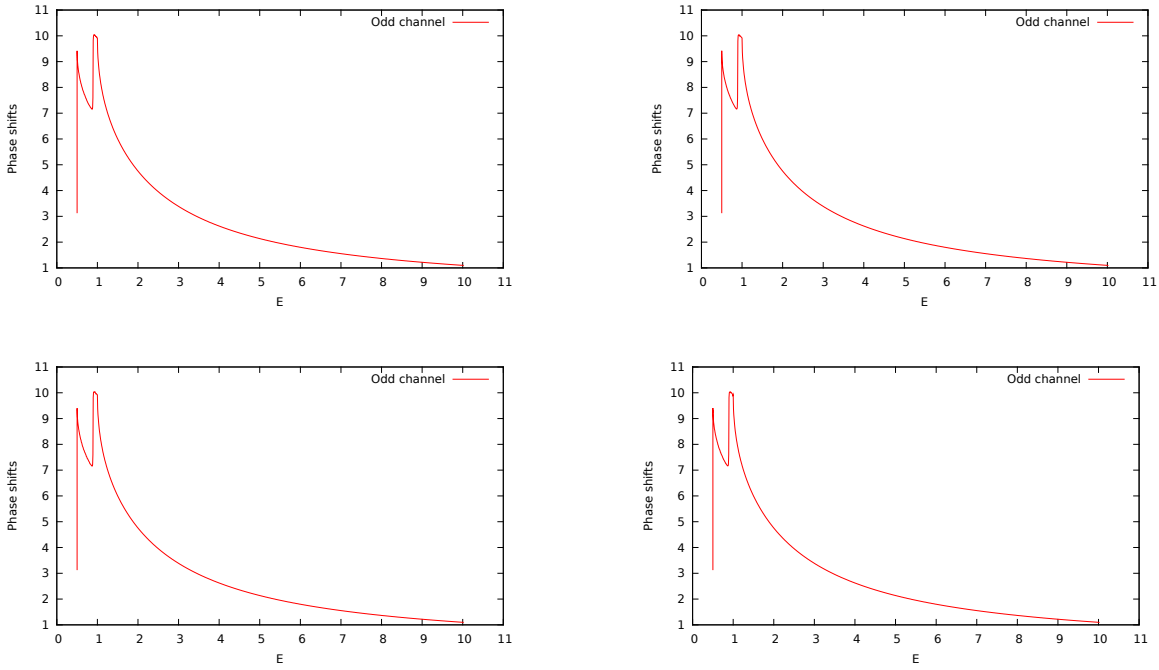

Figure 5.5: Behaviour of phase shifts for the exponential potential P_4 if $\mu > \Delta m$. Clockwise from top left: rmax = 10, 20, 30, 40 (odd channel, $m_1 = 0.5$, $m_2 = 1$, $\mu = 0.9$).

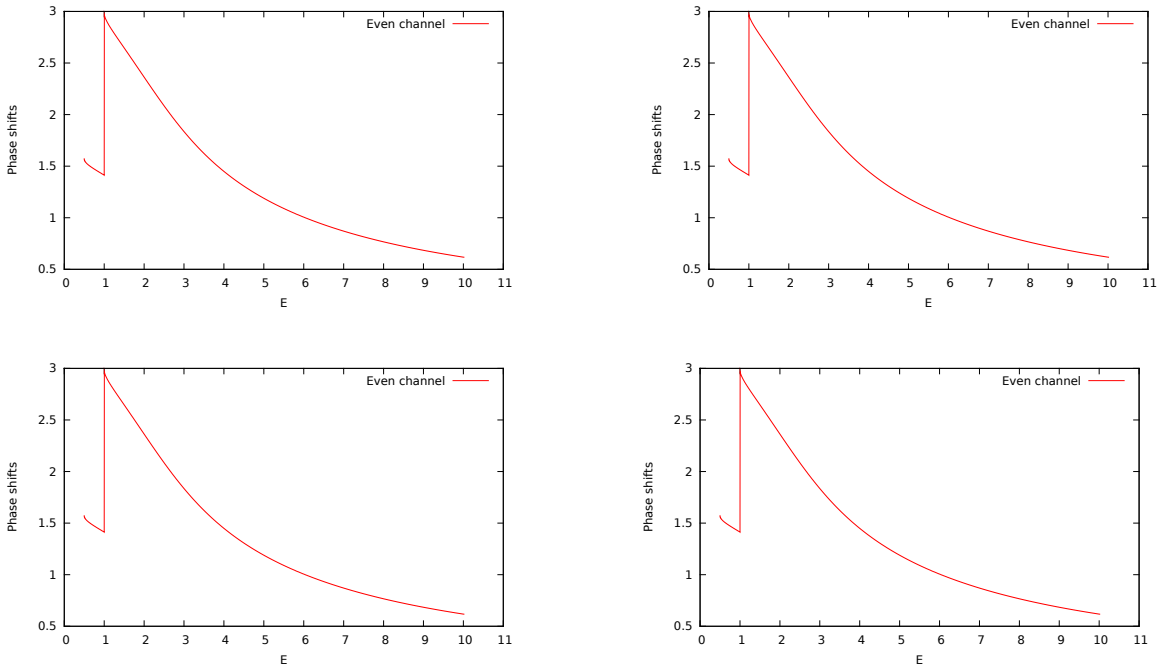

Figure 5.6: Behaviour of phase shifts for the Gaussian potential P_5. Clockwise from top left: rmax = 10, 20, 30, 40 (even channel, $m_1 = 0.5$, $m_2 = 1$, $\mu = 2$).

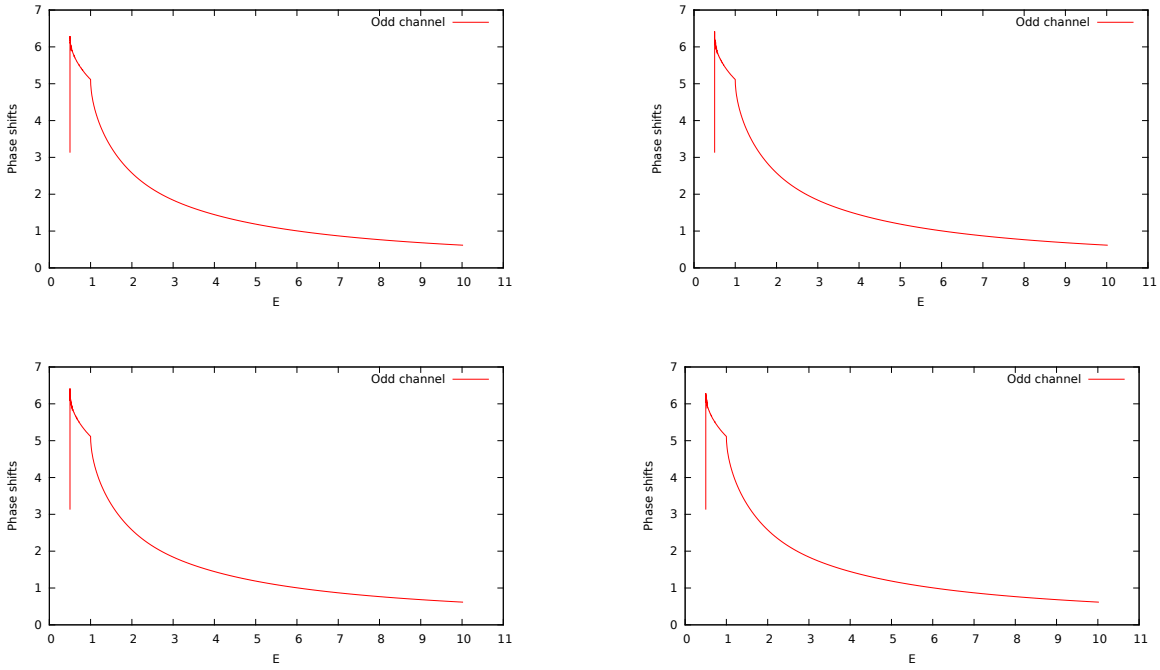

Figure 5.7: Behaviour of phase shifts for the Gaussian potential P_5. Clockwise from top left: rmax = 10, 20, 30, 40 (odd channel, $m_1 = 0.5$, $m_2 = 1$, $\mu = 2$).

While the phase shifts for the exponential potential are well-behaved, we see that the Gaussian potential appears to have a vertical 'jump' discontinuity near $E = 1$ for these parameters (see figures below). The apparent 'jumps' in the other figures are not a problem, but rather a feature, as they occur at $E = m_2$, and correspond to the results of Levinson's theorem. We may worry that the former discontinuities correspond to a discontinuity of the S-matrix as a function of the energy, which is physically undesirable. We can investigate this issue by plotting the entry S_{11} of the S-matrix, as this is the only interesting entry below the mass gap. The figures below make it clear that the S-matrix is still a continuous function of E. Since this implies that the phase shifts must also be a continuous function of E, we may wonder why there is a jump at all. The resolution of this paradox is provided in [26]. That reference makes it clear that we must add $\frac{\pi}{2}$ to the phase shift below threshold in the even channel, i.e. the correct formula for the phase shift in the even channel below threshold is

$$\delta_+(E) = \frac{\pi}{2} + \frac{1}{2i} \ln \det S_+, \tag{5.14}$$

where the S-matrix in the even channel, S_+, is to be constructed as in the discussion in chapter 4. The corrected plot of figure 5.6 is provided below.

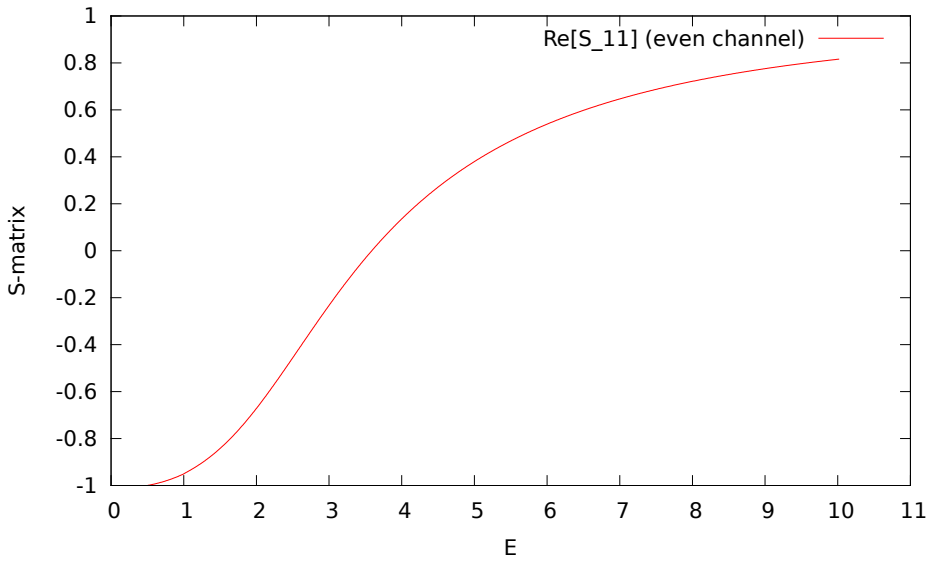

Figure 5.8: Behaviour of $\mathrm{Re}(S_{11})$ as a function of energy for the Gaussian potential P_5 (even channel, $m_1 = 0.5$, $m_2 = 1$, $\mu = 2$)

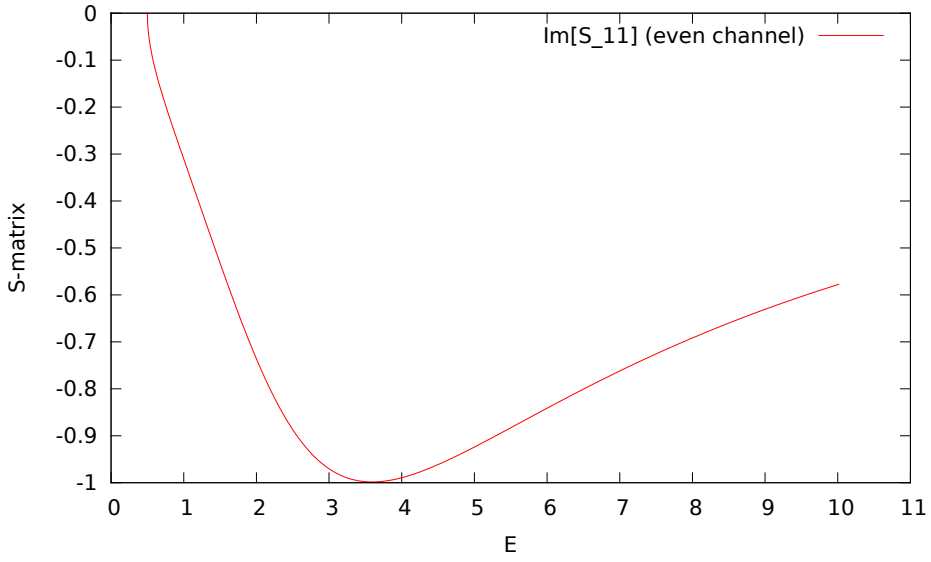

Figure 5.9: Behaviour of $\mathrm{Im} = (S_{11})$ as a function of energy for the Gaussian potential P_5 (even channel, $m_1 = 0.5$, $m_2 = 1$, $\mu = 2$)

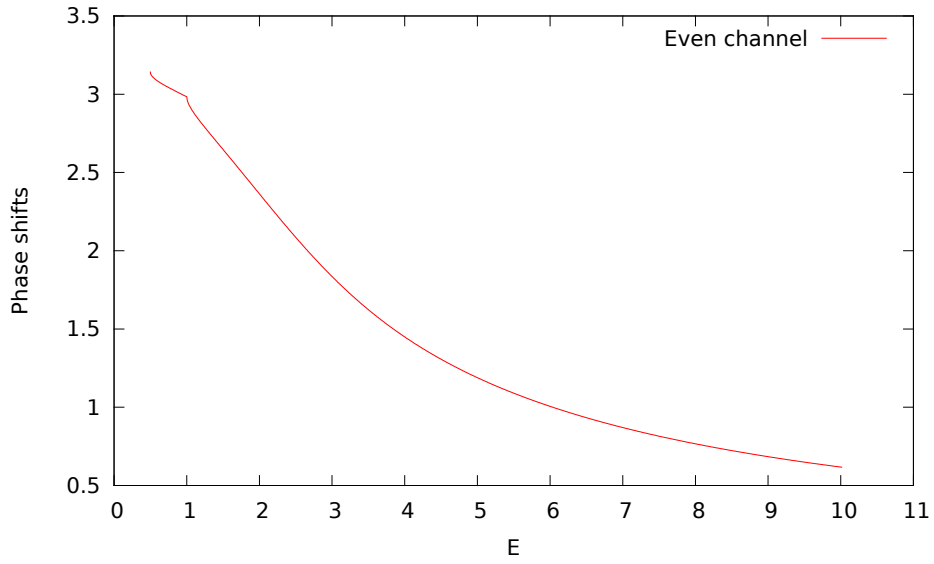

Figure 5.10: Corrected behaviour of phase shifts for the Gaussian potential P_5 (even channel, $m_1 = 0.5$, $m_2 = 1$, $\mu = 2$, $rmax = 10$)

5.2 Numerical results along the real momentum axis

In this section the results (up to four decimal places) of the numerical calculations along the real momentum axis for a specific potential with different parameters (i.e. both model and Runge-Kutta parameters) are presented for the coupled case. If we are to trust our results we require them to be numerically stable, in the sense that they must 'settle down' to a fixed value when the numerical parameters are chosen appropriately. The data are presented in several tables, as in the example of the uncoupled potentials that was performed as a consistency check (see section 4.6 for a reminder of the importance of the various parameters). We must also carefully consider the behaviour of the various pieces of the integral as outlined in subsection 5.1.3.

We consider the potential

$$V(r) = -e^{-\mu r} \begin{pmatrix} 0.6 & 0.4 \\ 0.4 & 0.6 \end{pmatrix}, \tag{5.15}$$

which corresponds to P_3 in appendix C. We could have included any number of other potentials; this one was chosen merely by way of convenience. All the other potentials investigated with the numerical program showed comparable properties with respect to stability of the integral for different numerical parameters, so endless tables of numerical data would give us no more insight into the problem in this thesis. We are not interested in any specific potential, only whether the spectral method is applicable. To that end it is sufficient to establish that the numerical data is well-behaved, which appears to be the case.

The VPE is calculated from equation (4.104), with the numerical piece reproduced here for convenience in the k_1 parameterisation:

$$\Delta E_{numerical} = \frac{1}{2}\sum_{j}^{b.s.}(\omega_j - m_1) - \frac{1}{\pi}\sum_{p=+1,-1}\int_0^\infty dk_1 \frac{k_1}{\sqrt{k_1^2 + m_1^2}}[\delta_p(k_1) - \delta_p^{(1)}(k_1)]. \tag{5.16}$$

The result of the numerical integral contributions (without the factor of $\frac{1}{\pi}$) in the even and odd channels are listed in the tables that follow. The figures show the behaviour of the integrand as a function of k_1. Tables of numerical data listing the bound state energies are also included.

	$m_1 = 0.5$, $m_2 = 1$, $\mu = 0.9$			$m_1 = 0.5$, $m_2 = 1$, $\mu = 1$		
	$ntt = 101$	$ntt = 501$	$ntt = 2001$	$ntt = 101$	$ntt = 501$	$ntt = 2001$
$\epsilon = 10^{-5}$						
$(0, \Delta m)$	-0.3239	-0.3239	-0.3239	-0.3139	-0.3139	-0.3139
$(\Delta m, \Delta m + \delta k_1)$	-0.0611	-0.0322	-0.0171	-0.0542	-0.0287	-0.0153
$(\Delta m + \delta k_1, \tilde{k}_1)$	-0.2073	-0.2442	0.2608	-0.1910	-0.2238	-0.2386
$(\tilde{k}_1, \infty)$	-0.0003	-0.0003	-0.0003	-0.0003	-0.0003	-0.0003
Σ	-0.5928	-0.6007	-0.6023	-0.5596	-0.5668	-0.5683
$\epsilon = 10^{-10}$						
$(0, \Delta m)$	-0.3239	-0.3239	-0.3239	-0.3139	-0.3139	-0.3139
$(\Delta m, \Delta m + \delta k_1)$	-0.0611	-0.0322	-0.0171	-0.0542	-0.0287	-0.0153
$(\Delta m + \delta k_1, \tilde{k}_1)$	-0.2073	-0.2442	-0.2608	-0.1910	-0.2238	-0.2386
$(\tilde{k}_1, \infty)$	-0.0003	-0.0003	-0.0003	-0.0003	-0.0003	-0.0003
Σ	-0.5928	-0.6007	-0.6023	-0.5596	-0.5668	-0.5683

Table 5.1: Integral contribution to the VPE (even): Numerical results for the integral contribution to the VPE of a coupled system in the even channel over the specified intervals ($\tilde{k}_1 = 10, rmax = 100$)

	$m_1 = 0.5,\ m_2 = 1,\ \mu = 0.9$			$m_1 = 0.5,\ m_2 = 1,\ \mu = 1$		
	$ntt = 101$	$ntt = 501$	$ntt = 2001$	$ntt = 101$	$ntt = 501$	$ntt = 2001$
$\epsilon = 10^{-5}$						
$(0, \Delta m)$	0.0386	0.0386	0.0386	0.0286	0.0285	0.0285
$(\Delta m, \tilde{k}_1)$	-0.0002	0.0006	0.0008	0.0019	0.0026	0.0027
$(\tilde{k}_1, \infty)$	-0.0003	-0.0003	-0.0003	-0.0003	-0.0003	-0.0003
Σ	0.0380	0.0389	0.0391	0.0302	0.0309	0.0309
$\epsilon = 10^{-10}$						
$(0, \Delta m)$	0.0386	0.0386	0.0386	0.0286	0.0285	0.0285
$(\Delta m, \tilde{k}_1)$	-0.0002	0.0006	0.0008	0.0019	0.0026	0.0027
$(\tilde{k}_1, \infty)$	-0.0003	-0.0003	-0.0003	-0.0003	-0.0003	-0.0003
Σ	0.0380	0.0389	0.0391	0.0302	0.0309	0.0309

Table 5.2: Integral contribution to the VPE (odd): Numerical results for the integral contribution to the VPE of a coupled system in the odd channel over the specified intervals ($\tilde{k}_1 = 10, rmax = 100$)

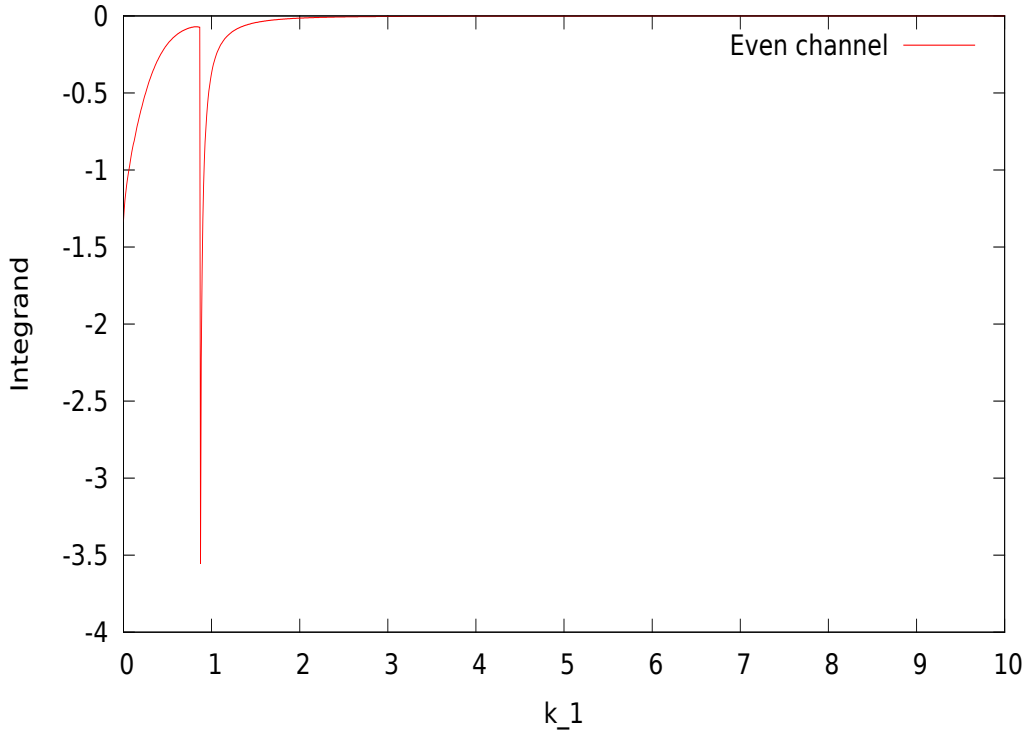

Figure 5.11: *The integrand* $\frac{k_1}{\sqrt{k_1^2+m_1^2}}\sum[\delta(k_1)-\delta^{(1)}(k_1)]$ *corresponding to the data in the tables above (even channel, ntt=101,* $\mu = 0.9$*)*

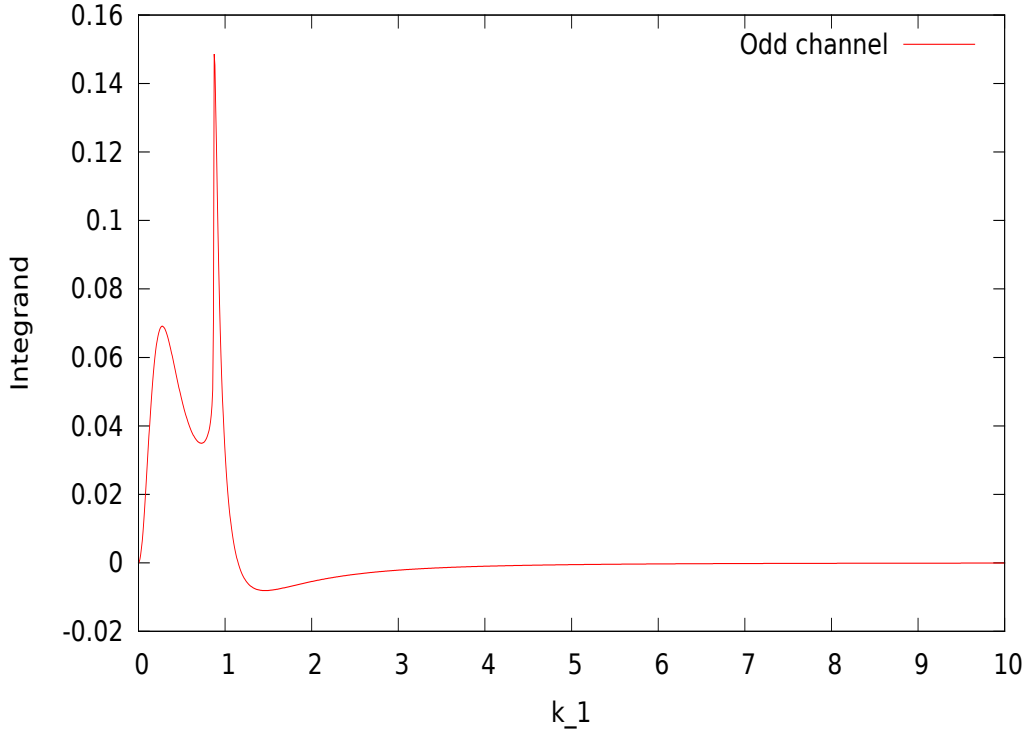

Figure 5.12: *The integrand* $\frac{k_1}{\sqrt{k_1^2+m_1^2}}\sum[\delta(k_1)-\delta^{(1)}(k_1)]$ *corresponding to the data in the tables above (odd channel, ntt=101,* $\mu = 0.9$*)*

	$m_1 = 0.5$, $m_2 = 1$, $\mu = 0.9$			$m_1 = 0.5$, $m_2 = 1$, $\mu = 1$		
	$nttH = 101$	$nttH = 201$	$nttH = 1001$	$nttH = 101$	$nttH = 201$	$nttH = 1001$
$nk = 201$						
BSE	0.0413	0.0415	0.0415	0.0622	0.0623	0.0623
$nk = 801$						
BSE	0.0413	0.0414	0.0415	0.0621	0.0623	0.0623

Table 5.3: Numerical results for the bound state contribution to the VPE in the even channel ($L = 10$)

	$m_1 = 0.5$, $m_2 = 1$, $\mu = 0.9$			$m_1 = 0.5$, $m_2 = 1$, $\mu = 1$		
	$nttH = 101$	$nttH = 201$	$nttH = 1001$	$nttH = 101$	$nttH = 201$	$nttH = 1001$
$nk = 201$						
BSE	-	-	-	-	-	-
$nk = 801$						
BSE	-	-	-	-	-	-

Table 5.4: Numerical results for the bound state contribution to the VPE in the odd channel. Note that there aren't any. ($L = 10$)

5.3 Numerical Check of Levinson's Theorem for two coupled fields

The proof of Levinson's theorem presented in appendix A depends crucially on the analyticity of the Jost function in the upper complex momentum plane. Since we also expect analyticity in the coupled problem, Levinson's theorem should hold in that case as well. This can be verified numerically. To investigate this issue we consider a number of different potentials, and indicate the number of bound states that our program counts. It does so in two ways; by explicitly calculating the binding energies, and by calculating the sum of the phase shifts at the threshold, for energies close to m_1. If the program finds, for a given potential in one spatial dimension, that there are n bound states, then we expect to find that $\delta(E)|_{m_1} = n_-\pi$ in the odd channel, and $\delta(E)|_{m_1} = \pi(n_+ - \frac{1}{2})$ in the even channel[23], where $n = n_- + n_+$ is the total number of bound states. Both n_- and n_+ are obtained by the part of the program that finds the bound state energies. The results are summarised in the following tables. It is taken for granted that the numerical parameters have been appropriately chosen to guarantee stability, as discussed previously. The potentials are labelled P_1 to P_6, and are listed in appendix C (P_2 is the free case).

[23]This differs slightly from the case in three spatial dimensions. See reference [27].

	$m_1 = 0.5,\ m_2 = 1,\ \mu = 0.9$				$m_1 = 0.5,\ m_2 = 2,\ \mu = 2.1$			
	P_1	P_2	P_3	P_6	P_1	P_2	P_3	P_6
n_-	0	0	0	0	0	0	0	0
E^2	-	-	-	-	-	-	-	-
$\delta(E)\|m_1$	0	0	0	0	0	0	0	0

Table 5.5: Checking Levinson's theorem for two coupled fields: Counting bound states (odd channel)

	$m_1 = 0.5,\ m_2 = 1,\ \mu = 0.9$				$m_1 = 0.5,\ m_2 = 2,\ \mu = 2.1$			
	P_1	P_2	P_3	P_6	P_1	P_2	P_3	P_6
n_+	0	0	1	1	0	0	1	1
E^2	-	-	0.0415	-0.1464	-	-	0.1892	0.9075
$\delta(E)\|m_1$	-1.5708	0	1.5708	1.5708	-1.5708	0	1.5708	1.5708

Table 5.6: Checking Levinson's theorem for two coupled fields: Counting bound states (even channel)

If we specifically consider the results for P_1 to P_3, we see that this corresponds to the physical situation of starting with a small repulsive potential, and then gradually tweaking the parameters so that it goes through zero ($V(r) = P_2$) and then becoming slightly attractive. The resultant phase shifts correspond to the behaviour expected from [27], which we take to mean that the results correspond to the correct physical situation.

We conclude that our numerical program counts states in accordance with Levinson's theorem in one spatial dimension for potentials P_1 to P_3, and P_6, and that this strongly suggests that the Jost function is analytic for these potentials. This is essentially a connection between the numerical scattering data and the topology of the Riemann surface associated with the Jost function. Specifically, we are counting the number of poles of the surface in figure 4.1.

As stated previously, the restriction on the parameter μ prevents us from investigating potentials with more than one bound state. This is a technical issue that should be surmountable by further investigation of the differential equations from which the phase shifts are extracted.

However, the issue is more complicated. For certain potentials it appears that Levinson's theorem does not hold. This is the case for potentials with values on the diagonal that are large with respect to those those on the off-diagonal, as the following table shows. This implies that we must be very careful when using the methods developed in this thesis to calculate the $O(\hbar)$ corrections to interacting scalar

fields, as they may not be applicable to certain potentials. This is an issue that warrants further attention, but we are in general satisfied with the robustness and validity of this approach, as long as this issue is taken into consideration.

	$m_1 = 0.5,\ m_2 = 1,\ \mu = 0.9$				$m_1 = 0.5,\ m_2 = 2,\ \mu = 2.1$			
	P_4	P_5	P_7	P_8	P_4	P_5	P_7	P_8
n_-	1	0	1	1	1	0	0	0
E^2	0.0431	-	0.1994	0.1922	0.0651	-	-	-
$\delta(E)\|m_1$	3.1416	3.1417	3.1418	3.1419	3.1414	3.1413	0	0

Table 5.7: Investigating the failure of Levinson's theorem for certain potentials : Counting bound states (odd channel)

	$m_1 = 0.5,\ m_2 = 1,\ \mu = 0.9$				$m_1 = 0.5,\ m_2 = 2,\ \mu = 2.1$			
	P_4	P_5	P_7	P_8	P_4	P_5	P_7	P_8
n_+	0	1	0	0	0	0	1	1
E^2	-	0.0269	-	-	-	-	-0.1904	-0.1986
$\delta(E)\|m_1$	1.5708	1.5708	1.5708	1.5708	1.5708	1.5708	1.5708	1.5708

Table 5.8: Investigating the failure of Levinson's theorem for certain potentials : Counting bound states (even channel). Note that the correction from equation (5.14) has not been included.

6 Discussion

During the course of this thesis we have seen how tools from potential scattering theory can be applied to calculate vacuum polarisation energies in the context of Quantum Field Theory. We began by discussing the properties of the quantum vacuum in a general manner, with several comments about the Casimir effect and how it may be interpreted to arise from shifts in the zero-point energy due to the presence of conducting plates.

We then reviewed various results from potential scattering theory. This included the notions of the regular and Jost solutions, which have their origin in different boundary conditions for the solutions of the radial Schrödinger equation. The notions of scattering phase shifts, the scattering cross section and the S-matrix were also introduced, as was the partial wave decomposition. Levinson's theorem was introduced as an important tool of the spectral method. The density of states was heuristically constructed by placing the system in a box of finite length. This notion was extended to the continuum by considering the difference between the density of states of interacting and free scattering systems. A simple example was considered to illustrate how all these ideas can be brought together to determine the vacuum polarisation energy of a scalar field interacting with a static background field. This required the identification of terms of the Born series with Feynman diagrams, for which a proof was outlined. This identification makes it clear that the spectral method is only applicable to renormalisable field theories, and requires the usual counterterms to render the theory finite.

We continued by showing how a certain model describing two interacting fields in the context of QFT is equivalent to the two channel regular solution from scattering theory. This was achieved by introducing the kink solution, a soliton that interpolates between the two vacua of one of these fields. We looked at small fluctuations around this classical solution, and expanded the Lagrangian density to quadratic order. Some formal manipulations and use of the stationary ansatz then allowed us to recover the regular solution in two channels. We also established that the regular series in one channel converges.

Next, we introduced the field theoretic formalism of our toy model that describes two interacting scalar fields with a mass gap in $(1+1)$ dimensions. The system was quantised by the standard approach of enforcing equal-time commutation relations between the field operator components and the components of the conjugate momenta in the Heisenberg picture. The Euler-Lagrange equations were used to obtain the equation of motion. The fields were then expanded in a Fock decomposition, choosing the covariant normalisation and identifying the expansion coefficients as the Jost solutions, rather than plane waves. The annihilation and creation operators were likewise defined. The commutation relations for these operators were calculated. We then proceeded to derive the necessary equation for the energy density, which is the component $\hat{T}_{00}$ of the energy momentum tensor.

Following on from this, we extended the scattering theory formalism to describe two fields. A

Green's function was introduced, and its imaginary part was identified with the local spectral density. This was then used to rewrite the expression for the energy density obtained previously. This enabled us to derive an expression for it along the imaginary k_1 axis, after appropriate Born subtractions and evaluation of the integral corresponding to the energy density along a contour in the complex k_1 plane.

Starting with a specific ansatz for the form of the scattering wavefunctions, and appropriate boundary conditions, a number of ordinary, second-order complex differential equations were derived. It was shown how the scattering phase shifts of two scalar fields with a mass gap interacting via a radial and Hermitian potential can be extracted from these equations. This was done for both the even and odd channels, and both inside and outside the mass gap. It was also shown how the S-matrix can be constructed from these equations. A similar analysis was performed to find the differential equations from which the first Born approximation to the phase shifts could be extracted. It was then explained how the bound state energies can be determined numerically for a given potential.

The applicability of the numerical method was demonstrated by comparing the numerical results of our Fortran 90 program to known analytic results for two uncoupled Pöschl-Teller potentials. Excellent agreement was established.

In the next chapter a number of issues related to the numerical integration of the phase shifts were discussed. The necessary connection between scattering theory and the field theoretic formalism was made via equation (5.3). An additional restriction on exponential potentials was found if we wish to make the ansatz inspired by the dispersion relations. We saw that this issue is related to the chosen boundary conditions, and is thus not a fundamental restriction of the method. Results along the real k_1 axis were presented, and it was established that the relevant integrals are numerically stable.

Finally, we confirmed that the numerical results for the scattering phase shifts of two interacting scalar fields with a mass gap in one spatial dimension agree with Levinson's theorem for a number of potentials. While the numerical confirmation of Levinson's theorem for these potentials allowing one bound state strongly suggests that the Jost-like function for two interacting scalar fields with a mass gap in $(1+1)$ dimensions is analytic in those cases, we would ideally like to extend this result to potentials with more bound states. This issue is currently unresolved, but should in principle only require another look at the DEQs and further development of the numerical program. An analytic proof of the analyticity of the Jost function is also desirable, as it is currently outstanding.

A more serious issue is the failure of Levinson's theorem for certain potentials. This is a problem that requires further investigation.

The most obvious avenue of further research would be to investigate a similar model in higher spatial dimensions. While $(1+1)$ dimensions presents a useful 'laboratory' to investigate effects like that discussed here, a world with one spatial dimension is not very rich in dynamics, and bears little resemblance to our own.

It is also conceivable to extend the model by considering more fields, in however many spatial dimensions. However, the analytic properties of the scattering data quickly become difficult to deal with when we have more than two fields.

A further hurdle is the dearth of experimentally detected scalar fields, which makes it a difficult matter to connect the results with experiments in the real world. As the situation stands, the only fundamental scalar field known to exist in nature (as of early 2014) is the Higgs. The main point of interest of the toy model considered in this thesis is the treatment of the integrals occurring near

the mass thresholds, their physical relevance, and whether the Jost function approach of the spectral method is applicable. The various bosons occurring in the electroweak theory (i.e. the Higgs, W's and the Z) also have different masses, so this thesis can be seen as the first small step in applying spectral methods to more realistic interacting field theories with mass gaps.

Appendices

Appendix A: Proof of Levinson's Theorem for s-wave

As noted in section 2.3.2 , this section contains a proof of Levinson's Theorem [19] for s-wave ($l = 0$) and regular potentials in three spatial dimensions. We start by considering the following contour integral along an arbitrary closed path in the complex plane:

$$\oint_C dz \frac{P'(z)}{P(z)} = \oint_C dz \frac{d}{dz} \ln[P(z)]. \tag{1}$$

We assume here that $P(z)$ is a polynomial of arbitrary order, $P(z) = A(z - z_1)(z - z_2)...(z - z_n)$, where the z_j are its nondegenerate roots. Then the above becomes

$$\begin{aligned} \oint_C dz \frac{P'(z)}{P(z)} &= \oint_C dz [\frac{1}{z - z_1} + \frac{1}{z - z_2} + ... + \frac{1}{z - z_n}] \\ &= 2\pi n i \end{aligned} \tag{2}$$

where n is the number of roots of $P(z)$ lying inside the contour C, since

$$\frac{1}{2\pi i} \oint_C dz \frac{1}{(z - a)^n} = \begin{cases} 0 & \text{if } a \text{ is not contained in } C \\ 0 & \text{if } a \text{ is contained in } C \text{ but } n \neq 1 \\ 1 & \text{if } a \text{ is contained in } C \text{ and } n = 1. \end{cases} \tag{3}$$

We can then establish Levinson's theorem as follows: we consider the contour C_0 along the x-axis from $-R$ to $+R$ that skips the origin with a small semicircle of radius ϵ above the real axis, plus the semicircle at R in the upper complex k-plane (see figure 1 below) and evaluate the contour integral of the derivative of the natural logarithm of the Jost function $F(k)$ along C_0 by taking the simultaneous limits $R \to \infty$ and $\epsilon \to \infty$. Since we know (property 4 from section 2.3.2)[24] that $F(k)$ is analytic in the upper k-plane we can use the above to obtain

$$\frac{1}{2\pi i} \oint_{C_0} dk \frac{F'(k)}{F(k)} = \lim_{\substack{\epsilon \to 0 \\ R \to \infty}} \frac{1}{2\pi i} [\int_{C_1} + \int_{C_2} + \int_{C_3} + \int_{C_4}][dk \frac{F'(k)}{F(k)}] = n \tag{4}$$

where n is the number of bound states inside the contour at the binding energies $-\kappa_j^2$. Note that our construction of C in the figure below allows us to apply Cauchy's theorem to a multiply connected domain. Explicitly,

$$\oint_C dk \frac{F'(k)}{F(k)} = 0, \tag{5}$$

so

$$\oint_{C_0} dk \frac{F'(k)}{F(k)} = \sum_{j=1}^{n} \oint_{C(i\kappa_j, r)} dk \frac{F'(k)}{F(k)} = 2\pi i n, \tag{6}$$

where $C(i\kappa_j, r)$ is the circle of some small radius r centered at $i\kappa$.

We now use the properties of the Jost function to evaluate the integral along $C_1 + C_2 + C_3 + C_4$

[24] Further properties in this appendix refer to those occurring in the same section.

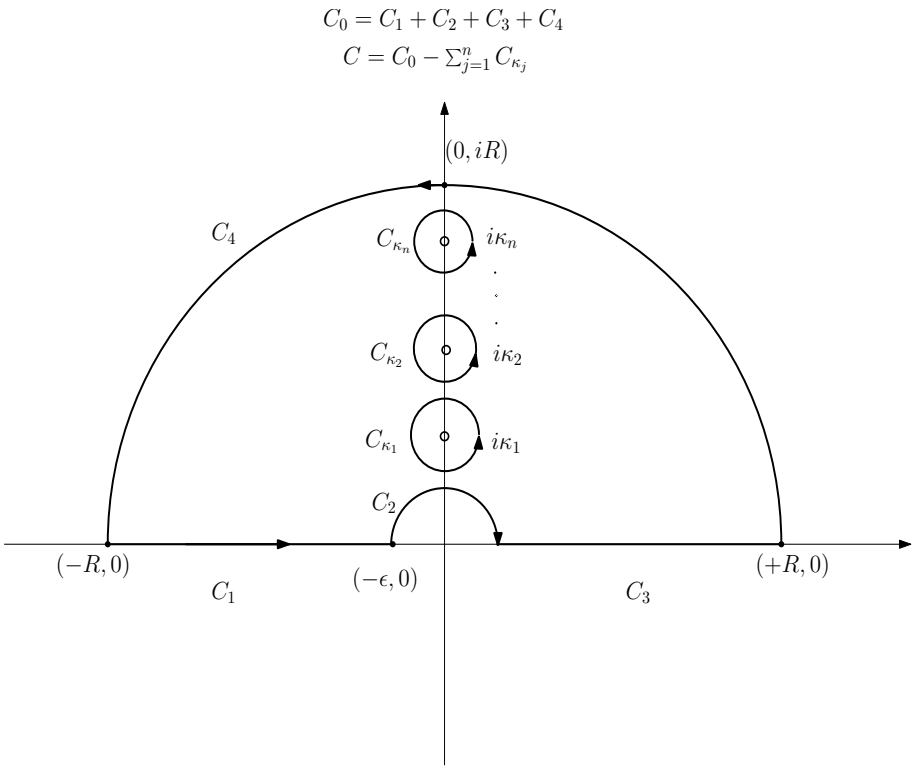

Figure 1: *Integration contour used in the proof of Levinson's Theorem for the s-wave*

term by term.

C_1 and C_3: From property 2 we have, for real k, $F(k) = |F|e^{-i\delta(k)}$, so $\int dk \frac{F'(k)}{F(k)} = -i \int dk \frac{d}{dk}\delta_l(k)$ if the integration is along the real axis. Then

$$\begin{aligned}\frac{1}{2\pi i}[\int_{C_1} + \int_{C_3}][dk\frac{F'(k)}{F(k)}] &= \frac{-i}{2\pi i}[\int_{-R}^{-\epsilon} + \int_{+\epsilon}^{+R}][dk\frac{d\delta(k)}{dk}] \\ &= \frac{1}{2\pi}[-\delta(-\epsilon) + \delta(-R) - \delta(+R) + \delta(+\epsilon)]. \end{aligned} \tag{7}$$

We take the limit as the radius of the semi-circle goes to $+\infty$, to ensure that we enclose all the bound states, and the limit as the radius of the small semi-circle goes to zero to deal with possible poles there (i.e. $F(0) = 0$). We define $\delta(\infty) = 0$, which establishes the physically reasonable expectation that a particle incident at infinite energy won't be perturbed by a regular potential, and is equivalent to requiring the S-matrix element to go to unity for large k (since $\delta(k) = 2\pi$ implies that $S = \mathbb{I}$). Then, since $\delta(-k) = -\delta(k)$ (property 7), the above contributes $\frac{1}{\pi}\delta(0)$ to the total integral along the contour C, after taking the appropriate limits.

C_4: From property 3 we have $\lim_{|k|\to\infty} F'(k) = 0$ so that the semicircle contributes nothing to the integral.

C_2: For the small semicircle we make use of the fact that as $k \to 0$ along the upper complex plane

$F(k) = O(k)$ and $F(k)^{-1} = O(k^{-1})$. So

$$\frac{1}{2\pi i}\int_{C_2} dk \frac{F'(k)}{F(k)} = \frac{1}{2\pi i}\int_{\pi}^{0} d\theta = -\frac{1}{2} \tag{8}$$

if $F(0) = 0$, and 0 otherwise.

Summing the contributions and rearranging we get Levinson's theorem in three spatial dimensions,

$$\delta(0) = \begin{cases} n\pi & \text{if} \quad F(0) \neq 0 \\ \pi(n + \frac{1}{2}) & \text{if} \quad F(0) = 0 \end{cases} \tag{9}$$

which gives us a remarkably simple relationship between the phase shifts at $k = 0$ and the number of bound states for a large class of potentials of type (2.10). The generalisation to $l > 0$ is

$$\delta(0) = n\pi, \tag{10}$$

which is proved as above without the complication at $k = 0$.

In one spatial dimension the result in the symmetric channel changes [27] to

$$\delta(0) = \pi(n - \frac{1}{2}), \tag{11}$$

which is relevant to our discussion of the analyticity of the Jost function of two coupled scalar fields in chapter 5.

Appendix B: Numerical Methods

This appendix contains a concise overview of the various numerical methods and algorithms used during the course of this thesis, with appropriate references. Unless otherwise stated, all the numerical algorithms were implemented in Fortran 90, after a rather lengthy and unsuccessful attempt at implementing them in C from scratch[25].

Numerical Integration

The numerical integration method used was the 5-point Newton-Cotes formula, also known as Boole's rule[26]. Like all Newton-Cotes formulas, of any order n, Boole's rule approximates the integral of a function over an interval by integrating the Legendre interpolating polynomial associated with it. The Legendre interpolating polynomial of order n is the polynomial which passes through the points $(x_1, f(x_1)), \ldots, (x_n, f(x_n))$, given by

$$P(x) = \sum_{j=1}^{n} f(x_j) \prod_{\substack{k=1 \\ k\neq j}}^{n} \frac{x - x_k}{x_j - x_k}. \tag{12}$$

[25] This is not recommended.

[26] Due to a misprint in the 1972 edition of Abramowitz and Stegun's venerable 'Handbook of Mathematical Functions with Formulas, Graphs, and Mathematical Tables' this is widely known as Bode's Rule.

Given the value of a function at n points, the actual form of the Newton-Cotes formula which approximates the integral of the function over an interval can then be obtained by constructing this polynomial and integrating it. To do so for $n = 5$ is very tedious, so the reader is directed to reference [28] for the following result: Given five equally spaced data points, $\{f(x_1), \ldots, f(x_5)\}$, with $x_{i+1} - x_i = h$ for $i = 1 \ldots 4$, the integral

$$\int_{x_1}^{x_5} dx f(x) \tag{13}$$

is approximated by

$$\frac{2}{45}h(7f(x_1) + 32f(x_2) + 12f(x_3) + 32f(x_4) + 7f(x_5)) - \frac{8}{945}h^7 f^{(6)}(\zeta), \tag{14}$$

where the ζ occurring in the error term is some number between x_1 and x_5.

Numerical solution of differential equations

The standard method used to solve the numerous differential equations in this thesis was a 4th-order Runge-Kutta (RK) algorithm with adaptive step-size control, which is equivalent to a RK algorithm of 5th-order. The logic is straightforward: one first computes the result of taking two 'small' steps of the independent variable (in this thesis this would be the spatial variable) with the solver, then compares this with the result of taking one 'large' step equal to the sum of the two smaller steps. The difference is used to estimate the error of the large step. If this is larger than some specified error tolerance, then the data is discarded and the step-size decreased. The process is continued until the magnitude of the error is acceptably small, at which point the solution is accepted and the independent variable incremented. The computational overhead is not too bad [29]: If the exact solution of advancing a single function y from x to $x + 2h$ is denoted by $y(x + 2h)$, and the two approximate numerical solutions for one large step and two small steps by y_1 and y_2 respectively, then they are related by

$$\begin{aligned} y(x + 2h) &= y_1 + (2h)^5\theta + O(h^6) \\ y(x + 2h) &= y_2 + 2(h^5)\theta + O(h^6). \end{aligned} \tag{15}$$

Here θ is a value that remains constant over the interval and is of order $\frac{d^5y}{dx^5}$. We can define

$$\Delta = y_2 - y_1 \tag{16}$$

to eliminate the constant θ above to get the local extrapolation

$$y(x + 2h) = y_2 + \frac{\Delta}{15} + O(h^6). \tag{17}$$

We see that this is accurate to *fifth* rather than fourth order. While we may initially think that each of the RK steps require four evaluations of the DEQ, for a total of twelve, the endpoints are the same, so that only eleven are required. Since we are achieving the accuracy of the smaller stepsize, this must be compared to eight evaluations, for an overhead factor of 1.375, which buys us the improvement of fifth-order accuracy while using the largest permissible step-size.

If we are interested in the value of some 2×2 matrix function F at the origin, the 2nd-order DEQs for F are integrated *backwards* (with the chosen precision) from 'spatial infinity' to the origin. The choice of an appropriate value for the independent spatial variable which corresponds to 'far away' is determined by the length scale of the potential. The value of the dependent variables at the first step is determined by the boundary conditions. In the case where F corresponds to the function occurring in the ansatz $\psi_a(r) = FA$, as in section 4.4, a fifth independent function $\delta(r)$ is also introduced, which does not suffer from the mod π ambiguities mentioned there.

The numerical integrator itself takes as input the value of the 2×2 matrix F, its first spatial derivative F', the value of the function δ and δ', the step-size Δx and current position xs, and the value of the energy. The physical parameters of the theory, like the masses of the fields and the specific form of the potential, are provided in a separate module. The output of the integrator is the value of F and F' at the advanced step. Because of Fortran's highly efficient implementation of matrix multiplication, it is convenient to represent the system as a 5×5 matrix as follows:

$$\textbf{Input}: \quad z1 = \left(\begin{array}{cc|c} F_{12}(xs) & F_{21}(xs) & \\ F_{21}(xs) & F_{22}(xs) & \\ \hline & & \delta(xs) \end{array}\right) \qquad zd1 = \left(\begin{array}{cc|c} F'_{12}(xs) & F'_{21}(xs) & \\ F'_{21}(xs) & F'_{22}(xs) & \\ \hline & & \delta'(xs) \end{array}\right) \tag{18}$$

$$\textbf{Output}: \quad z2 = \left(\begin{array}{cc|c} F_{12}(xs-\Delta x) & F_{21}(xs-\Delta x) & \\ F_{21}(xs-\Delta x) & F_{22}(xs-\Delta x) & \\ \hline & & \delta(xs-\Delta x) \end{array}\right)$$

$$zd2 = \left(\begin{array}{cc|c} F'_{12}(xs-\Delta x) & F'_{21}(xs-\Delta x) & \\ F'_{21}(xs-\Delta x) & F'_{22}(xs-\Delta x) & \\ \hline & & \delta'(xs-\Delta x) \end{array}\right). \tag{19}$$

We apply this procedure inside a DO loop that increments the energy. Because the DEQs inside and outside the mass gap differ, we have two DO loops that access different Runge-Kutta routines.

In practice the integrator also solved for another 2×2 matrix of coupled DEQs, corresponding to the first Born approximation, and another independent DEQ for the symmetric channel (which entails different boundary conditions), but the above diagram is conceptually clear.

The calculation of the phase shifts and the first Born approximation thereof, at a given energy and in both channels, then corresponds to the solution of ten 2nd-order, complex, ordinary differential equations. This is equivalent to forty 1st-order, ordinary, real-valued differential equations. These take the value of the energy as a parameter, so that we may think of the equations at different energies as unique. The size of the energy intervals is provided as a numerical parameter. So, for instance, for two hundred values of the energy we must solve eight thousand 1st-order DEQs to the specified accuracy to calculate the VPE. In practice, for numerical testing, the program would solve over six

million equations in one run.

Numerical checks on the differential solver

The program used to solve the DEQs occurring in this thesis is complex enough that we need some way of checking that the output is sensible. There are many ways in which errors can enter into the solution of the DEQs (not the least of which is sign errors, which there are many opportunities for). We list here some of the ways in which the consistency of the numerical data was established at various points:

- The S-matrix is required to be unitary at every point in the simulation (from the postulates of quantum mechanics). This is easily checked, and a deviation would indicate something amiss. In the mass gap we only require that the element S_{11} have magnitude of unity. Outside the gap we must remember to normalise the S-matrix with respect to the incoming flux. In practice the off-diagonal elements of the S-matrix, when calculated numerically, will be non-zero, but should be very small (typically of the order 10^{-10} to 10^{-15}). This is to be expected, and not an indication of an error, as long as they remain small for the entire duration of the simulation.

- The numerical output can be compared to the result for a potential with known analytic results. Deviation from this would indicate an error. This was done for two uncoupled Pöschl-Teller potentials [24], with different masses, achieving excellent agreement (see section (4.6)).

- We can diagonalise the problem for equal masses, decoupling the fields, and the numerical output should correspond with that of the undiagonalised problem. For instance, the equation from which the phase shift for two fields with equal masses and a radial potential $V = V(r)$ is extracted is

$$F'' - 2ikF' - VF = 0. \tag{20}$$

  If we diagonalise the potential by the unitary matrix U, this becomes

$$\tilde{F}'' - 2ik\tilde{F}' - D\tilde{F} = 0, \tag{21}$$

  where $D = U^\dagger VU$ and $\tilde{F} = U^\dagger FU$. The boundary conditions restrict the form of F so that the off-diagonal elements remain zero. These two equations should then yield the same numerical data if the approach is consistent. This check was performed for a number of potentials.

Despite all the care that has been taken to be sure that the numerical data is sensible, the nature of the problem that was investigated is such that it would be wise to take the numerical results for the coupled fields with a pinch of salt. Specifically, a negative result for the analyticity should be viewed with suspicion. A positive result is much less likely to be false, simply because it is extremely unlikely that unrelated functions just happen to have the same value when integrated along different axes in the complex momentum plane.

Calculating binding energies

In section 4.5 the method for calculating binding energies for a given potential was outlined. While the general procedure was outlined there, the diagonalisation algorithm used appears in *Numerical*

Recipes in Fortran 77 [30] on page 460. The algorithm is well suited to diagonalising real symmetric matrices, using a sequence of orthogonal similarity transformations equivalent to rotations of a plane. These are called Jacobi rotations.

It may happen that for very tightly bound potentials the numerical results for the squared binding energies are negative. If this is the case the numerical routine used to determine the energies will return NaNs ('not a number'), as the routine expects the output to consist of positive real numbers. It is then clearly not possible to calculate the VPE along the real momentum axis, as the binding energies enter as central ingredients. This will be the case if the ground state of the system does not correspond to vanishing fields. We can however still use these results to investigate Levinson's theorem.

The integrals occurring in the calculation of the binding energies were computed using Boole's rule (see above).

Appendix C: Potentials used to check numerical results and Levinson's theorem for two coupled scalar fields with a mass gap in $(1+1)$ dimensions

$$P_1 = \begin{pmatrix} 0.6 & 0.4 \\ 0.4 & 0.6 \end{pmatrix} e^{-\mu r}. \tag{22}$$

$$P_2 = 0. \tag{23}$$

$$P_3 = -P_1. \tag{24}$$

$$P_4 = -\begin{pmatrix} 10 & 0.4 \\ 0.4 & 10 \end{pmatrix} e^{-\mu r}. \tag{25}$$

$$P_5 = -\begin{pmatrix} 10 & 0.4 \\ 0.4 & 10 \end{pmatrix} e^{-\mu r^2}. \tag{26}$$

$$P_6 = -\begin{pmatrix} 1.0 & 0.4 \\ 0.4 & 1.0 \end{pmatrix} e^{-\mu r^2}. \tag{27}$$

$$P_7 = -\begin{pmatrix} 2.0 & 0.4 \\ 0.4 & 2.0 \end{pmatrix} e^{-\mu r}. \tag{28}$$

$$P_8 = -\begin{pmatrix} 2.0 & 0.6 \\ 0.6 & 2.0 \end{pmatrix} e^{-\mu r}. \tag{29}$$

BIBLIOGRAPHY

[1] G. Gabrielse, D. Hanneke, T. Kinoshita, M. Nio, and Brian C. Odom. New Determination of the Fine Structure Constant from the Electron g Value and QED. *Physical Review Letters*, 97:030802, 2006.

[2] H.B.G. Casimir and D. Polder. The Influence of retardation on the London-van der Waals forces. *Physical Review*, 73:360–372, 1948.

[3] N. Graham M. Quandt and H. Weigel. Spectral Methods in Quantum Field Theory. *Lecture Notes in Physics, Springer-Verlag*, 2009.

[4] N. Graham, R.L. Jaffe, and H. Weigel. Casimir effects in renormalizable quantum field theories. *International Journal of Modern Physics A*, 17:846–869, 2002.

[5] E. Farhi, N. Graham, P. Haagensen, and R.L. Jaffe. Finite quantum fluctuations about static field configurations. *Physics Letters B*, 427:334–342, 1998.

[6] H. Weigel, M. Quandt, and N. Graham. Stable charged cosmic strings. *Physical Review Letters*, 106:101601, 2011.

[7] E. Farhi, N. Graham, R.L. Jaffe, and H. Weigel. Searching for quantum solitons in a (3+1)-dimensional chiral Yukawa model. *Nuclear Physics B*, 630:241–268, 2002.

[8] J.P. Blaizot and G. Ripka. Quantum theory of finite systems. *MIT press Cambridge*, 1986.

[9] P.C.W. Davies. Scalar particle production in Schwarzschild and Rindler metrics. *Journal of Physics A*, 8:609–616, 1975.

[10] W.G. Unruh. Notes on black-hole evaporation. *Physical Review D*, 14:870, 1976.

[11] T. Ching. Relativity, Gravitation and Cosmology: A Basic Introduction. *Oxford University Press*, 2006.

[12] S. Weinberg. The Cosmological Constant Problem. *Reviews of Modern Physics*, 61:1–23, 1989.

[13] S. J. Summers. Yet More Ado About Nothing: The Remarkable Relativistic Vacuum State. *by H. Halvorson (Cambridge University Press, Cambridge)*, pages 317–341, 2011.

[14] D. Tabor and R.H.S. Winterton. The direct measurement of normal and retarded van der Waals forces. *Proceedings of the Royal Society of London. A. Mathematical and Physical Sciences*, 312:435–450, 1969.

[15] M.J. Sparnaay. Measurements of attractive forces between flat plates. *Physica*, 24:751–764, 1958.

[16] R.L. Jaffe. The Casimir effect and the quantum vacuum. *Physical Review D*, 72:021301, 2005.

[17] R.G. Newton. Scattering Theory of Waves and Particles. *McGraw-Hill Book Company*, 1966.

[18] K. Chadan and P.C. Sabatier. Inverse Problems in Quantum Scattering Theory (Second Edition). *Spinger-Verlag New York*, 1989.

[19] N. Levinson. On the uniqueness of the potential in a Schrödinger equation for a given asymptotic phase. *Danske. Vid. Selsk. Math. Fys. Medd.* ***25****, 1-29*, 1949.

[20] N. Graham, R.L. Jaffe, V. Khemani, M. Quandt, M. Scandurra, H. Weigel, et al. Calculating vacuum energies in renormalizable quantum field theories: A New approach to the Casimir problem. *Nuclear Physics B*, 645:49–84, 2002.

[21] U. Mosel. Path Integrals in Field Theory: An Introduction. *Springer-Verlag*, 2004.

[22] F. Calegero. Variable Phase Approach to Potential Scattering. *Academic Press, New York and London*, 1967.

[23] R. Rajaraman. Solitons and Instantons: An introduction to solitons and instantons in Quantum Field Theory. *North-Holland Amsterdam*, 1982.

[24] G. Pöschl and E. Teller. Bemerkungen zur Quantenmechanik des anharmonischen Oszillators. *Zeitschrift für Physik*, 83:143–151, 1933.

[25] R.F. Dashen, B. Hasslacher, and A. Neveu. Nonperturbative methods and extended-hadron models in field theory. II. Two-dimensional models and extended hadrons. *Physical Review D*, 10:4130, 1974.

[26] N. Graham, M. Quandt, and H. Weigel. On the Casimir Energy of Frequency Dependent Interactions. *arXiv:1406.0748 [hep-th]*, 2014.

[27] G. Barton. Levinson's Theorem in One-dimension: Heuristics. *Journal of Physics A*, 18:479–494, 1985.

[28] M. Abramowitz and I. Stegun. Handbook of Mathematical Functions with Formulas, Graphs, and Mathematical Tables. *ERIC*, 1972.

[29] W.H. Press, S.A. Teukolsky, W.T. Vetterling, and B.P. Flannery. Numerical Recipes in C: The Art of Scientific Computing. *Cambridge University Press*, 1992.

[30] W.H. Press. Numerical recipes in Fortran 77: The Art of Scientific Computing (Second Edition). *Cambridge University Press*, 1992.